Title
Microstructural Development During Processing of Ethoxide-Derived Titania

Author
Shalz, M.L.

Publication Date
1991-05-01

LBL-30789

Lawrence Berkeley Laboratory
UNIVERSITY OF CALIFORNIA

Materials & Chemical Sciences Division

Microstructural Development During Processing of Ethoxide-Derived Titania

M.L. Shalz
(M.S. Thesis)

May 1991

Prepared for the U.S. Department of Energy under Contract Number DE-AC03-76SF00098

DISCLAIMER

LBL-30789

MICROSTRUCTURAL DEVELOPMENT DURING PROCESSING OF ETHOXIDE-DERIVED TITANIA

Mark L. Shalz
M.S. Thesis

MATERIALS SCIENCE
AND
MINERAL ENGINEERING
University of California
Berkeley, CA 94720

and

MATERIALS SCIENCE DIVISION
Lawrence Berkeley Laboratory
University of California
Berkeley, CA 94720

May, 1991

This work was supported by the Director, Office of Energy Research, Office of Basic Energy Sciences, Materials Sciences division of the U.S. Department of Energy under Contract No. DE-AC03-76SF00098

Microstructural Development During Processing of Ethoxide-Derived Titania

by

Mark Loren Shalz

Abstract

The diameter of nominally monosized titania particles, synthesized by the controlled hydrolysis of titanium tetraethoxide, varied among batches between 0.25 and 0.35 μm under seemingly identical precipitation conditions. The internal structure of the powder particles was examined by TEM of ultramicrotomed sample compacts. With these techniques, the as-prepared powders were shown to be agglomerates of fine units on the order of tens of angstroms in size. As-prepared powders appeared amorphous under standard X-ray diffractometer scans using Cu Kα radiation, however, electron diffraction revealed short range ordering. The first two diffraction rings in TEM diffraction patterns correspond to lattice spacings of ≈3.6 and ≈2.4 Å for the as-prepared powders.

The temperature for the transformation of as-prepared powders to anatase ranged from 335°C to 420°C, and the anatase to rutile transformation temperature ranged from 500°C to 990°C (as determined by crystallization and dilatometric studies). The observed variations occurred among different powder batches. In thermal pretreatment studies, sample phase content varied as a function of the pretreament temperature; e.g., samples pretreated at 500°C and 600°C and then annealed at 900°C were composed of rutile and a mixture of anatase and rutile, respectively. However, identical pretreatments of similar

samples produced the reverse phase content after the 900°C anneal; i.e., the sample pretreated at 500°C contained a mixture of anatase and rutile and in the compact annealed at 600°C, only rutile was detected.

The enthalpy of the transformation of the as-prepared powder to anatase, determined by differential scanning calorimetry, was dependent upon powder batch and atmosphere, indicating that the as-prepared powder reacts with O_2 on transforming. The transformation enthalpy of experiments performed in flowing air varied from -337 to -367 J/gm and the transformation enthalpy for powders heated in flowing argon ranged form -248 to -300 J/gm.

To Carla, Loren, Maria, Theresa, Kevin, Joseph, Katherine and in Memory of Louis and Dorothy.

Table of Contents

Table of Figures

Table of Tables

ACKNOWLEDGEMENTS

Foremost I would like to acknowledge the advice and guidance that my thesis chairman and research supervisor, Professor Andreas Glaeser, provided throughout the course of this project. I would like to thank him for the time and effort he gave to reading and editing the numerous drafts, versions, sections and pieces of this document. I have learned a lot from him and appreciate his patience and support and I look forward to working with him during my PhD research.

I also thank the other professors of my thesis committee, Clayton Radke and Ronald Gronsky, for their time spent reading and editing this work. Their suggestions were helpful in producing the final version of this thesis.

Life is not all work, and there are several persons who have provided light and humorous repose during the evolution and life of this thesis. They are current and former lab mates, Tony Tomsia, Harold Ackler, Jim Powers, Annabel Nickles, Rich Hashimoto, James Stolken, Mark Locatelli, Ken Johnson, Ellice Luh, Juergen Roedel, and Craig Carter. I give special thanks to Tony Tomsia for the extensive use of his computer for word processing and for performing computations. His generosity and good spirit were always appreciated.

I would also like to thank my family. My parents have always supported and encouraged my academic and scientific interests and for that I am truly grateful. As a special matter I would like to acknowledge the friendship of my brother, Kevin, a fellow Cal student. The time we spent playing cards, basketball, pool and especially our Tuesday-Thursday

water polo matches were especially helpful in keeping an even balance between academics and recreation in my life. I treasure all the hours we spent together here. Good luck as you graduate.

My sincerest thanks go to my wife, Carla. I thank her for her patience in seeing me through this work. Her love encouraged me to succeed and her spirit gave me life when all seemed hopeless.

The author acknowledges the support of the U.S. Department of Energy under Contract Number DE-AC03-76SF00098.

1 INTRODUCTION

In recent years, interest in the synthesis of ceramic powders through liquid chemistry[79-93] has increased. In particular, several metal oxides and metal oxide systems have been produced by the hydrolysis of metal alkoxides and double metal alkoxide solutions[79-93]. Ceramic powders produced by chemical means provide several advantages. Chemical homogeneity may be improved by using co-precipitation techniques for multi-component systems (e.g., barium titanate[82,87] has been synthesized by the simultaneous hydrolytic decomposition of barium bis isopropoxide and titanium tetrakis tertiary amyloxide[87]). Components may be mixed in solution so that the distinct metal ions are mixed at the nanometer scale instead of micron scale as is expected using classical techniques of powder grinding and mixing. Control of particle size and distribution is possible by controlling reaction temperature and reagent concentrations, (e.g., the work done by Barringer[70] on synthesizing titanium dioxide demonstrates control of particle size with reagent concentration). Powder morphology can be controlled by adjusting reagent conditions, pH, temperature as well as through the use of chemical additives. For example, investigators have been able to synthesize hematite particles which are spherical[90], cubic[92,93], spindle-type[91], or have other shapes[90], by controlling these variables. Purity of the resulting powders may be controlled. The purity of chemically derived powders depends on reagent purity and any impurities which may enter the system during handling. In the present study, titanium dioxide was synthesized by the hydrolysis of titanium tetraethoxide.

These powder production methods are relatively new for producing ceramic powders (post WW II)[79]. For the last 40 years, TiO_2 has been commercially produced using the sulfate-process and the chloride-process. The end product has the tetragonal anatase structure. In contrast, for TiO_2 produced by the hydrolysis of titanium tetraethoxide, atomic ordering is indicated in electron diffraction patterns; however the data does not identify the phase as either anatase or rutile. Thus, one expects these powders and "conventional" titania powders to behave differently on heating.

Edelson showed that the microstructural development of alkoxide-derived titania powders may be influenced by heating at temperatures which are low when compared to the normal sintering temperatures of titania[60]. After nominally identical annealing treatments in an HCl atmosphere (to accelerate coarsening phenomena) both a fine-grained structure with a narrow size distribution and grains nearly twenty times larger than the surrounding grains were observed. These differences were attributed to differences in low temperature thermal history, and its effects on the crystallization behavior and polymorphic transformation behavior of the TiO_2 used. A good discussion on the relationship between transformation kinetics and grain growth kinetics and how they may relate to microstructural evolution (in particular, grain size and grain size distributions in annealed compacts of particles which are actually agglomerates of fine units) may be found in Reference 69.

Two recent papers have shown that there is interest in producing ethoxide-derived TiO_2 on a large scale[38,57]. Production on a large scale implies that there is interest or will be interest in using this powder commercially (most likely in the electronics industry where the quantities used are relatively small compared to the titania used in, for example, the paint pigment and paper industry). The benefits would be a product of high purity, depending mostly on reagent purity and handling techniques, and a reduced firing temperature which can in turn broaden the range of materials that can be co-fired with TiO_2. As part of the process of transforming the powder to a useful product the green compact will eventually need to be thermally treated. One expects the performance of the final product will depend on grain size, phase content, chemical homogeneity, and microstructure, and thus, it is important to characterize the response of this powder to thermal treatment.

This research focuses specifically on determining the effects of low-temperature anneals on the microstructural evolution in ethoxide-derived TiO_2 compacts, and on studying the crystallization and phase transformation characteristics of this powder. Those

characteristics of ethoxide-derived TiO_2, which differentiate it from TiO_2 produced by the sulphate-process or chloride-process, may also be found in other alkoxide-derived powders, and thus, the results of this study may have broader applicability.

2 LITERATURE REVIEW .

TiO_2 has been the subject of numerous studies including experiments addressing the anatase to rutile transformation[1-24], TiO_2 synthesis by chemical methods[27,35-41,57,70], and the sintering of titanium dioxide under various experimental conditions[25-34]. The present study examines the effects of thermal treatments on the microstructural evolution of ethoxide-derived TiO_2, and therefore it is useful to have an understanding of prior work. The following summarizes the findings on the above topics.

The transformation of anatase to rutile has been researched extensively. Figure 1 shows reported values for the transition temperature for "pure" titania and titania containing additives.

MacKenzie's[11-13] work on the anatase→rutile phase transformation concentrated on differentiating the effects which different cation and anion dopants and reaction atmospheres have on the transformation. The motivation for his work was discrepancies in the literature. He wished to perform a series of experiments under very controlled conditions. In his work he discusses the effects of ionic impurity size and valency and how size and valency may possibly affect the transformation. He postulated that cations which enter substitutionally into the anatase lattice and which had a lower valency than Ti^{4+}, increased the concentration of anion vacancies, which, consequently, is assumed to facilitate the transformation. Interstitial impurities were assumed to hinder the transformation. The transformation temperature could be reduced by as much as 200°C depending on the impurity. MacKenzie also performed experiments to determine the effect of impurities on the activation energy of the transformation. Impurity additions increased the activation energy. To study the kinetics of the transformation, percent of anatase converted versus time data were fit to a contracting spherical interface model (he found that other kinetic models, in particular first order and nucleation and crystal-growth fit the data equally well). For the conversion of "pure" anatase, the contracting spherical interface model yields an activation energy of

468 kJ/mol. Similarly, Czanderna et al.[3] studied the conversion of "spectroscopically pure" anatase to rutile and fit their data to a second order rate law. The calculated activation energy was ≈418 kJ/mol.

Iida and Ozaki[7] focussed on the role which minor additives, annealing atmosphere and preparation method had on the anatase to rutile transformation and on the grain growth of TiO_2. Probably the most revealing of their studies concerned the effects of TiO_2 preparation techniques on the transformation of anatase to rutile. They prepared TiO_2 by decomposition of ammonium titanium sulfate, titanium oxalate and titanium hydroxide (the oxalate and hydroxide were derived from the ammonium titanium sulfate, and the hydroxide was prepared by three different techniques). The transformation to rutile varied with preparation method, which indicates that the differences may be related to residual impurities. Although it is not mentioned in their paper, the data appear to show a correlation between anatase grain size and conversion to rutile. Their data show that the TiO_2 which had larger grain sizes after heating at 900°C for 3 h converted more readily to rutile. This agrees with the findings of Edelson[69] and is also consistent with earlier observations by Mackenzie[11]. They also found that reducing atmospheres promote the transformation. Decomposition of titanium hydroxide in an atmosphere of flowing air resulted in 70% conversion to rutile whereas an atmosphere of static air resulted in 48% conversion to rutile. They concluded that the difference may be due to the more rapid removal of H_2O from the decomposition of titanium hydroxide in the flowing air. In contrast, MacKenzie proposed that H_2O promoted the transformation by facilitating bond rupture through the formation of $Ti(OH)^{3+}$ ionic species which readily diffused along grain boundaries. Obviously more investigation is required.

Shannon and Pask[21] summarized the literature (through 1964) addressing the effects of impurities on the anatase → rutile transformation. Shannon and Pask found that CuO, deposited on the surface of anatase, promoted the transformation reaction for up to 1 wt% CuO, based on total sample weight. (1 wt% of CuO present as a monolayer corresponds to

a particle diameter of ≈0.27 μm. The reference did not state the particle size of the material studied). Similar effects with Fe_2O_3 additions were observed by Heald[5]. Shannon and Pask suggested that impurities initiate a surface reaction which promotes the conversion. Once the anatase surface is completely covered by the impurity, additional amounts should have little effect on the transformation. The weight percent at which further additions of the impurity had no effect would represent a limiting amount of the transformation promoting additive. To test this hypothesis one could determine the limiting weight percent of CuO for several anatase samples with different specific surface areas. The limiting weight percent should increase with specific surface area.

The formation of other Ti-O phases at the surface, for example Magnelli phases, or the formation of other phases through reaction of the anatase with added impurity metals, may act as nucleating sites for rutile[21]. Using single crystals of anatase, Shannon and Pask[22] studied the transformation to rutile and determined the reaction initiated on the anatase surface and that the reaction was topotactical. The {112} pseudo-closed-packed planes of oxygen in anatase were retained as the {100} pseudo-closed-packed planes in rutile. Similarly, Cimino et al.[2] (1980) concluded that ReO_2 particles (produced by the decomposition of NH_4ReO_4 in an inert atmosphere < 400°C) act as nuclei for the anatase → rutile transformation.

Besides the naturally occurring TiO_2 phases, rutile, anatase, and brookite, investigators have produced another phase of TiO_2 by application of high pressure at high temperatures. The new phase of TiO_2 (known as TiO_2 II) has the α-PbO_2 structure and was found to be stable at atmospheric pressure up to 340°C. The pressure-temperature studies of Dachille et al.[4] indicated pressure-temperature boundaries for which the transformations anatase → TiO_2 II, brookite → TiO_2 II and TiO_2 II → rutile occur. However their inability to reverse the reactions leads one to suspect that anatase, brookite, and TiO_2 II are all metastable with respect to rutile at atmospheric pressure (Jameison et al.[8]). In fact, no study

was found for which rutile converted to anatase or brookite, however, at high pressures (>150 kbars) and temperatures below 340°C Linde[10] found that polycrystalline rutile samples converted to the TiO_2 II α-PbO_2 structure.

Several past studies have been concerned with the sintering of rutile. Table 1 summarizes the findings. Compare the results of O'Bryan et al.[31] and Grotyohann et al.[29] presented in Table 1. For seemingly identical experiments, neck growth rates are significantly different. After the same sintering time, the neck diameter to particle diameter ratio on the larger particles (1000 μm dia.) was twice that on the smaller particles (78 μm dia.). From the scaling laws of Herring one would predict that the larger particles would require more time for sintering to a comparable geometry (neck diameter to particle diameter ratio); however, in OBryan's work the time was shorter. The reason for the discrepancy is not known. However, it may be related to the sample purity. From the graph (Figure 1) and discussion on reported transformation temperatures it is clear that impurities (even in small quantities) affect the transformation of anatase to rutile. The phase transformation proceeds by an activated process which may be related to the diffusion of TiO_2 to the neck region; i.e., both processes may depend on, for example, O^{2-} vacancy concentration which in turn may be strongly dependent on impurity concentrations.

In this study, temperature activated shrinkage processes (e.g., sintering and phase transformations) within ethoxide-derived TiO_2 compacts were studied using constant heating rate dilatometry techniques. Activation energies were extracted assuming volume and boundary diffusion models.

Several techniques (besides the chloride and sulfate-processes which combined produce ≈2.8 million metric tons per year of TiO_2) for preparing TiO_2 have been studied. Czanderna[41] (1957) describes a procedure whereby "spectroscopically pure" TiO_2 may be prepared by dissolving silica-free titanium metal in an ammonicial solution of 90% H_2O_2.

Year	Reference	Experiment	Particle Size μm	Diffusion Mechanism	ΔH $\frac{kcal}{mole}$	Atm.	T °C	Comments
1962	33	Sphere to plate	1000	Vol. Diff. n=5		1μm vacuum	1200 - 1275	Isothermal Experiments
1964	29	Sphere to sphere	75	Evap-Cond		air	1300	x/a = 0.2 after 1000 min
	"	"	53	"		"	1350	
	"	"	75			N_2	1300	Sintering occurred slower in N_2
	"	"	53			"	1350	
1966	31	Sphere to sphere	1000	Surf. Diff. $\left(\frac{x}{a}\right)^n = kt$	68±5	air	1100 - 1350	Temp.= 1300°C x/a = 0.4 after 1000 min
	"	"	"	Surf. Diff. n=7	"	$\frac{P(H_2)}{P(H_2O)} = 10$	900 - 1050	x/a < 0.08
				Unknown n=2	"	"	"	x/a > 0.08
1967	26	Compact shrinkage	0.35 ±0.05	Grain boundary diffusion	76.9 ±2.5	Air	700 - 1130	Isothermal Experiments
1987	32	Powder compact coarsening	0.2	Evap-Cond.		HCl	1200	Isothermal Experiments
1983	25	Compacts of hydrolyzed $Ti([OCH(CH_3)_2]_4$	0.04	N/I	N/I	Air		Compacts sintered to 99% density at T < 900°C
1983	70	Compacts of hydrolyzed $Ti(OC_2H_5)_4$	0.35	Vol. Diff. during intermediate stage	72	Air	1060, 1100, and 1160	Isothermal dilatometry
"	"	"	"		64.9 ±5			Constant heating rate dilatometry
1986	28,69	"	"	N/I	N/I	Air	300 - 1200	Constant heating rate dilatometry[1]

N/I Not investigated

[1]Shrinkage of compacts investigated throughout heating range. Identified observed dilation with specific mechanisms exhibiting shrinkage; e.g. phase transformations, excess reagent combustion, water removal, sintering etc.

Table 1. Summary of TiO_2 sintering studies.

Drying of the peroxide resulted in titania gel which transformed into anatase crystals ≈3 mm on an edge. Suyama and Kato[36] (1976) studied the reaction

$$nTiCl_{4\,(g)} + nO_{2(g)} \rightarrow 2nCl_{2(g)} + nTiO_{2(s)}$$

at high temperature (T > 850°C) and under several experimental conditions of reaction temperature, oxygen concentration and titanium tetrachloride concentration. They also investigated the effects which certain additives have on the formation of titania through this reaction[35] (1985). Komarneni et al.[39] (1985) have shown that TiO_2 gels (clear yellow, aero hydrogels), may be synthesized by vigorously mixing titanium alkoxides in 30% H_2O_2. These gels appeared amorphous by X-ray diffraction and show some diffuse rings by selected area diffraction in the TEM. These rings coincided with some reflections of brookite. On heating to 300°C and 400°C the gels transformed to anatase of particle sizes of ≈10 - 25 nm. Barringer (1983), Edelson (1986), and Jean and Ring[56] (1986) produced titania in small batch processes (≈1 gram of powder per batch) using an alkoxide, specifically titanium tetraethoxide. By hydrolyzing the ethoxide with H_2O, spherical (≈ 0.3μm) titanium dioxide particles of a narrow size distribution (appearing amorphous under X-ray diffraction) were precipitated. These powders were shown to be agglomerates of nanometer sized particles[28]. Edelson, and Ring and Jean controlled particle agglomeration by performing the synthesis in the presence of HPC (hydroxypropyl cellulose) dispersant. This technique was extended by Nahass and Owen[38] (1988) to a continuous-flow reactor using triethylamine as the steric stabilizer instead of HPC. It has also been reported (Seigal et al.[37], 1989) that TiO_2 may be generated by the gas-condensation method; i.e., ultrafine Ti metal is condensed onto a substrate in an inert atmosphere at low temperature and then allowed to oxidize as the ultrafine Ti particles are warmed in an oxygen atmosphere to room temperature.

This short review points out a few characteristics of the TiO_2 system which are worth noting. First, the anatase to rutile transformation is not completely understood and is strongly affected by impurities. In this study, in order to limit problems associated with impurities, contamination was kept to a minimum by using high purity reagents during the synthesis

of the powder. Secondly, the review on sintering of TiO_2 shows that the sintering mechanisms vary and are not completely defined. Therefore the sintering of ethoxide-derived TiO_2 should be and is considered in this work. And thirdly, it is apparent that the titania preparation techniques affect microstructural evolution during heat treatment and therefore should be considered when interpreting the present results.

3 EXPERIMENTAL PROCEDURES

3.1 Powder Synthesis

Titania was chemically synthesized in a glovebox[¢] containing an N_2 atmosphere dried by Drierite®[f] desiccant. Anhydrous ethanol, filtered through 0.2 μm filter membranes[£], was used as the reaction medium (bulk solution within which synthesis was carried out). Reagent concentrations, based on the total solution volume, were 0.15M titanium tetraethoxide[#], 0.45M H_2O[a], and 0.005 g HPC (hydroxypropyl cellulose, molecular weight 100,000) per cm^3 of total solution. These concentrations duplicate those used by Edelson[28]; they provide monodispersed, unagglomerated powders with a yield > 50% based on the complete reaction of the titanium tetraethoxide[27,28,57].

For some batches a stock solution was used; i.e., a solution containing H_2O, HPC, and filtered ethanol in the correct proportions and of twice the necessary concentrations was made and kept in a polyethylene bottle in the glovebox. At the time of synthesis, titanium tetraethoxide and filtered ethanol were mixed, and then quickly added to an equal volume of the stock solution being stirred with a Teflon® magnetic stirring bar (300-500 rpm) in a polypropylene reaction beaker. Mixing continued for only 2-4 more seconds. TiO_2 precipitated within 7 to 9 s after mixing was stopped.

For several batches, the titanium tetraethoxide was added to the anhydrous ethyl alcohol inside the glovebox but the precipitation reaction was performed outside of the glovebox . One of these batches was made with a water concentration of 0.75M with no HPC added, and an additional batch was made with 0.75M water and 0.342×10^{-3} g HPC per cc of total solution (usually 200 ml). Powders will be denoted by their preparation as follows:

[¢]Labconco Model No. 50004
[f] W. A. Hammond Drierite Company, Xenia, Ohio
[£]Gelman Sciences Inc., Prod. No. 64814, TMC-200, Lot No. 4174055
[#]Aldrich Chemical Company lot numbers 07213HP and 04011LT
[a]The water was distilled and purified to 18.2 MΩ-cm by a Barnsted still model no. LR20344 and water purifier filter system part no. 16508

> Atmosphere/[$Ti(OC_2H_5)_4$]/[H_2O]/[HPC]/C,V, or S, where atmosphere is either dry N_2 or Air;[$Ti(OC_2H_5)_4$] and [H_2O] are quoted as Molarity × 100 and [HPC] is 1000 × grams of HPC per cc of total solution. C stands for centrifugally settled powders; V stands for vacuum-filtered reagents; S indicates that stock solutions were used. For example, a powder batch identified as N_2/15/45/5/S indicates that the powder was synthesized in a dry nitrogen atmosphere, with concentrations of titanium tetraethoxide, water and HPC equal to 0.15 M,0.45 M, and 0.005 g of HPC per cm^3 solution respectively, and was made from a stock solution containing the H_2O and HPC.

These procedures differ from the previously reported synthesis techniques [27,28,57] in that the titanium tetraethoxide solution and HPC solution were not always filtered. Vacuum filtering HPC solutions is extremely difficult (see Section 4.1) and attempts to do so were eventually abandoned.

The amount of TiO_2 synthesized in each batch was not recorded because it was desirable to reduce handling. Because the amount of powder produced in each batch was small, different experiments had to be performed with different batches of powder. Therefore batch to batch variations among experiments could not be eliminated, and this should be kept in mind.

3.2 Powder Wash and Dispersal

Newly prepared powder was allowed to equilibrate in the glovebox for approximately 10 min. After this period, the wash and centrifugal classification procedure began. The procedure duplicated that of Edelson[69][e] with the following modification: some batches of powder were dispersed[f] in basic NH_4OH solution (pH ≈ 10.5 before dispersion), and then the pH was adjusted by adding more NH_4OH to the suspension followed by redispersal. This process was continued until the pH remained near 10.5 after dispersion (suspension pH was estimated by using pH test paper, Micro Essential Laboratories Inc.).

---

[e]Coarse particles in the suspension were settled, the supernatant was removed, and then the fines in the supernatant were redispersed in an H_2O + NH_3OH solution with a pH ≈ 10.5. These wash steps were repeated at least four times.

[f]Heat Systems-Ultrasonics, Inc., Model No. W-375, equipped with a one half inch sapphire tipped horn which was used to prevent titanium contamination from standard titanium horns. The suspensions were usually dispersed at 590 to 70% of full scale for 2 to 3 min.

For powder prepared outside the glovebox, no wash procedure was followed[57]. These powders were centrifuged at 3600 rpm (equivalent to an acceleration of ≈25,000 and ≈17,000 m/sec/sec at the bottom and middle of the centrifuge tube respectively) for 3 minutes to remove coarse material. This settled material was discarded, and the fines in the remaining supernatant were settled in the ethyl alcohol at 1200 - 1500 rpm (equivalent to an acceleration of ≈3500 and ≈2400 m/sec/sec at the bottom and middle of the centrifuge tube respectively) for 24 h. These powders were then dried under 8.47×10^4 Pa (25" Hg) vacuum at room temperature.

3.3 Compact Formation; Settling and Drying

The following procedures apply to the powders synthesized within the glovebox.

In the final dispersion step, the nominal solids concentration was adjusted to be between 10 and 40 volume percent. Compacts to be used in dilatometer studies were settled in covered flat-bottomed Teflon® centrifuge tubes (fashioned out of 3/4" dia. rods). Those used in sintering studies were settled in covered polycarbonate centrifuge tubes. The centrifuge speed was approximately 800 rpm (equivalent to ≈1200 and ≈800 m/sec/sec at the bottom and middle of the centrifuge tube respectively) and settling lasted over 24 h.

After settling the powder, the resulting pellets were dried. To speed drying, the supernatant was carefully removed with a pipette until it could no longer be removed without disturbing the settled powder. The compacts were then dried in air at room temperature for several days followed by drying at 60°C for several days in a vacuum of ≈ 6.7×10^4 Pa (20" Hg).

3.4 Heat Treatments

The experiments of Edelson[60] show that low-temperature history may affect the microstructural development of alkoxide-derived titania compacts. To study the relationship between thermal history and microstructural development, experiments were performed with extremes in heating rates and differences in low-temperature heat treatment.

3.4.1 High Heating Rate

Samples used in TEM experiments were heated rapidly. The furnace[Δ] and an alumina crucible were preheated to the desired temperature (ranging from 400°C to 825°C). When the sample was loaded, the preheated crucible was removed from the furnace to facilitate loading, and then reinserted into the funace. The furnace atmosphere was still air. These samples came from a single batch of powder N_2/15/45/5/CV, Batch 3 (See Section 3.1 for nomenclature).

3.4.2 Low Heating Rate

Powder compacts from one batch were dried at 140°C under 25" Hg vacuum for 136 h and then heated in air[ΔΔ] up to 1000°C. Compacts were removed at specific temperatures during the heating ramp. Starting at 140°C, the furnace set point was increased to the next removal temperature every 20 to 30 min. See Figure 2 for a temperature profile during the experiment. Samples were removed from the furnace at the following temperatures: 140, 200, 275, 300, 320, 335, 350, 400, 450, 500, 550, 600, 650, 700, 750, and 1000°C. The compacts were allowed to soak at 400°C for ≈110 min, 800°C for ≈8 h and 1000°C for 2 h. X-ray and SEM techniques were then used to characterize compact grain size and phase content.

3.4.3 Low-Temperature Pretreatment

Experiments were performed to assess the effect of low-temperature preheating on sintering. Compacts of N_2/15/45/5/S powder (Batch 24) were used for these experiments. The compacts came from a single batch and were broken into 30 to 40 pieces approximately 9 mm^3 each. In order to avoid disintegration during annealing, the samples had to be slowly heated to 400°C to remove water and ammonium hydroxide, and to burn off unreacted reagents. The heating schedule followed was close to 1°C/min up to 200°C under an initial vacuum of 6.7×10^4 Pa (20" Hg, Precision Vacuum Oven, CGA Corporation , Model #19).

[Δ] Thermolyne Model No. 30400, accuracy ±1°C.
[ΔΔ] ibid.

During this segment, water and ammonia were removed as evidenced by the aroma of NH_3 over the crucible and condensation on the furnace window. From 200 to 330°C the compacts were heated in air; the furnace's (Thermolyne #30400) set point was increased by 10°C every 5 min. This range corresponds to decomposition of the HPC and initiation of crystallization to anatase. The next segment consisted of soaking the compacts at 337°C for 9 h. This treatment was necessary to avoid extensive cracking and crumbling of the compacts as crystallization to anatase was slow enough at this temperature. Lastly, the set point was increased 5°C every 5 min until 400°C was reached, after which the samples were removed from the furnace and stored in a capped glass vial. The compacts could now be introduced into a hot furnace without disintegrating.

These thermally conditioned compacts were divided into four groups of five or six samples in each group, and preannealed for 2 h at either 400, 500, 600, or 700°C. All compacts heated at one temperature were heated simultaneously. Subsequent anneals of the preannealed compacts were performed at either 800, 900, 1000, or 1100°C. Again, all compacts annealed at one temperature were annealed simultaneously. Thus, each sample was subjected to one 2 h preanneal at either 400, 500, 600, or 700°C and one 1 h high-temperature anneal at either 800, 900, 1000, or 1100°C. Samples which have undergone such a treatment will be denoted as follows: two hour pretreatment temperature/one hour high-temperature anneal. For example, a sample identified as 400/900 implies that the sample was pretreated for two hours at 400°C and the annealed at 900°C for one hour. The designation, 500/None, implies that the sample underwent a two hour 500°C pretreatment only.

Top surface micrographs, as well as some fracture surface micrographs, were recorded and phase content was analyzed by X-ray diffraction.

3.5 Differential Scanning Calorimetry (DSC)

As the compacts are heated, several reactions occur which result in sample shrinkage. Many of the mechanisms have been outlined before, e.g., removal of reagents and

polymorphic phase transformations[28,69]. Knowing the sign and magnitude of the heat of reaction for these processes will aid in deciphering when each reaction occurs. This information was obtained from a differential scanning calorimeter and when analyzed in conjunction with dilatometry data, one may interpret the observed reactions with greater confidence.

Results of the heating rate experiments indicate that the characteristics of the anatase to rutile transformation may depend on heating rate. In order to study the effect of heating rate on this reaction, experiments were performed within the range of heating rates 4 - 500°C/min (500°C/min was the calorimeter's limit).

Powder from several batches[¶] was analyzed with a PERKIN ELMER 7 SERIES differential scanning calorimeter. The main component of the calorimeter was composed of two chambers. An empty sample pan was placed in the right chamber; an identical pan containing a sample (a typical sample size was on the order of 5 to 15 mg of powder) was placed in the left chamber. During an experimental run, both chambers are heated and cooled such that they followed the desired heating schedule (temperature profile). The difference between the power input to each chamber was recorded as a function of temperature and time. Because the pans were nearly identical in shape and mass, the power difference is assumed to be due entirely to the presence of the powder in the left chamber.

Samples were heated in standard aluminum, carbon and gold pans at 4, 10, 20, 40, 50, 100, 200, 300, 400, and 500°C per minute within the range 30 to 725°C. Some powders were preheated in air at 200, 250 and 450°C for 2 to 4.5 h before being placed in the calorimeter. A schedule indicating the combinations of heating rate, temperature range, powder batch, atmosphere, and pretreatment studied is listed in Table 16 of Appendix 2. In order to evaluate the accuracy of the measurements, most runs were performed at least twice. Sample weight loss was also recorded. Baseline measurements (calorimeter output with

[¶] Air/15/75/5 (Batch 9), N_2/15/75/0/C (Batch 13), N_2/15/75/0.34/C (Batch 14), N_2/15/45/5/SC (Batch 16), and N_2/15/45/5/SC (Batch 18). See the section on powder synthesis for a description of the nomenclature.

just empty pans in each chamber) were recorded and subtracted from most of the experimental runs. Baselines had to be redetermined when sample pans (carbon, gold, or aluminum) or heating profiles were changed.

3.6 Dilatometry

As stated previously, several reactions (e.g., the anatase → rutile transformation, H_2O loss, sintering, and organic material burn-off) occur when alkoxide-derived titania is heated. These reactions result in sample shrinkage which may be measured in a dilatometer[28]. That is, one may associate these thermally activated changes in the pellet with the features of the dilatometer curve. As a consequence, if one transforms the powder to anatase prior to inserting it in the dilatometer, one expects the curve's peak due to the as-prepared powder transforming to anatase to disappear. By measuring sample dilation one may quantify three aspects of the reactions: 1) when it initiated, 2) when the reaction ceased, and 3) the reaction's contribution to the total sample shrinkage. With this in mind the following dilatometry experiments were performed.

Centrifuged compacts of as-prepared and hydrothermally treated (to convert to anatase) powders were used in dilatometry runs. Hydrothermally treated powders were powders heated in boiling water of pH initially greater than 10 (necessary to stabilize the suspension against coagulation) for 24 h (this treatment has been shown to transform the as-prepared powder to anatase, Reference 69). During the hydrothermal treatment, a condenser was placed on top of the heated flask to prevent loss of liquid. The suspension of hydrothermally treated powder was then redispersed in a cell disrupter, and a compact formed as described earlier, Section 3.3 Compact Formation; Settling and Drying. The centrifuged pellets were cut into 3 or 4 pieces along the settling direction. They were generally 3 to 6 mm in length with a triangular cross sectional area near 5 mm^2.

Die pressed compacts of ground powders thermally pretreated in air at 250°C, or 400°C were also used in dilatometry experiments.

All samples were heated between platinum foil disks over platinum foil in an alumina sample holder. The atmosphere was ambient and the instrument used was a Harrop Model TDA-H1-PP6 dilatometer. Because the dilatometer furnace was maintained at an initial temperature of 300°C the samples were slowly introduced into the furnace over a period of 1 to 2 h. Once at 300°C, the compacts were heated to 400°C at 1°C/min (a soak period, lasting over 20 min at 335°C, was employed for compacts of powders not thermally pretreated). From 400°C to the maximum temperature (at least 1000°C) the compacts were heated at 4°C per minute. To follow the length and temperature variation of the compact, the output from the dilatometer's LVDT and the sample thermocouple were automatically read and stored in a computer approximately every 15 to 20 seconds. Data acquisition began at either 300 or 400°C.

Sample identification will be as follows: Powder Batch Number / Pretreatment / Centrifugally settled, (C), or Die Pressed, (DP). For example, if a sample is designated as 17/H/DP then that dilatometry sample was prepared from Batch 17 powder (See Section 3.1 and Section 8.1 for details on powder batches) which was hydrothermally treated in boiling H_2O for 24 h and then pressed into a pellet.

3.7 Ultramicrotomy

3.7.1 Introduction

For TEM studies, ultra-thin (thickness < 150 nm) sample areas which are transparent to electrons are needed. Due to sample geometry, strength, and chemistry, conventional techniques of ion milling and jet polishing for preparing samples for transmission electron microscopy do not work well in preparing a porous ceramic powder compact. Therefore, an alternative technique, used extensively in the biological sciences for preparing specimens for light and electron microscopy, was employed.

The methods adopted were those of ultramicrotomy, a technique whereby ultra-thin sections (5 nm under perfect conditions and 70 nm routinely, using a diamond knife) of a sample may be cut. This allows for TEM viewing of the internal structure of the TiO_2

particles and of the evolution of the contact between adjacent particles. The following is a description of microtoming on a modern microtome. The use of ultramicrotomy to prepare TEM specimens allows for viewing the internal microstructure of the TiO_2 particles (something which had not yet been done in detail) and the neck region between two adjacent particles. Refer to Figures 3-8 for definitions of microtomy terms.

3.7.2 Description of Ultramicrotomy

3.7.2.1 Setup

The specimen, which is generally embedded in an epoxy or acrylic resin, is secured to the microtome arm through a chuck which operates similarly to the chuck on a drill press. The chuck has rotational and angular adjustment capabilities to allow for complete orientation of the specimen block (sample block). An appropriate microtomy knife is locked into the microtome's knife stand (knife holder). The reservoir behind the knife is filled with a fluid, such as water, so that the cut sections may float free from the knife during sectioning. The fluid level is such that the fluid just wets the edge of the knife and is horizontal. An extremely important and meticulous alignment of the knife and specimen block face then follows. This alignment varies from sample to sample and must be performed carefully in order to avoid damaging the knife and specimen when sectioning commences. Once the alignment has been completed, sample sectioning may be started.

3.7.2.2 Sectioning

When the microtome's motor is engaged, its arm cycles up and down. On the microtome used, Sorvall MT 6000, the cutting speed (arm speed) could be adjusted from 0.1 to 10's of mm per second. On the downstroke the specimen block face is brought down onto the knife edge, thus cutting the specimen and producing a section. The section floats on top of the boat fluid. At the bottom of the stroke, the microtome arm retracts a small amount allowing the specimen block to pass the knife edge on the upstroke without touching

it. At the top of the stroke the arm advances an amount set by the operator (the desired section thickness). When this cycle is continuously repeated, sections float off the edge of the knife and form a continuous ribbon. See Figure 6.

3.7.2.3 Retrieving and Coating Sections

Sections are usually collected on a carbon-film-covered TEM grid. They are picked up by lowering the grid onto the section ribbons while holding it parallel to the surface of the knife boat (trough) fluid. The sections on the grid are then dried and carbon coated for TEM observation. Although sectioning may sound simple, the technique requires much experience to produce useable sections and to diagnose and correct problems during cutting when they occur. The importance of the alignment cannot be stressed enough. A change of less than 1° in a setting, for example, knife angle, may mean the difference between success and complete failure in sectioning.

For the interested reader, more information on microtomy may be found in References 73-78.

3.7.2.4 Knife

Before proceeding with a description of the sample preparation, some discussion relating to the cutting edge used is appropriate. The most often used cutting edge for microtomy is a freshly cleaved piece of glass. Special devices exist (for example, the LKB KnifeMaker) for cleaving 1" × 1/4" glass strips to be used as knives. The freshly cleaved glass provides an adequately sharp edge for cutting thin sections of soft tissues, but fails for cutting harder material like bones, teeth, metals and ceramics. For these materials, diamond knives are used (see Figure 4). The diamond knife offers many advantages over the glass knife: it is extremely hard, is very sharp (10's of atoms across at the edge of a brand new knife), can be resharpened, is ready to use, has a long life if treated properly and has precision ground angles. The diamond knife used in this study was manufactured by Micro Engineering, Huntsville Texas and had a 3 mm cutting edge.

3.7.3 Sample Preparation for Ultramicrotomy

3.7.3.1 Ultramicrotomy Sample Preparation: General

Almost every material cut with a microtome requires a unique preparation technique which is developed through a trial and error process that is guided by the findings of other investigators. For most biological materials, one usually embeds the tissue to be microtomed in an epoxy resin (for example, Spur Epoxy Resin), cures the resin according to set heating schedules, and then prepares the blockface for sectioning by shaping it with a single-edged razor blade. Although the size of the block face achieved in this manner is quite large ($\approx$1 mm^2), the softness of the material being cut allows one to cut these larger areas successfully.[Æ]

On the other hand, metals and ceramics are orders of magnitude harder than animal and plant tissues, and therefore, these steps require modification. Preparation of sample blocks for ultramicrotomy requires the embedding of the sample in a suitable resin; i.e., a resin which i) cures to a hardness close to that of the sample's, ii) will not adversely react with the sample, iii) is easy to work with, iv) will adhere to the sample, v) has good cutting characteristics , and vi) has low viscosity for sample penetration. LR White® (London Resin Company) hard acrylic resin was chosen because it fulfilled these requirements.

The one drawback in using this resin is that the recommended curing schedule requires heating at 60°C for 20 to 24 h while excluding oxygen from the surface of the resin. However another curing schedule not requiring oxygen exclusion was found in the literature and tried[75].

3.7.3.2 Embedding

Several embedding techniques were tried. 1) This method is that described by Blake et al.[78]. One bores a shallow hole (1/4" deep × 1/8" diameter) into a 2" piece of 5/16" diameter

[Æ] Specimen preparation is not as simple as it may sound because one must be careful in materials selection to avoid reactions of the resin with the tissue, and reactions between the resin and stains used later on in the preparation for microscopy. Heat effects during resin curing and many other compatibility problems can arise.

Lucite® rod. See Figure 7A. The sample is placed into the 1/8" diameter hole which is then filled with the resin. Curing the resin then proceeds according to Csenscits'[75] recipe, 1 h at 90°C without excluding oxygen. 2) This method is the same as the first except an attempt to exclude oxygen from the surface while curing at 90°C was made by using microscope slide coverslips to cover the resin surface. 3) Vacuum curing was tried. 4) Embedding at 60 and 90°C was tried in BEEM®[9] conical top and bottled neck top embedding capsules (Ted Pella Cat. #'s 130-130-SPC and 130-SPB respectively). See Figure 7B. However, difficulties encountered with the above methods warranted a new embedding technique. In the final method, size 00 gelatin capsules and bottleneck BEEM® capsules were used because of their low oxygen permeability. The bottleneck portion of the BEEM® capsule was removed with a razor blade and placed tip down in the gelatin capsule. The capsule was filled with resin and the sample was dropped into the bottleneck. The gelatin capsule was closed and the resin cured according the manufacturers recommendations, 60°C for 20-24 hours. After curing, the gelatin capsule was easily removed, as well as the tip BEEM® bottleneck capsule, rendering the tip reusable (see Figure 8).

3.7.3.3 Block Face Shaping

3.7.3.3.1 Block Face Shaping: Introduction

Once the sample has been successfully embedded, it is necessary to shape it properly for ultramicrotomy. This means removing resin material to expose the sample and then shaping the exposed sample tip, also known as the block face, to a small trapezoid (See Figure 3). To save on diamond knife lifetime and to achieve ultra-thin sections the block face of hard samples should be made as small as possible.

3.7.3.3.2 Shaping

Four block face shaping methods were tried. 1) Material was trimmed away with a single edge razor blade under a binocular microscope as biologists do. This was tried on

[9] Trademark of Better Equipment for Electron Microscopy, Inc.

the Lucite® embedded samples. 2). The method suggested by Blake et al.[78] was also tested. With this method the material around the sample in the Lucite® rod is removed by a sanding wheel. A specialized jig (described in detail in Reference 78) was used to hold the Lucite® rod at a specific fixed angle to the sanding wheel. The sample was sanded to the proper shape by rotating the rod in the jig and sanding as necessary using 200 grit SiC paper for quick removal of the bulk excess resin and Lucite®. 600 grit paper was used for the final shaping. 3) The lucite rods were held by hand while sanding instead of being held in the jig. 4) The fourth method used, and the one adopted, was rather simple. As a result of embedding in the gelatin enclosed BEEM® capsule tops, the specimens ended up embedded in the resin at the tip of a bottle shaped neck. Therefore, no rough shaping of the specimen block was required (This can be seen by comparing the sample location in Figures 7A and 7B). The block face was accurately shaped under a binocular microscope using a miniature aluminum sanding wheel (covered with 600 grit SiC paper) attached to the shaft of a 1.5 volt hobby motor. No lubricating fluid was used during sanding and the acrylic shavings were removed from the lapping paper with a jet of compressed air. With practice, the block face could be sanded to a trapezoid of less than 25 μm on each side. (See Figure 14)

3.8 Characterization

3.8.1 TEM, SEM, and BET Measurements

Ultramicrotomed samples were viewed in two different transmission electron microscopes, a Phillips 301 and a Phillips 400. The Phillips 301 was mainly used to view areas of ultramicrotomed cross-sections containing several particles while the Phillips 400 was used to obtain microdiffraction patterns of individual TiO_2 grains.

As-prepared powder, powder compacts, and annealed samples were viewed in an ISI DS-130 scanning electron microscope. Because TiO_2 is not a conductor, samples were gold coated for 2 to 2.5 min in a Polaron Instruments Inc. SEM Coating Unit E5100 gold

evaporator to reduce charging during observation. They were placed ≈1.5" from the gold target and the argon beam current was set at 20 ma. In order to see the effect which the gold coating had on surface morphology, some samples were viewed without being coated.

Surface area measurements (Quantachrome QSJR-1) were performed only on as-prepared or dried samples. The single point BET method was employed using an adsorption gas of 30% N_2, 70% He.

3.8.2 X-RAY Diffraction

X-ray scans were performed on a Siemens Diffractometer equipped with a DACO microprocessor and personal computer for diffractometer control and data acquisition. Because sample amount and crystallite size were extremely small, powders to be analyzed were placed into a special holder made out of plexiglass. See Figure 9. Ground powders were packed into the cup of Figure 9A and compacted with a glass slide until the surface was smooth and flush with the top surface of the holder. For samples which could not be ground, a different holder was used. See Figure 9B. The sample to be examined was first polished and then placed on top of a small piece plasticene and pressed down with a glass slide. This ensured that the sample's surface was flush with the holder's top surface.

Samples which were fragile (e.g., samples of as-prepared powder compacts and compacts which had undergone only slight necking during heat treatment and were still extremely porous) were embedded in LR White® hard acrylic resin before being polished. Once embedded a smooth surface could be produced on the sample which could then be used in the diffractometer.

The Scherrer formula:

$$t = \frac{K\lambda}{B\cos\theta}$$

$$B = \sqrt{B_i^2 - B_{ref}^2}$$

t = crystallite thickness,
B_i = measured peak width (FWHM) of the sample in radians,
B_{ref} = measured peak width (FWHM) for instrument broadening,
λ = X-ray wavelength (1.54060 Å),
K = constant between 0.94 (gaussian shaped peak) and 1.0.

θ = Bragg angle.

was used to calculate grain size. The X-ray background intensity was estimated and subtracted from the scans before the full width at half maximum (FWHM) was determined. Standards with large grains were run in order to obtain the necessary data so that instrumental peak width broadening effects could be subtracted from diffraction peak widths.

3.8.3 Chemical Analysis

The powders used in this study were prepared in the same laboratory as Edelson, using the same apparatus and techniques. Therefore, the purity of the powders was assumed to be the same as that quoted in Reference 69.

4 RESULTS AND DISCUSSIONS .

4.1 Observations on Powder Preparation

The literature[28,57,60] states that the ethoxide containing solution and water-HPC containing solution mixed in the powder synthesis, can be filtered through 0.2 μm nominal pore diameter filter membranes prior to mixing. However, in this study, it was extremely difficult, if not impossible, to vacuum filter the solution containing the HPC. To discover the difficulty, filter membranes used for filtering the ethanol-HPC solution were examined in the SEM. Figures 10A and 10B show filter membrane surfaces of unused 0.45 μm nominal pore size filters and of filters which had been used to filter a solution of ethanol and HPC respectively. (Note that the micrograph magnifications are identical.)

The effects of the HPC are quite remarkable. Both the pore density and the average size of the available pores are greatly reduced. This accounts for the observed reduction in the flow of the filtrate with time. The initial filtrate flow (under vacuum) was a steady stream which rapidly slowed to a few drops per second after 15 to 25 ml of solution were filtered. Even HPC-ethanol solutions which had been stirred at room temperature for over 24 h exhibited this behavior. This implies that either the HPC molecular size or, the smallest units into which the HPC dissolves on simple mixing (the solution was mixed using a magnetic stirring rod at at least 500 RPM), are on the order of tenths of microns. Private communications with Edelson revealed that vacuum filtration of the HPC-ethanol solution was abandoned because of this problem. An alternative to vacuum filtration may be pressure filtration. In this study it appears that not filtering the solutions did not harm the experiments. In the current study all the ethanol used (and only the ethanol) was filtered through 0.2 μm membranes.

4.2 As-Prepared Powder Characteristics

At this point it is necessary to define some terms which will be used throughout. The largest "particles" observed in the SEM and TEM will be termed particles or powder particles. TEM observation of ultramicrotomed powder particles show that within the

particles (powder particles) are finer units. These finer units will be generally termed primary particles, primary units or particulates. Thus, the powder particles are agglomerates of primary particles.

Powders used in experiments were prepared under the conditions outlined in Section 3.1. Average particle size was found to vary among batches prepared under nominally identical conditions. The high resolution SEM micrographs in Figures 11 and 12 reveal structural differences in powders prepared with and without HPC dispersant. X-ray diffraction patterns of as-prepared material show no signs of crystallinity, however, electron diffraction patterns of ultramicrotomed, as-prepared powder, display diffuse rings, an observation consistent with short-range atomic ordering.

4.2.1 Powder Characteristics - Influence of Synthesis Technique

Average particle size differed among batches which were supposedly prepared under similar conditions. There are two potential causes for the differences. First, during the synthesis, the stirring of the water-containing and ethoxide-containing solutions that were being mixed lasted for only 3 - 5 seconds, which may have been insufficient to homogenize the solution fully before the onset of polymerization reactions. This being the case, the degree of mixing may have varied from batch to batch and thus the reagent concentrations within the reaction beaker would vary. Barringer[27] showed that particle size was dependent on reagent concentrations. This non-uniformity in reagent concentrations could produce the observed variation in particle size among seemingly identically prepared powders. A second possibility is also related to the experimental procedure. The ethanol-titanium tetraethoxide solution was poured from a beaker into the stirred beaker containing the ethanol-water-HPC solution. When the titanium tetraethoxide was added to ethanol, the solution needed to be mixed by swirling the contents of the beaker. After pouring the contents into the second solution, some ethoxide often remained unmixed in the beaker. This amount varied, and thus, the concentration of the ethoxide during the reaction varied. This could also cause the observed differences in particle size.

4.2.2 Powder Characteristics - General

Table 2 lists the average particle size for as-prepared powder from several batches. Several items are worth noting. Where powders have been settled into a cake and top and bottom surface micrographs are available, bottom surface micrographs show powders with a larger average diameter than do top surface micrographs. This observation is similar to that reported by Jean and Ring[57]. Differential settling rates during compact formation result in a particle size distribution which varies in the direction parallel to the settling axis. This is easy to understand as particles settling according to Stokes law (The particle settling velocity is proportional to the particle radius squared). Note that even for nominally monodispersed powders, as used in the present study, particle size segregation is still expected.

Morphological differences exist between powders prepared with and without HPC as displayed in Figures 11 and 12 respectively. In one case, Figure 11, definite sub-units are visible and the powder particles are seen as agglomerates of these finer sub-units. These sub-units are on the order of 40 nm as measured from the SEM micrograph. In Figure 12 these sub-units appear to be absent. Close inspection of the micrograph shows some fine structure. However, it is not know whether this is a result of the gold coating or representative of the titania. Neither Jean[57] nor Barringer[27,70] report such particle morphologies.

The fine particles (i.e. particulates, sub-units) of Figure 11 were detected in all powders prepared with HPC; however the size of these particulates differed among batches. The differences in the sub-unit sizes (measured from SEM micrographs of seveal batches) did not correlate with the variation in particle (an agglomerate of the sub-units) sizes. Note that these sub-units are not the primary-particles seen in ultramicrotomed powder (TEM) and discussed in Section 4.2.

Previous researchers have examined the crystallinity of the as-prepared powder using standard X-ray diffraction[27,28] and low angle X-ray diffraction[72]. Standard X-ray diffraction techniques provided no indication of crystallinity[27,28] for as-synthesized powder; the current

study produced similar results. However, preliminary low angle X-ray diffraction studies by Moss[72] indicate reflection peaks are produced from as-prepared powder. These peaks do not match those of anatase.

ID#	Description	Particle Diameter nm	Comments
B3	N_2/15/45/0.635/C	381 ± 24	Top Surface
B9	Air/15/75/5	169 ± 19	Settled in ethanol on to microscope stub. Powder not washed.
B17	N_2/15/45/5/SC	321 ± 32	Internal Surface. AKA B17S1
B17	N_2/15/45/5/SC	320 ± 32	24 h hydrothermal treatment
B18	N_2/15/45/5/SC	306 ± 26	Top surface
B18	N_2/15/45/5/SC	365±26	Bottom surface
B19	N_2/15/45/5/SC	277 ± 30	Top Surface
B19	N_2/15/45/5/SC	299 ± 30	Bottom Surface
B24	N_2/15/45/5/SC	255 ± 29	Top Surface
B24	N_2/15/45/5/SC	263 ± 26	Bottom Surface
B26	N_2/15/45/0	501 ± 68	Suspension dried on SEM stub
B27	N_2/15/45/5	272 ± 31	Suspension dried on SEM stub

Table 2 Average powder particle size (i.e. largest units observed). The error quoted is one standard deviation. Powder synthesis variables. Nomenclature: Atmosphere / $[Ti(C_2H_5)_4]$ (Molarity) * 100 / $[H_2O]$ (Molarity) * 100 / [HPC] (gm/cc) * 1000 / S = stock solution used; C=centrifugally classified.

Electron diffraction patterns of ultramicrotomed as-prepared powders (the same powder which showed no crystallinity in standard X-ray diffraction scans), show definite signs of atomic ordering; i.e., very diffuse rings and individual spots (Figure 13). Measurements taken directly off a negative, show the first two rings correspond to lattice spacings of ≈3.6 and ≈2.4 Å (camera constant ≈ 23 Å-mm). The error in these measurements is estimated at ±10% due to the difficulty in measuring the ring diameters. These lattice spacings do not match those of: anatase, any another recorded polymorph (JCPDF) of TiO_2, or any of the Magnelli phases (Ti_nO_{2n-1} n=2...10). Using electron diffraction, Barringer[70]

reported that powders aged for 3 months in water showed signs of crystallinity near the edge (reported as anatase), whereas Edelson[69] reported that the as-prepared powders appear amorphous.

BET surface area measurements were performed on two batches of powder, Batch 3 (N_2/15/45/0.635/CV) and Batch 18 (N_2/15/45/5/CS). These powders had specific surface areas of approximately 210 m^2/g and 360 m^2/g, respectively. This difference exists most likely because of procedural differences experienced during synthesis. Note that the HPC concentrations were different for each batch. If the HPC molecules were to act as nucleating sites, then it is conceivable that for the Batch 18 powder more nuclei would be formed and the resulting powder would have a specific surface area larger than that for Batch 3 powder[f]. This assumes that the yield is the same for each batch. The considerations of Section 4.2.1 may also play an important part in determining the surface area of powders. The titania powders synthesized are agglomerates of ultrafine primary units as discussed by Edelson[69]. The powder nucleation regime during the synthesis is a function of the reagent concentrations. If this nucleation regime varies due to differences in local or overall reagent concentrations, then the nuclei number density will also vary from batch to batch. Thus, after the growth period for the primary particles, the final particulate size (sub-units comprising the agglomerates) will vary.

It should be pointed out that the derivation of the BET adsorption equation assumes that multilayer formation of the adsorbate (N_2) is possible. However, the area around the contact points of sub-units may limit the formation of multilayers and therefore the surface areas calculated with the BET equation should be interpreted with caution. The information gained by studying the adsorption of N_2 on ethoxide-derived titania by determining complete adsorption isotherms would help in interpreting single point BET results.

---

[f]Filtering the Batch 3, HPC containing solution, as well as the lower HPC concentration of the Batch 3 powder, decreases the number density of HPC molecules in solution.

4.3 Ultramicrotomy

4.3.1 Embedding

In the present study, all embedding techniques employed (Section 3.7.3.2), except the last one, proved to be less than 50% effective. Their low effectiveness was the result of two recurring problems, resin cracking and incomplete curing.

Most samples cured at 90°C contained cracks in the resin. The cracks appeared around the sample and often extended to the surface. This resulted in the samples being held loosely in place by the resin, and therefore, the samples had to be discarded. The high failure rate is most likely due to an increase in resin shrinkage rate caused by exceeding the curing temperature recommended by the manufacturer. On many occasions the resin had not been cured to a hardness sufficient to allow for proper sectioning, possibly due to the presence of O_2 during curing. To try to remedy the problem, microscope slide coverslips were placed on top of the Lucite® rods to enclose the resin while it cured. This did not substantially increase the embedding success rate. Vacuum curing was tried, but under a relatively weak vacuum (≈15" Hg, and therefore too high of an oxygen pressure) components of the resin volatilize, and therefore the method was not pursued. BEEM® capsules (See Figure 7B) were found to be permeable to oxygen, and therefore, proper curing could not be achieved using them. Rapid curing also caused severe distortion of these capsules. High temperature embedding at 90°C in BEEM® capsules was also ineffective. The capsules warped and the resin did not cure completely. The problems encountered in the above attempts all result from incorrect curing temperature and atmosphere even though success in using these methods (Csenscits et al.[75]) has been reported. During this study, they were not successful enough to warrant continued use. The final embedding method described, Section 3.7.3.2, using gelatin capsules, was adopted and proved to be over 90% successful.

4.3.2 Block Face Shaping

As stated previously, four methods were used to shape the specimen block faces: i) shaping using a razor blade, ii) sanding away excess material from the sample while holding

the sample in a specialized jig, iii) sanding while hand holding the sample, and finally iv) sanding under a 40 power binocular using a miniature sanding wheel. The method with the greatest success rate was the latter. For details on the difficulties encountered with each method see Appendix 1.

Figure 14 is representative of the block face size which may be obtained with practice. This particular sample is ≈25 μm on a side. When compared to biological samples block faces, which are ordinarily ≈1 mm per side, this is a significant improvement.

4.3.3 Sectioning Results

Figures 15-19 represent typical sections of as-prepared and heat treated titania powders. Micrographs of sections of as-prepared powder and powders which had been heated at or below 400°C (shown in Figures 15, 16, and 20) show that the sections were cut well, i.e., there was very little particle pull out and resin tearing. For the samples annealed at higher temperatures (Figures 17-19,21)sectioning was not as successful. It appears that instead of slicing the particles, the particles cleaved along grain boundaries or else pulled out of the resin. The particle pull out is evidenced by the holes in the resin. Improvement in resin-particle adhesion would improve sectioning, resulting in thinner sections for viewing in the TEM. A product, such as Dow Corning Z-6050 has been suggested as an adhesion aid. It is an organo-functional silane which allows it to react with or to "couple" organic polymers and inorganic surfaces. Also, for the powders heated at 800°C, particle penetration by the resin is necessarily absent due to grain growth and densification of the powder. For this powder, better adhesion is definitely desired.

In some cases it may be desirable to control the sectioning direction. For examples, observations parallel to a specific lattice plane in a single crystal may be necessary. If care is taken it is possible to orient the sample in the block face so that when the block face is shaped the desired surface is exposed. The results of trying to section a compact parallel to the settling direction is displayed in Figure 21. The alignment of the powder particles is more pronounced when the figure is viewed along a diagonal.

4.4 Internal Structure of Titania

Due to the techniques of ultramicrotomy, it was possible to study the internal structure of ethoxide-derived titania. Figures 15 to 19 show the evolution of the internal structure of ethoxide-derived titania powders heated at increasing temperatures. Figure 15 is a cross section of as-prepared powder. (See Figure 13 for the electron diffraction pattern of the as-prepared powder). Close examination of the micrograph reveals features (possibly crystalline material) on the order of 40Å. This size is on the same order of magnitude as the crystal size measured by X-ray line width broadening of powders slowly heated to 400°C. However, it is an order of magnitude smaller than the sub-units seen in SEM micrographs, Figure 11. This may suggest that when the as-prepared powders transform at ≈300 - 400°C, several anatase grains may nucleate within the same particulate (sub-units seen in SEM micrographs). This would account for the smaller grain size seen in the transformed powder. In contrast, the difference in particulate sizes seen in as-prepared powders and the powders heated at 400°C may reflect differences between the as-synthesized powders. Only Batch 3 powders were ultramicrotomed and viewed in the TEM. The X-ray line broadening measurements reflect particulate size in Batch 24 powders. Performing similar experiments using a single batch of powder may clarify this point.

Figures 20A and B and Figures 16A and B are bright field and electron diffraction patterns from Batch 3, (N_2/15/45/0.636/CV), powder which had been hydrothermally treated (Figure 20) and which had been annealed for 15 min in air at 400°C (Figure 16). The diffraction patterns show that both powders are crystalline. Measurements of the diffraction rings show that both anatase and brookite are present. The broad rings in Figure 20B indicate that the crystallites within the hydrothermally treated powders are smaller than the crystallites that produce the sharper rings in Figure 16B. Possibly a longer hydrothermal treatment would result in material with a crystallite size similar to the powder heated at

400°C for 15 min. The smallest units for the 400°C, 15 min sample and the hydrothermally treated sample are ≈60 Å. This crystal size is similar to that found for the untreated powders and shows that very little growth has occurred during the crystallization.

For powders heated at 500°C for 24 h (Figure 17), the crystallite size ranges from 10 nm to 45 nm. This represents nearly a ten fold increase in particle size. A second, continued, anneal at 590°C for 30 min produced little change in the crystallite size range. Accurate measurements of individual crystallites would be necessary to see if the treatment had any effect on the size distribution.

Increasing the second anneal to 650°C for 30 min (Figure 18) resulted in definite grain growth. The maximum grain sizes now are on the order of 170 nm and the smallest crystallites still are present. The smaller grains are most likely in the process of shrinking at the expense of the growth of the larger grains.

Finally, ultramicrotomed powders annealed at 800°C and held for 1 h are shown in Figure 19. The maximum crystallite size is ≈350 nm with an average crystallite size ≈270 nm. The micrograph shows that at this temperature grain growth is rapid enough to cause pore-boundary separation during grain growth. However, because the distance to vacancy sinks, e.g., grain boundaries and free surfaces, is relatively short, it is expected that this internal porosity should decrease with longer anneals.

4.5 Heat Treatments

Initial experiments indicated that the transformation of the as-prepared powder to anatase, rutile, and/or brookite may be heating rate dependent. The results of experiments conducted to determine if such a relationship exists follow.

4.5.1 Crystallization Study: High Heating Rate

Extremely high heating rates were achieved by dropping TiO_2 compacts directly into a preheated crucible and placing the crucible back into the furnace for the required annealing time. Observation of the compact, immediately after it had been placed in the crucible, showed that a reaction occurred after approximately 3-5 seconds. The periphery of the

compact blackened and then a black ring moved toward the center of the sample. This was followed by extreme crumbling of the compact; i.e., the compact broke apart and formed a small pile at the bottom the crucible. The dark ring is most likely associated with the burn-off of organics, whereas the sudden transformation of the as-prepared powder to a crystalline phase is likely one cause of the compact disintegration. The crumbling may also result from the fast desorption of adsorbed gases, specifically, H_2O. If the permeability of the compacts is not sufficiently high to allow for the gas to escape, the internal pressure may become large enough to breakup the compact. The permeability of the compact depends inversely on the square of specific surface area, and thus, is proportional to the square of the particle size. For nanoscale particles, the permeability will be extremely low. A simple calculation shows that the pressure may reach hundreds if not thousands of atmospheres. The moles of adsorbed H_2O may be estimated as follows. Measurements of mass loss in dilatometry samples showed that ≈33% mass loss occured in compacts which were not intentionally dried. A centrifuged compact having a volume of ≈30 mm^3 (3.0×10^{-5} liters) and a mass of 0.1275 g would initially contain 1.17×10^{-3} moles of H_2O assuming that 50% of the mass lost (16.5% of the initial mass) was due to the evolution of H_2O. This is not an unreasonable estimate. Assuming ideal behavior of evaporated H_2O yields an internal pressure of ≈2000 atm. The compacts certainly could not remain intact if they experienced this magnitude of pressure.

Crystallographic results of the high heating rate experiments are presented in Table 3. The three TiO_2 polymorphs anatase, brookite and rutile, were observed to occur in only one batch of rapidly heated powder (Batch 3, N_2/15/45/5/CV, see Section 3.1 for nomenclature). Table 3 shows that the phases present depended on the annealing temperature. As the annealing temperature was increased, the intensities of the anatase and brookite diffraction patterns decreased and the intensity of the rutile diffraction pattern increased. This can be seen in the series of Figures 22A to 22D (TEM diffraction patterns)

Some possibilities exist to explain the behavior observed. For the 400°C anneal, both anatase and brookite are found in the sample. Most likely the initial powder transformed on heating to both anatase and brookite. The possibility that the one of these phases results from the transformation of the other is unlikely; i.e., in another experiment in which the rapidly heated powder sample was held at 400°C for over 24 h, a diffraction pattern similar to the one in Figure 22D in ring intensities and positions resulted. Thus, both phases were stable at 400°C and have probably resulted from the transformation of the original powder.

Anneal Temperature,. and Time	ANATASE	BROOKITE	RUTILE
400°C, 15 min	V ST	ST	none
500°C, 1440 min	V ST	ST	VVW
610°C, 120 min	ST	W	ST
700°C, 45 min	none	none	ST

Table 3. Strength of TEM diffraction pattern rings. The powder is from Batch 3, N_2/15/45/5/CV. The nomenclature is as follows: VW = Very Weak intensity in diffraction pattern, M = Moderate intensity, and ST = strong intensity.

As with the samples rapidly brought to 400°C in air, the powder heated at 500°C for 24 h shows strong anatase and brookite rings in its electron diffraction pattern; however, the diffraction pattern also contains spotty rings associated with rutile (See Figure 22B). The rutile is the product of either the starting powder, anatase and/or brookite transforming into the rutile phase. Annealing powder from the same batch at 500°C for an extended period, perhaps seven days, may clarify the point. At high enough temperatures (greater than 700°C), only rutile appears as seen in Figure 22D.

4.5.2 Crystallization Study: Low Heating Rate

In the low heating rate experiments (Batch 23, N_2/15/45/5/CS) the crystallization of the powder was followed closely. The results of X-ray diffraction studies, which show the phase evolution and particle size evolution within the powder (through X-ray peak width broadening), are summarized in Figure 23 and Table 4.

Removal Temperature, °C	Crystallite Size, Å
350	11
400	22
450	20
500	22
550	25
600	31
650	27
700	34
750	61
1000	91

Table 4. Crystallite size as a function of removal temperature for slow heating crystallization study. See Section 3.4.2 for a description of the experiment. Compacts from Batch 23, N_2/15/45/5/C/S.

There was no significant change in the X-ray diffraction pattern up to 335°C. Figure 23A is the diffraction spectrum of the as-prepared powder after it had been heated to 335°C. The absence of any peaks in the spectrum might lead one to believe that the powder is amorphous after such a treatment, however, electron diffraction patterns show evidence of atomic ordering in the as-synthesized powder. At 350°C, the anatase (101) peak ($2\theta = 25.38°$), and peaks corresponding to other anatase crystallographic planes, appeared. See Figure 23B. The (101) peak's broadness indicates a small particle size (refer to Table 4 for a compilation of the grain size development).

Figures 23C and 23D show the X-ray diffraction spectra for compacts removed at 400 and 750°C. In these spectra there is no conclusive evidence (in the form of noticeable diffraction peaks) that the compact contains brookite or rutile. These phases have not yet appeared at these temperatures as they had in the samples which had been heated rapidly. The absence of brookite may be due directly to the results of slow heating. When the samples are heated slowly, the H_2O present in the compacts evaporates and is mostly gone by 250°C[69,70]. At this temperature the transformation of the as-prepared powder to a crystalline phase has not yet occurred. According to MacKenzie[11-13], residual H_2O in titania produced by the sulfate process may play an important role in determining the transformation kinetics

of the reaction anatase $\rightarrow$rutile. Mackenzie hypothesizes that H_2O reacts with Ti^{4+} and O^{2-} creating charged $Ti^{4+}(OH^-)_n$ species. A similar mechanism may be responsible for the transformation of the as-prepared powder to brookite on rapid heating. During the slow heating, most of the initial water is absent in the compact at the observed transformation temperatures ($T > 335°C$).

To test the above hypothesis regarding the presence of brookite in rapidly heated powders, three compacts, (N_2/15/45/5/SC, Batch 24), were rapidly heated to 400°C and then annealed for 15 min. Before annealing the compacts were prepared as follows: i) as-prepared powder, i.e. no treatment, ii) dried at 200°C, and iii) dried at 200°C and then saturated with water. X-ray diffraction scans showed that all three compacts contained no detectable amounts of brookite or rutile. Therefore, it is not conclusive that residual water affects the transformation of the as-prepared powder. These experiments demonstrate that variations exist among different batches of powders synthesized under nominally identical conditions. Highly controlled laboratory techniques, whereby homogeneous powders among batches may be produced, would aid indetermining the transformation mechanisms occurring.

4.5.3 Effects of Low Temperature Pretreatment

As outlined in Section 3.4.3 each sample in the pretreatment study was subjected to two anneals, an initial anneal at a temperature $\leq 700°C$ (the pretreatment) and a second anneal at temperatures $\geq 800°C$. The intent of these experiments was to assess the effect which the isothermal pretreatments might have on the microstructural evolution of the compacts when annealed at "normal" sintering temperatures of TiO_2. These experiments were motivated by findings of Edelson[60,69]. Figures 24-29 represent mostly fracture surfaces of the samples in this study. Pretreatment temperature increases clockwise and high temperature treatment temperatures increase with each page of figures. The following summarizes the results of the current experiments and discusses their implications.

Previous researchers[28,69] found that top surface micrographs were representative of the internal microstructure of the annealed compacts of ethoxide-derived titania, however this study revealed that internal structure may vary greatly from that seen in top surface images. As an example, compare Figures 24 and 29C. (Top and fracture surface micrographs of sample 600/1100. See Section 3.4.3 for nomenclature.) Therefore, because of the difference in microstructure seen between top and fracture surfaces, both fracture surface and top surface micrographs will be reported and considered in the evaluation of the pretreatment study (only top surface micrographs were available for the samples in Figures 25A,D and 29B,D. In fact, for one sample, the microstructure across a fracture surface was inhomogeneous. See Figures 30A-C. A cause for this inhomogeneity is discussed at the end of this section.

The analysis will begin with an evaluation of the effect of the pretreatment on the compacts used for the experiments. Initial particle structure was determined by electron diffraction (Batch 3 powder, 15/45/5/CV, see Section 4.2 for details) to contain some atomic ordering[§]. Slowly heating the compacts to 400°C, to avoid cracking, resulted in compacts of anatase powder.

The two hour pretreatments resulted in a change of particle (agglomerate) and grain sizes. Particle sizes were determined from SEM micrographs and grain sizes were determined by X-ray line broadening. Results are summarized in Table 5. Except for the sample treated at 400°C for 2 h, measurements from top surface SEM micrographs indicate that particle (agglomerate) size decreases with increasing pretreatment temperature. On the other hand, grain sizes resulting from the X-ray line broadening experiments increase with pretreatment temperature and are approximately five to eleven times smaller than the sizes determined by the SEM images. This supports one of Edelson's conclusions, i.e., that the as-synthesized powders (the spherical agglomerates on the order of 0.35μm) are actually

[§]Atomic ordering (in different batches of as-prepared powders prepared in this lab) has been observed by Simon Moss using low angle X-ray diffraction techniques [72].

agglomerates of finer units. When the powder is heated, the fine particles (which comprise the agglomerate) transform to anatase. The shrinking of the agglomerates is understood as the sintering of the fine particles (crystallites seen in the TEM micrographs of Figure 16 and Figure 20) and the increase in grain size is seen as the coarsening of the fine crystalline units comprising the agglomerates (Cross Reference Section 4.4, TEM of ultramicrotomed particles). Thus, different phenomena are being observed in each measurement.

It is interesting to note that fracture surface micrographs show the opposite trend in particle (agglomerate) size evolution. Unfortunately only fracture surface micrographs from two samples are available. Most likely this is not due to differential settling during the centrifuging step because the powder was classified to produce a monodispersed compact. One possibility is that the atmosphere inside the compacts is near equilibrium. Depending on the surface tension of the crystallites composing the agglomerates, the equilibrium vapor pressure within the compacts may be 50 to 75% greater than the vapor pressure over a surface of zero curvature. Because the compacts were annealed in open crucibles the compact volume near the surface will not be in equilibrium with the atmosphere. The densification processes occur by grain boundary and volume diffusion whereas coarsening may occur through an evaporation-condensation mechanism. Within the compact, coarsening may also proceed and does. (The driving force is the reduction of particle surface area.) However, at the compact surfaces, material is lost beyond the free surface into the crucible and furnace atmosphere and coarsening will not occur (material escapes before condensing). Experiments which maintain an equilibrium atmosphere around the sample during annealing might clarify this point.

	SEM		X-RAY
Pretreatment	Top Surface	Fracture Surface	Polished Surface
As Prepared	255 ± 55	N/A	Some Atomic Order
Slowly Heated to 400°C	232 ± 26	N/A	21
400°C 2 h	200 ± 28	N/A	22
500°C 2 h	230 ± 20	258 ± 28	23
600°C 2 h	210 ± 20	290 ± 43	29
700°C 2 h	200 ± 21	N/A	40

Table 5. Particle size in nanometers from SEM micrographs and X-ray line broadening for TiO_2 (Batch 24 powder, N_2/15/45/5/CS) having undergone the indicated thermal treatments. The 2 h anneals followed slow heating to 400°C.

	SEM
Pretreatment	Grain Size from Top Surface 1100°C annealed samples. (nm)
400°C 2h	939 ± 350
500°C 2h	773 ± 259
600°C 2h	934 ± 299
700°C 2h	757 ± 280

Table 6. Particle size in nanometers from top surface SEM micrographs of Batch 24 powder having undergone the indicated thermal treatments. The 2 h pretreatment anneals followed slow heating to 400°C. The 1 h anneal at 1100°C followed the pretreatment.

Compacts for whieh the final anneal occurred at 1100°C appear in Figures 29A-D. Only top surface micrographs are available for the samples in Figures 29B and 29D. Grain size measurements from top surface micrographs of each sample are listed in Table 6. The grain size measurements show that considerable grain growth has occurred. In fact, grain size has increased by at least one order of magnitude over samples which have only undergone the two hour pretreatment.

Samples for which fracture surface micrographs are available reveal that the internal structures are quite different from those seen in the top surface images. The top surface micrographs would lead one to believe that the compacts had sintered to near theoretical density. However, fracture surfaces show that this is not necessarily the case. Compare

Figure 24 and Figure 29C. Figure 29C reveals the samples internal structure. Grains are facetted and the density is relatively low when compared to the top surface micrographs. The facetting is the result of the elimination of high growth rate planes (kinetic considerations) and/or the development of low energy crystallographic planes. In the present case, this produces coarser grains. The porosity is connected which implies that the sample is within the intermediate stage of sintering.

An interesting observation was the inhomogeneity of the internal structure of the sample pretreated at 400°C for two hours and then annealed at 1100°C for an hour. The Figures 30A-C illustrate the differences. Within the center of the sample, (the darker region in Figure 30C), the microstructure consists of grains which are rounded and smooth and it appears to be much denser than the region containing facetted grains. (This is a probable reason for the difference in contrast between the center of the micrograph and the outside area.) The cause of this inhomogeneity is not known however at least one cause can be proposed. As with the variation in crystallite size (noted above for samples having only undergone pretreatment) being attributable to a non-equilibrium atmosphere, the present effect may also be related to the internal atmosphere. It was noted that the top surface micrographs would lead one to believe that the sample was nearly 100% dense. Being dense the surface then acts as effective seal around the sample imposing a mechanical constraint to further densification. This results in an atmosphere which is both homogeneous and in equilibrium with the internal material. One would then expect that changes occurring by evaporation-condensation mechanisms within the sample may proceed. This may be the case for the observed facetting. Thus, the microstructure is expected to change as the surface porosity disappears. However, this does not explain why the facetting occurs within a ring around the center of the samples.

In samples annealed at 1000°C, facetting is also apparent, yet to a lesser degree than that found in the samples annealed at 1100°C. Within apparatus detection limits, the compacts are rutile. Comparing the top surface micrographs to the fracture surface images,

there appears to be a correlation between top surface density, and facetting and coarsening of grains within the compacts. That is, the denser the top surface is, the coarser the grains are, the more facetted they are and the internal microstructure appears less dense. This being the case, the arguments above may apply here. The difference in microstructure appearing between samples annealed at 1000 and 1100°C are most likely attributable to the different annealing temperatures. Longer anneals at 1000°C should result in highly facetted grains as seen in the 1100°C samples.

The greatest variation in microstructure as a function of pretreatment temperature was seen among samples annealed at 900°C. Not only were grain size and shape different among compacts but also the phase content was different. In fact, the phase content of samples annealed at 900°C varied even between supposedly identical treatments. For example, samples pretreated at 500 and 600°C initially, were composed of pure rutile and a mixture of rutile and anatase, respectively. These experiments were repeated and the opposite configuration was observed; i.e. the sample pretreated at 500°C contained a mixture of anatase and rutile and the compact pretreated at 600°C contained only rutile (note that the differences were seen after the 900°C anneal). For compacts annealed at 900°C for 1 h, sample density also varied as a function of pretreatment. For the compacts pretreated at 400 and 600°C, (Figures 27A and 27C respectively) density, as determined from SEM micrographs of fracture surfaces, is estimated to be greater than 90% of theoretical density and for the other compacts the density is estimated between 60 and 75%. The compacts of greater density had grain sizes and distributions which were more uniform. It is not unexpected that microstructural differences were more pronounced at this annealing temperature. From dilatometry data, it is seen that 900°C is within the observed temperature range for the anatase to rutile transformation. Thus, the dissimilarities may result from the characteristics of the anatase to rutile transformation.

4.6 Dilatometry

4.6.1 Dilatometry: Introduction

The results of the constant heating rate dilatometry experiments are presented in four sections. Each section considers compact dilation within a progressively higher temperature range. The data gathered during an experiment consisted of temperature versus LVDT (Linear Variable Differential Transformer) voltage output. The voltages will not be reported but instead linear contraction ($\Delta L/L_i$, where L_i is the initial sample length) versus temperature will be plotted. This normalization allows the data for each sample to be plotted and compared on the same graph.

Linear contractions may be derived from the voltage readings as follows. The LVDT output is directly proportional to the change in sample length. Thus

$$\Delta L = L(T_2) - L(T_1) = -a \cdot [V(T_2) - V(T_1)] = -a \cdot \Delta V$$

where $L(T_1)$ and $L(T_2)$ is the sample's length at T_1 and T_2 respectively and a is the proportionality constant determined by the following experimental condition[1]:

$$\Delta L_{max} = (L_f - L_i) = -a \cdot \Delta V_{max} < 0$$

or

$$a = -\frac{(L_f - L_i)}{\Delta V_{max}}$$

$$= \frac{(L_i - L_f)}{\Delta V_{max}}$$

$$> 0$$

T = Temperature
L_f = final length of the sample
L_i = initial length of the sample.

One may then write for the length contraction

[1] a is a constant which should not vary significantly from run to run; it is a property of the LVDT

$$\frac{-\Delta L(T)}{L_i} = \frac{L_i - L(T)}{L_i}$$

$$= a \cdot \frac{\Delta V(T)}{L_i}$$

and if the voltage of the LVDT is initially zeroed then

$$\frac{-\Delta L(T)}{L_i} = \frac{a \cdot V(T)}{L_i}$$

It is also of interest to determine the percent change in sample density between two points on the contraction curves. As Figure 31 shows, the dilation curves may be divided into sections corresponding to regions of increased rates of shrinkage. Values of density changes may then be tabulated for each region and then compared to the density change expected for specific reactions (e.g., the anatase to rutile transformation).

The equation for calculating a sample's density change between two temperatures is derived below. Assume a cubic sample of side l_1, mass m_1 and density ρ_1 at temperature T_1 and side l_2, mass m_2 and density ρ_2 at temperature T_2. Then the fractional density change may be written as:

$$\frac{\rho_2 - \rho_1}{\rho_1} = \frac{\frac{m_2}{l_2^3} - \frac{m_1}{l_1^3}}{\frac{m_1}{l_1^3}}$$

$$= \frac{m_2}{m_1}\left(\frac{l_1^3}{l_2^3}\right) - 1$$

Substituting for l_1 and l_2 terms involving the initial length, l_i, and the change in length, $-a\Delta V$, the resulting equation for the fractional change in density involves only measured terms:

$$\frac{\rho_2 - \rho_1}{\rho_1} = \frac{m_2}{m_1}\left(\frac{1 - \frac{a\Delta V(T_1)}{l_i}}{1 - \frac{a\Delta V(T_2)}{l_i}}\right)^3 - 1$$

For calculating percent volume change the following equation is similarly derived:

$$\frac{\Delta V}{V_1} = \frac{V_2 - V_1}{V_1} = \frac{l_2^3 - l_1^3}{l_1^3}$$

$$= \left(\frac{l_2}{l_1}\right)^3 - 1$$

$$= \left(\frac{1 - \frac{a\Delta V(T_2)}{l_i}}{1 - \frac{a\Delta V(T_1)}{l_i}}\right)^3 - 1$$

This derivation assumes that the sample's densification is uniform and isotropic.

4.6.2 Shrinkage Region 1: Initial Crystallization and Organic Removal

Region 1: Room temperature to ≈420°C:

The actual data does not represent as smooth a curve in this region as Figure 31 suggests. In this region the LVDT output of the dilatometer was generally monotonic and had the general shape of Figure 31. However, the position and height of the shrinkage regions varied from sample to sample. The differences within Region 1 are most likely attributable to variations in sample insertion. As stated in Section 3.6, the sample holder was slowly introduced into the 300°C dilatometer furnace over a period of 1 to 2 h. During this period the sample temperature could not be accurately controlled. Similarly, the furnace temperature oscillated about the current setpoint on ramping. These oscillations (+/- 10°C max.) diminished steadily from 400°C until they were necessarily absent at temperatures above 600°C.

The shrinkage in this temperature range results from several processes: transformation of the as-prepared powder to anatase and/or brookite, water loss, evolution of NH_3, decomposition of HPC, and burnoff of unreacted reagents, e.g. ethanol and titanium tetraethoxide. The water loss and burnoff of unreacted reagents have been reported by Edelson[69] and Barringer[70], respectively.

To assess the changes which occur in this temperature range, compacts were heated in air and inspected periodically. The evolution of NH_3 during the initial heating was confirmed by the aroma of ammonia above compacts during drying. NH_3 is first noticed

when the sample temperature is near 110°C and the aroma of NH_3 is generally unnoticeable above 190°C. These temperatures, of course, depend on heating rates and the time intervals between samplings. No effort was made to quantify the amount of NH_3 which was evolved.

Reaction of HPC, and possibly reactant burnoff, during heating was evidenced by a change in color of the compacts, and in some cases, compact cracking. At approximately 175°C, compacts heated in air began to change color from white to light brown with a few black and dark brown spots distributed on the surface of each. As the temperature was increased, the compacts darkened further, becoming dark brown at 220°C. At 275°C, the samples began to lighten indicating that the material was being decomposed and subsequently removed (i.e., burnt). When the furnace temperature had reached 300°C and remained there for over 12 h, the compacts were considerably lighter in color than they were at 275°C, and by the time the furnace reached 375°C (six hours later) the compacts appeared as white as they had before being heated.

To compare these changes with those that occur in a thin covering of HPC on heating, the following experiment was conducted simultaneously. Four cm^3 of a room temperature saturated solution of HPC in ethyl alcohol was evaporated from a 4 cm^3 alumina crucible. This produced a coating of HPC on the inside of the crucible. This crucible was heated adjacent to the one containing the compacts discussed in the previous paragraph. At 175°C a light brown (almost yellow) ring appeared inside the crucible at the intersection of the wall and bottom. Further heating to 220°C resulted in the entire inner surface becoming brown, and at 275°C dark brown. At 360°C the burnt HPC was gone from a ring around the opening of the crucible, and at 375°C, the crucible was almost entirely free of burnt HPC. The temperatures at which these changes occurred correlate well with the changes seen in the compacts. Therefore, the sample color changes in the powder compacts between the temperatures 175°C and 375°C are most likely due to the decomposition and subsequent burn-off of HPC.

Table 7 lists the relative % density changes for three samples within the first region. The relative density change between temperatures T_1 and T_2 is defined as:

$$\frac{\Delta\rho}{\rho_i}\% = \left(\frac{\rho_2 - \rho_1}{\rho_1} \times 100\right),$$

where ρ is the compact density. Because density equals mass/volume, a loss of mass at constant volume would result in a decrease in density. Mass loss, however, is usually accompanied by a corresponding contraction. Therefore, the relationship between mass loss and volume change will dictate the percent change in density. It should be noted that much of the low temperature density change observed is associated with the mass loss of the samples and this significantly affects calculated density changes; e.g., a 30% volume decrease coupled with a 30% mass decrease will result in no density change. Similarly, it is easy to see that a negative density change is also realizable under these circumstances.

The powder for samples D4, D5, and D10 came from Batch 17 (N_2/15/45/5/SC). The powder used for D10 was not subject to hydrothermal treatment. However, the powder used in samples D4 and D5 was boiled for 24 h in H_2O prior to compact formation (this treatment is described in Section 3.6). In the following analysis it is assumed that all of the sample mass loss occurred during the first range of dilation ($T < 420°C$). The % mass loss recorded for samples D4, D5 and D10 were 34, 32, and 31 %, respectively. The small differences in mass loss among these samples cannot account for the large differences in density observed, (See Table 7), between the compacts of hydrothermally pretreated powders (samples D4 and D5) and the compact of untreated powder (sample D10). The differences must result from different dilations.

Assuming that the hydrothermal treatment transformed the powder to anatase, one expects that the density changes observed in the first region for compacts of treated powders to be less than that for compacts of powder which did not receive the hydrothermal treatment (i.e. the dilation due to transformation to the crystalline phase would be absent in treated

Sample	Sample Description	$\frac{\Delta\rho}{\rho_i}$%	Expected $\frac{\Delta\rho}{\rho_i}$% for powder transformation[1]
D4	Powder Batch 17. Placed in 100°C H_2O for 24 h and then centrifugally settled into a compact	14	0
D5	Identical to D4	23	0
D10	Powder Batch 17. Centrifugally settled into a compact. No pretreatment	41	24%

[1]Assumes that the hydrothermal pretreatment for D4 and D5 completely transforms the powder to anatase.

Table 7. Density changes occurring within the first range of shrinkage on the dilatometer plot. Room temperature to 420°C

powders). This is evident when comparing the density changes in samples D4, D5, and D10, which were 14, 23, and 41 % respectively. Here it has been assumed that the initial atomic structure of the powder is the only difference between compacts of hydrothermally pretreated powder and compacts not pretreated. If an initial powder density of 3.1 g/cm^3 for as-prepared powder is assumed, (as measured in Reference 70), then the expected density change due to the transformation of the as-prepared powder to anatase is 24%. The results show that the density change in sample D10 is almost twice the density change expected for the as-prepared to anatase transformation. This indicates that the dilation and mass loss due to other mechanism, e.g., water removal and material burn-off, contribute significantly to the density changes in this temperature range. The density changes observed in D4 and D5 (the hydrothermally pretreated powders) are less than 24% which implies that the density changes due to other mechanisms are less than that due to the crystallization transformation but are nevertheless significant and consistent with the changes observed in D10.

The work of Edelson[69] showed that water loss occurs to at least 360°C and therefore density changes will reflect this. As the transformation in air of the as-prepared powder initiates in the range 300°C to 350°C it is not possible to completely separate the density

changes from the two mechanisms. Experiments which remove the water and react remaining reagents and HPC within the compacts prior to any transformation of the as-prepared powder would better quantify the density changes due to the transformation.

Another consideration is the extent to which the hydrothermal treatment transformed the powder. If the hydrothermally treated powders were completely transformed during the treatment, no sample dilation in this low temperature region would be due to phase changes. However, there is no evidence to indicate that the powders are completely transformed by the 24 h hydrothermal treatment. Therefore, the transformation of as-prepared powder to anatase in the pretreated powders, may still be responsible for some of the low temperature shrinkage.

It is also conceivable that hydrothermal treatment may have another effect on the powder. It may have "washed" the powder by removing or reacting excess reagents, e.g., residual ethanol and unreacted titanium tetraethoxide. Nevertheless, one expects the effect on the sample dilation due to these possible changes to be small when compared to the dilation due to the loss of adsorbed H_2O and the transformation of the as-prepared powder to anatase (and possibly brookite).

Powders for three samples, D15, D18 and D19, were preheated in air at at least 360°C, but not over 400°C, for 3.5 h. The effect of the pretreatments on the powders was to remove water and react any excess reagents as stated before, as well as to transform the as-prepared powders to anatase. This is confirmed in the dilation versus temperature plot in that no dilation occurred at temperatures less than 400°C in compacts formed with these pretreated powders.

4.6.3 Shrinkage Region 2: Anatase Sintering

Region 2: ≈400°C to 700 - 970°C:

The total relative density and volume changes occurring in this region for several compacts is recorded in Table 8. The range of density change spans 19 to 38 %.

Sample	Temperature Range °C	Relative % Density Change	relative % Volume Change
D4/17/Hydro/C	420 - 971	37	-27
D5/17/Hydro/C	420 - 953	33	-25
D8/16/None/C	420 - 759	33	-24
D9/16/None/C	420 - 759	33	-25
D10/17/None/C	420 - 733	33	-25
D13/24/200°C[£]/DP	420 - 808	32	-25
[¶]D15/21/400°C 3.5 h/DP	420 - 821	19	-16
D17/24/200°C[£]/C	420 - 816	33	-25
D18/20/360°C/DP	420 - 827	38	-27

[¶] The data for sample D15 did not show a distinguishable region in this temperature range for intra-agglomerate densification and therefore, the end temperature probably has been under estimated. This suggests that an overlap between shrinkage mechanisms occurred; i.e. intra-agglomerate densification and the anatase to rutile phase transformation occurred simultaneously over a large enough temperature range to conceal the termination of intra-agglomerate densification.

[£] Slowly heated to 200°C to allow for drying without cracking the compact.

Table 8. Temperature range and relative density and volume changes in the shrinkage region just prior to that attributed to the anatase to rutile.

To identify the mechanism(s) contributing to this portion of the total dilation, these results are viewed in light of the results of the crystallization/heating-rate experiments and TEM micrographs of microtomed annealed powders. The crystallization/heating-rate study (Cross Reference Secton 4.5) showed that the transformation of anatase to rutile occurs mostly above 650°C, and in some cases was not yet complete at 1000°C. For most dilatometer samples, the majority of the dilation within the current temperature range occurred below the observed temperature range for the transformation of anatase to rutile. Thus, the observed dilation must have a different cause.

TEM observations of microtomed powders reveal that it is possible to transform the as-prepared powder to rutile by annealing at 700°C for 45 min (direct insertion into the hot zone of the furnace). However, the powder transforms to anatase and/or brookite by annealing at 400°C (Cross Reference 4.5.1, Crystallization Study: High Heating Rate). Similarly, electron diffraction patterns of powder which had been preannealed at 500°C for

[£]Slowly heated to 200°C to allow for drying without cracking the compact.

24 h and subsequently annealed at 590°C show almost completely continuous rings due to anatase and brookite reflections and extremely spotty rings due to rutile reflections. This was the case for Batch 3 (N_2/15/45/0.635/CV) powders. These observations suggest that the transformation from anatase to rutile, even though it may occur within part of the temperature ranges recorded in Table 8, does not proceed to an extent which would contribute significantly to the dilation observed below 590°C. These results reinforce the interpretation that the observed dilation in Region 2 of Figure 31 is not due to the anatase to rutile transformation.

In some Differential Scanning Calorimetry (DSC) experiments (those conducted with Batch 13 powder, N_2/15/75/0/C) a second exothermic reaction occurring between ≈400 and 650°C (the onset and duration of the reaction depended on the heating rate, Section 4.7 Differential Scanning Calorimetry (DSC)). For one sample run at 4°C/min in air, the exothermic peak spanned 427 to 471°C. Even though sample shrinkage may initiate within this temperature range in some of the dilatometry experiments, the region associated with anatase sintering continues over at least 300°C (see Table 8) It then appears that the reaction associated with this peak does not correspond to shrinkage in dilatometer samples. In fact, there is no evidence of this exothermic reaction within the second range of shrinkage in the dilatometer plots. The regions are smooth and show no irregularity in the dilation curve of Figure 31 as would be expected if the reaction contributed significantly to the shrinkage in this temperature range. The expected effect on the dilation curve is depicted in Figure 32. Note that the exothermic peak being discussed was only seen in Batch 13, N_2/15/75/0/C, powder. (See Section 3.1 for a description of powder batch nomenclature.)

As stated by Edelson[69], the likely process contributing to the majority of the shrinkage in this region is intra-agglomerate densification. Considering the TEM micrographs of powders annealed between 400 and 650°C (Figures 16-18), it is apparent that considerable coarsening and intra-particle densification has occurred. In several cases, pores are seen trapped within grains. It is believed that the porosity which they represent is far less than

the original porosity of the agglomerates. This implies that agglomerate densification is occurring within this region. An analysis of this densification follows and will be similar to that of Young and Cutler[34].

The analysis begins with Equation 1 which was derived by Johnson[114]. It describes simultaneous volume and grain boundary diffusion of spherical single crystal particles. In the present analysis it is assumed that the "particles" are the primary, single crystal units which comprise the agglomerates. The "particle" size is therefore on the order of tens of nanometers and not 0.35 μm.

$$\left(\frac{\Delta L}{L_o}\right)^{2.06} d\frac{\frac{\Delta L}{L_o}}{dt} \cong \frac{2.63\gamma\Omega D_v\left(\frac{\Delta L}{L_o}\right)^{1.03}}{kTa^3} + \frac{0.7\gamma\Omega bD_B}{kTa^4} \qquad \text{Eq. 1}$$

Where

$\Delta L = L_o - L$ = the change in length of the specimen.
L_o = the initial length of the specimen.
γ = the surface energy.
Ω = the vacancy volume.
bD_B = the grain-boundary diffusion coefficient (b is the effective grain-boundary width) = $D_{oB}e^{-Q/RT}$.
D_v = the volume diffusion coefficient = $D_{oV}e^{-Q/RT}$.
t = time.
T = absolute temperature.
k = the Boltzman constant.
a = the radius of the particles in the specimen.

Following Young and Cutler, one applies this equation to constant rate of heating experiments by making the substitution T = ct where c is the heating rate. Assuming that only one diffusion mechanism, either volume diffusion or grain boundary diffusion, is operating, Young and Cutler integrated (approximately) and then differentiated the appropriate forms of the above equation resulting in:

$$\frac{d(\Delta L/L_o)}{dT} \cong \left(\frac{2.14\gamma\Omega D_{oB}RT}{ka^4cQ}\right)^{1/3} \cdot \frac{Q}{3RT^2} \cdot \exp\left(-\frac{Q}{3RT}\right) \qquad \text{Boundary} \qquad \text{Eq. 2}$$

$$\frac{d(\Delta L/L_o)}{dT} \cong \left(\frac{5.34\gamma\Omega D_{oV}RT}{ka^3cQ}\right)^{1/2} \cdot \frac{Q}{2RT^2} \cdot \exp\left(-\frac{Q}{2RT}\right) \qquad \text{Volume} \qquad \text{Eq. 3}$$

These derivations rely on some assumptions (e.g., particle size is constant) and it is claimed that "the repeated manipulation (the approximations used combined with the integration and subsequent differentiation) obtains the best possible data processing ability". Their work was done during 1970 and it is assumed that the approximations and equation manipulations were performed to make tedious computations easier because a personal computer was not available to them. From the above equations, linear plots should result when plotting

$$\ln\left(T^{5/3}\frac{d\left(\frac{\Delta L}{L}\right)}{dT}\right) \quad \text{vs} \quad \frac{1}{T} \qquad \textit{Boundary} \qquad \text{Eq. 4}$$

$$\ln\left(T^{3/2}\frac{d\left(\frac{\Delta L}{L}\right)}{dT}\right) \quad \text{vs} \quad \frac{1}{T} \qquad \textit{Volume} \qquad \text{Eq. 5}$$

for grain boundary and volume diffusion. The slopes of the plot will be either -Q/3R for grain boundary diffusion or -Q/2R for volume diffusion densification mechanisms.

In this study, the exact equation (Equation 1 of Young et al.) is used to determine activation energies assuming that grain boundary or volume diffusion contribute to the densification of the agglomerates. Assuming these densification mechanisms are occurring separately, the exact differential equation leads to the following:

$$\ln\left(\left(\frac{\Delta L}{L_o}\right)^{1.03} T\frac{d\frac{\Delta L}{L_o}}{dT}\right) = \ln\left(\frac{2.63\gamma\Omega D_{ov}}{cka^3}\right) - \frac{Q}{R}\cdot\frac{1}{T} \qquad \textit{Volume} \qquad \text{Eq. 6}$$

$$\ln\left(\left(\frac{\Delta L}{L_o}\right)^{2.06} T\frac{d\frac{\Delta L}{L_o}}{dT}\right) = \ln\left(\frac{0.7\gamma\Omega D_{oB}}{cka^4}\right) - \frac{Q}{R}\cdot\frac{1}{T} \qquad \textit{Boundary} \qquad \text{Eq. 7}$$

Plotting the left-hand side of each equation vs 1/T should result in straight lines for which the slope determines the activation energies, Q.

To accomplish the analysis, $\Delta L/L_o$ vs T data were fit to third, fourth, and fifth order polynomials using the method of least squares. Generally, it was judged that third and fourth order polynomials gave more accurate results. This was due to the resolution of the LVDT

and its effect on the data recorded. With the analytical forms for the dilation versus temperature and the derivative of dilation versus temperature available, activation energies could be obtained from the preceding equations. Results are presented in Table 9.

Experiment	Powder/ Pretreatment	Volume Diffusion Calculated Activation Energy kJ/mol	Grain Boundary Diffusion Calculated Activation Energy kJ/mol
D18	15/45/5 360°C 4 h Die pressed	-180	-262
D15	15/45/5 3.5 h 400°C Die pressed	-175	-276
D19	15/45/5 Slowly heated to 400°C Die pressed	-154	-236
D13	15/45/5 Slowly heated to 200°C die pressed	-137	-223
D17	15/45/5 Slowly heated to 200°C Centrifugally settled compact	-124	-170
D9	15/45/5 No thermal pretreatment	-115	-166
D10	15/45/5 No thermal pretreatment	-106	-167

Table 9. Activation energy for anatase sintering assuming boundary diffusion dominates (second column from right) and volume diffusion dominates (far right column).

Note, the range of values for the calculated activation energies in Table 9 for both grain boundary and volume diffusion. The range is much larger than expected. The variations, however, do not appear to be random but instead correlated with the thermal pretreatment. The apparent effect of thermal pretreatment was to consistently increase the activation energy with longer, higher temperature pretreatments.

The analysis applied here assumes that density and grain size among powder compacts are identical. In Equations 6-7, the grain size, a, is assumed constant. The temperatures and temperature range at which these equations were applied were relatively low, i.e., 400°C - 500°C. If significant grain growth occurred within the compacts at these temperatures during the experiments, the predicted change in activation energy would be an apparent decrease in activation energy. (The slope of a plot following Equation 6-7 is negative. An increase in grain size would lower the y-intercept and therefore result in a smaller slope and smaller calculated activation energy). Therefore, samples experiencing more grain growth during anatase sintering should exhibit a greater decrease in the y-intercept and thus a greater decrease in the slope and activation energy than samples which experienced relatively less grain growth during the experiment. This is consistent with observations. Activation energies calculated from samples with little or no pretreatment were consistently smaller than the activation energies calculated from samples which had undergone some pretreatment. The pretreated samples experienced less relative grain growth[8] and therefore the deviation from the expected slope was less for the pretreated samples. As seen in TEM micrographs of ultramicrotomed powders, see Figures 16 and 17, some grain growth probably occurred.

Although not considered by Young and Cutler, the instantaneous rate of densification is also a function of the sample density. A general formula for the densification rate involving sample density explicitly is[131]:

$$\dot{\rho} = A \frac{\exp^{-Q/RT}}{T} \frac{f(\rho)}{d^n} \qquad \text{Eq. 8}$$

where

[8]Grain growth rates decrease with grain size and it is hypothesized that the effect of pretreatment was to increase crystallite grain size.

$$A = \frac{C\gamma V^{2/3}}{R}$$

and

$\dot{\rho}$ = instantaneous densification rate,
d = grain size,
γ = surface energy,
V = the molar volume,
R = gas constant,
T = the absolute temperature,
Q = the activation energy,
$f(\rho)$ = a function only of the density
C = a constant,
A = a material property insensitive to ρ, T, or d,
n = 3 for volume diffusion controlled densification and 4 for boundary diffusion controlled densification.

One way to apply this equation is to perform constant heating rate dilatometry experiments with several heating rates and with samples exhibiting minimal grain growth. One may then compute density versus time from the sample dilation and extract points of constant density from runs with different heating rates[131]. The dilatometer used in this work was limited to a heating rate of 4°C/min and therefore this method could not be applied. Considering the differences in apparent activation energy to be due to the difference in density of the samples (resulting from the different pretreatments and possibly from the powder synthesis) it is apparent that unless the analyses are performed at the same sample densities then different values for the activation energy, Q, will result.

Another observation worth noting is the smaller values calculated for the volume diffusion activation energy compared to the grain boundary diffusion activation energy. The origin of this effect is not understood but may be related to the grain growth of the fine particles within the agglomerates and to neglecting density changes in the calculations.

4.6.4 Shrinkage Region 3: Anatase →Rutile Transformation

Region 3: ≈780°C to 990°C

Relative percent density and percent volume changes which occurred in region 3 are reported in Table 10. If the shrinkage of samples D8 to D17 in the temperature range of Region 3 is attributed to the conversion of anatase to rutile, the temperatures presented in Table 10 are in agreement with the results of the crystallization study, which showed conversion to rutile did not occur at temperatures below 750°C in the slowly heated samples. It is also seen in Table 10 that the temperature corresponding to the completion of the anatase to rutile conversion is ≈990°C. The measured volume and density changes (which would be 9.6% and 10.6% respectively if the dilation in this region had been only the result of the anatase to rutile transformation) ranged from 10% to 17% and from 11% and 21%, respectively. This suggests that intra-agglomerate and/or interagglomerate densification are occurring as well in this region.

Sample	Temperature Range °C	Relative % Density Change	Relative % Volume Change
D8	759 - 968	21%	-17%
D9	759 - 990	20%	-17%
D10	733 - 973	20%	-17%
D13	808 - 990	11%	-10%
D15	821 - 1002	14%	-12%
D17	816 - 1002	15%	-13%

Table 10. Relative density and volume changes the third region of dilation in dilatometer experiments. This range is believed to coincide with the anatase to rutile transformation. A relative density change of 10.6% is associated with this transformation.

However, these results do not correspond to those of Edelson[69]. In his study, conversion to rutile and intra-agglomerate sintering was attributed to the shrinkage which occurred in the temperature range 425 to 800°C. In that study, a 50% relative decrease in volume occurs in this temperature range. In the present study, the relative volume change occurring over the range 420°C to ≈990°C (the temperature range which corresponds to

intra-agglomerate densification and the transformation of anatase to rutile in this study) was on the average 35% (D17, D15, D13, D10, D9, D8, D5). The difference may be due to the sample crumbling mentioned in Reference 69.

4.6.5 Shrinkage Region 4: Sintering of Rutile

The last region of shrinkage is most likely due to interagglomerate sintering. The temperature at which sintering began was taken as the temperature at which the final inflection point occurred in the dilation versus temperature plot . On average interagglomerate sintering began at 990°C and ended near the final temperature of the run. The density changes occurring among the samples due to interagglomerate densification are presented in Table 11.

Sample	Temperature Range °C	Relative % Density Change	Relative % Volume Change
D8 16/H/G	968-1342	33%	-25%
D7 17/H/C	1000-1324	56%	-36%
D9 16/none/G	990-1347	47%	-32%
D10 17/none/C	973-1276	48%	-32%
D13 24/200°C/DP	990-1344	45%	-31%
D15 21/400°C/DP	1002-1340	51%	-34%
D17 24/200°C/C	994-1339	49%	-33%
D18 20/360°C/DP	994-1339	64%	-39%

Table 11. Density changes occurring within the fourth range of dilatometer shrinkage. The most probable cause for the densification is interagglomerate sintering.

The density changes ranged mostly from 45 to 51% with one sample exhibiting a 33% change and another sample exhibiting a 64% change in density during interagglomerate densification. Packing inhomogeneities and initial packing density during crystallite agglomeration are suspected as the cause of this difference. Among die pressed, centrifugally settled, and gravitationally settled compacts, similar relative changes in density were observed. The compacts may not be distinguished by their relative change in density due to interagglomerate densification alone.

However, fracture surface micrographs, Figures 33A-C, reveal that the microstructure of the compacts are not all the same. Centrifuged and gravitationally settled powders exhibited similar sintered microstructures. Porosity is evenly dispersed and grain size is relatively uniform. Their densities were estimated graphically to be near 93%. On the other hand, die pressed compacts had a similarly dense microstructure in some areas. However, relatively large cracks within die pressed compacts were observed (See Figure 33C). These cracks are the result of poor packing in the green state. In all three types of compacts, part of the remaining porosity is internal to the titania grains. If grain growth continues, the internal porosity may be effectively trapped as vacancy sinks (grain boundaries) move out from grain centers, inhibiting complete densification.

4.7 Differential Scanning Calorimetry (DSC)

4.7.1 DSC Introduction

For DSC experiments several batches of powder were used B18 (N_2/15/45/5/SC), B13 (N_2/15/75/0/C), B26 (N_2/15/45/0), B27 (N_2/15/45/5), B9 (Air/15/75/5), B15 (N_2/15/45/5SC) (see Section 3.1 for a description of the powder batch nomenclature). Experiments were performed with powders thermally pretreated (annealed for at least 1 h at temperatures of at least 200°C) in air prior to being put into the DSC and with as-prepared powders. In this section, experimental runs will be distinguished by the powder used, heating rate, atmosphere and pretreatment. For example, an experimental run using powder from B18, a heating rate of 10°C/min in air and a pretreatment consisting of a 1 h anneal at 200°C will be designated B18/10/air/1 h 200°C. Experiments scanned several temperature ranges and will be noted.

4.7.2 DSC General

Output from the DSC fell into six categories, each distinguished by the shape of its output curve (see Figures 34A-F). Listed within each of these figures is a description of the experimental parameters and powder chemistry that produced the given curve. The shapes of the curves and their differences will be addressed.

In general, DSC runs spanning room temperature to more than 500°C displayed two common peaks, an endothermic peak occurring between ≈50°C and ≈250°C and an exothermic peak occurring between ≈390°C and ≈500°C. The endothermic peak is mostly due to the evaporation of water[69,70] and a smaller portion from the evaporation of NH_3 (See Section 4.6.2). This endothermic peak was observed even in samples pretreated at temperatures above the temperature range of the peak. Since the exposure of these (pretreated) powders to the atmosphere was limited, the presence of the endothermic peak implies that atmospheric water is readily adsorbed by the powders. Assuming internal pores within the agglomerates with sizes in the tens of angstroms range, it is conceivable that water would condense within the pores due to the reduced vapor pressure of capillary condensation. Decomposition of HPC, evidenced by color changes in the powder (See Section 4.6.2), and some removal of excess reagents may also occur within this temperature range. Further study is recommended in which heating rates as low as 0.5 and 1°C per minute are employed while keeping close track of mass loss. The specific heat associated with this peak may then be calculated and compared to the latent heat of evaporation of water. These data combined with BET surface area measurements may provide insight as to how the water exists within the powder; i.e., either adsorbed as a monolayer (or several molecular layers) onto the surface or condensed within pores.

[c]The origin of the exothermic peak between ≈390°C and ≈500°C is due to the transformation of powder to anatase, and possibly, a combination of anatase and brookite.

---

[c]The data for B13/Air/Various heating rates/pretreated 250°C 3.25 h will be omitted from the following paragraph because it exhibited a behavior quite different from the other powders.

These results have been established through X-ray and TEM analysis (See Sections 4.2, 4.4, 4.5). For the various powders tested, the onset temperatures, peak temperatures and specific heats differed from powder batch to powder batch yet were consistent for any particular combination of DSC experimental atmosphere and powder batch. The findings are summarized in Table 12.

Batch	Synthesis	PreT[1]	Atm/# runs	Onset °C	Peak °C	ΔH J/g
9	Air/15/45/5	None	Ar/1	398	420	-262
13	N_2/15/75/0	250°C 3.25 h	Ar/8	438±1	471±1	-300±8
13	" "	None	Air/1	367	445	-367
26	N_2/15/45/0	None	Ar/2	413±6	439±3	-284±12
26	" "	None	Air/3	411±2	439±1	-337±17
27	N_2/15/45/5	None	Ar/2	416±5	450±1	-275±1
27	" "	None	Air/3	416±2	446±3	-341±5
15	".."	None	Ar/1	377	443	-248
18	" "	None	Ar/3			-270±4
18	" "	200°C/1 h	Ar/2	458	495	-251±8

1 Pretreatment temperature

Table 12. Compilation of onset temperatures, peak temperatures, and transformation enthalpies for the transformation of powders to anatase. DSC heating rates were generally 40°C/min (see footnotes for exceptions).

Note the difference among the enthalpies, which are recorded in the last column of Table 12. This may be due to differences in internal structure of the as-synthesized powders. The hydrolysis and subsequent condensation of the titanium tetraethoxide to TiO_2 is represented schematically in Figure 35 according to the discussion by Barringer[70].

The condensation results in a network of titanium and oxygen atoms which possesses atomic ordering (See Section 4.2.2). Depending on the arrangement of these bonds during synthesis, the resulting powders may vary in their "closeness" to crystallinity; i.e., the number of bonds broken and formed during crystallization to anatase may vary with and within each batch of powder. These structural variations may have resulted from heterogeneities while

mixing during powder synthesis; i.e., nonuniform reagent concentrations within the reaction region. Different transformation enthalpies will then occur. Further experimentation using powders which are known to have been synthesized within a homogeneous reagent environment are in order.

Two cases exist for which reaction enthalpies (for the large exothermic peak) were measured for both pretreated and non-pretreated powders from the same batch. Transformation enthalpy for the powders which had been pretreated was smaller than for powders which were not pretreated. The pretreatments were 1 h at 200°C and 3.25 h at 250°C for B18 and B13 powders respectively. The data reflect that the longer pretreatment at the higher temperature had a larger effect on decreasing the transformation enthalpy than the lower temperature treatment. The transformation of the pretreated powder at 250°C was reduced to 81% of the non-treated powder's heat of reaction whereas the reaction energy of the powder with the 200°C pretreatment was reduced to 93% of that for the non-treated powder. This may seem contradictory to the X-ray analysis findings, (being that those experiments did not "find" any transformation to have taken place prior to 335°C for a Batch 3 powder), however, X-ray experiments were not successful in determining the atomic ordering within the as-prepared powder either. This was established by electron diffraction (See Section 4.2.2) experiments on as-prepared powders and is also being seen in research by Moss using low angle X-ray diffraction. The appearance of anatase in X-ray diffraction scans is then probably due to a combination of complete powder transformation and simultaneous grain growth which should improve the scattering efficiency of the powder.

Figures 34A-Dshow how the presence of HPC affects the DSC scan. Note that Figures 34A,B are from powders prepared using HPC dispersant and Figures 34C,D represent DSC scans from powders prepared without HPC. For the experiments conducted in flowing air (Figures 34A,C), three exothermic peaks (labeled 1,2 and 3 in the figure) are observed in the DSC scan for powders prepared with HPC and only two exothermic peaks (labeled 2 and 3) are observed for powders prepared without HPC. Peak three is the

exothermic reaction just discussed. The two peaks, 1, and 2 in Figure 34A have onset temperatures of 260±1°C, and 327±3°C respectively, whereas the onset temperature of exothermic peak 2 in Figurex 34C is 299±25°C. (These onset temperatures are measured as the temperature at which the curves begin an abrupt deviation from their "straight line" trajectory.)

The absence of peak 1 in scans for powders prepared without HPC implies that the exothermic reaction observed is related to the use of HPC in the powder synthesis. Figures C,D represent scans of powders run in an inert (argon) atmosphere. These scans show no sign of an exothermic reaction similar to the exothermic peak 1 of Figure 34A. This implies that peak 1 results from a reaction between a component in the powder and a component in air, most likely oxygen. Following the decomposition of HPC, this reaction could possibly be due to the reaction of remaining carbon with oxygen, which is discussed next.

The total area of the exothermic peak 1 corresponds to -0.38, -0.49 and -0.22 Joules for the three samples run in air; the scan encompassed the temperature range of this peak. (These energies are not to be interpreted as exact because of difficulties in establishing a baseline to measure against. However, they do represent the order of magnitude of the energy associated with the exothermic peak.) Using published data[132], the enthalpy of reaction (at 282°C, the average peak temperature) for $C_{(s)} + O_{2(g)} = CO_{2(g)}$ was calculated to be -394 KJ/mol carbon (or -3.047×10^{-5} g carbon/J). From these data the necessary mass of carbon reacting with O_2 to produce the measured enthalpy change may be computed. For the three peaks under consideration the corresponding masses of carbon are 0.011, 0.015, and 0.0067 mg (See Table 13 for a summary of the calculations).

The magnitude of the mass loss (for the energies of peak 1) associated with the reaction of carbon with oxygen, falls below the error limit of the equipment used. (The balance used had a precision of 0.01 milligrams with a measurement reproducibility of ≈0.02 milligrams; i.e., if one made a measurement, arrested the balance, and then immediately made another

Enthalpy of Peak 1 in Joules	milligrams of Carbon reacting with O_2 to produce the enthalpy change observed
-0.38	0.011
-0.49	0.015
-0.22	0.0067

Table 13 Milligrams of carbon reacting according to the equation $C_{(s)} + O_{2\,(g)} \leftrightarrow CO_{2\,(g)}$ at 282°C to produce the enthalpy change associated with peak 1 (Figure 34A).

measurement the readings could differ by as much as 0.02 milligrams.) This small loss is consistent with the findings of Jean and Ring[57] with regard to mass loss in ethoxide-derived titanium dioxide powders synthesized in the presence of HPC; the mass loss characteristics on heating powder synthesized in the presence of HPC dispersant were not measurably different from mass loss characteristics of titanium dioxide synthesized without HPC.

Peak 2 is present in scans of powder prepared with and without HPC dispersant. However, it is only found for powders heated in air. The observed exotherm, therefore, results from a reaction of a component in the air with that in the powder.

Peak 2 energies averaged -72±5 J/g and ranged from -67 to -77 J/g for powders heated at 40°C/min and synthesized with HPC (B27 powders). In contrast, enthalpy measurements of identical runs using powder synthesized without HPC were measured at -29, -70, -159, - and -154 J/g (B26 powders). The source of the variations among the powders produced without HPC is not known. It might result from incorrect sample mass measurements however this seems unlikely since this task was performed with the utmost care and consistency. Errors of a factor of two and five are unlikely. A more likely source for the differences may be in judging where these peaks began and ended. The peaks of B26 (15/45/0) were more shallow and not as consistent in shape as those of B27 (15/45/5).

A possible source for this exotherm is a partial rearrangement of the TiO_2 structure of the as prepared powder or possibly even Ti-O bonding resulting from the decomposition of unreacted Ti-ethanol radicals. The decomposition would be endothermic, however, if the resulting Ti-O bond were more favorable a net exothermic reaction would be observed.

An unusual result was observed in 15/75/0 (Batch 13) powders pretreated at 250°C for 3.25 h. The effect is shown in Figures 34E,F. The exothermic peak associated with the transformation of the pretreated powder to anatase is followed by a second smaller (in runs performed in flowing argon) exothermic peak, Figure 34F. This feature becomes more pronounced for runs performed in air as Figures 34E shows. It is not present in scans of pretreated or unpretreated powders of different batches.

To assess the nature of the first observed reaction, runs were performed that were stopped just prior (a good estimate based on previously observed onset temperatures) to the initial exothermic peak, and runs were performed that were stopped after the first peak yet before the second peak. An X-ray scan of the powder heated to the onset temperature indicated that the powder was "amorphous". The powder heated in air just to the "end temperature" of the first peak was shown to be anatase through X-ray diffraction.

The nature of the second reaction is not understood. X-ray diffraction of B13 15/75/0 powders heated to 700°C show only anatase is present. Therefore this peak is not due to the anatase→rutile transformation. Performing similar DSC experiments with another batch of powder synthesized with a water concentration of 0.75M and pretreated as before may indicate whether or not the water concentration plays a role in the appearance of the second peak. Further experimentation is needed to determine why this second peak is observed for pretreated 15/75/0 powder and not in as-prepared 15/75/0 powder. Tracking mass loss, as well as detecting and identifying any evolved gases, would be beneficial.

5 SUMMARY AND CONCLUSIONS

Nominally monosized titania, ≈0.35μm diameter particles were prepared by the controlled hydrolysis of titanium tetraethoxide in ethanol. Particle size was found to vary among batches of seemingly identically prepared powders. The yield of each batch was relatively low and, therefore, elimination of batch to batch variations among experiments could not be limited by using the same batch of powder for each experiment.

Ultramicrotomy was found to be a useful technique for preparing thin sections of powder particles to examine in the TEM. Combining these techniques made it possible to study the internal microstructural evolution of heat treated powders.. Difficulties in the ultramicrotomy technique included resin-sample adhesion. Adhesion might be improved by application of an organofunctional silane to the compact prior to embedding.

The crystallization study showed that the transformation of anatase to rutile may be heating rate dependent and varies among powder batches. As discussed in the introduction there are several reported values of the anatase→rutile transformation temperature. Further investigation of the variables which control the transformation in ethoxide derived powders is necessary.

The effects of low temperature thermal pretreatments reported by Edelson[60] were not observed in this study. However, other morphological characteristics relevant to determining sintering behavior were observed. Compact surfaces were seen to densify at a greater rate than the bulk. This placed a mechanical constraint on the samples which inhibited bulk densification and promoted coarsening. The result was porous, facetted regions within the compact.

Evolution of agglomerate internal structure as well as particle-particle densification could be followed in a dilatometer. Compacts which had been hydrothermally pretreated exhibited a smaller linear shrinkage at temperatures corresponding to the transformation of as-prepared powder, than did compacts of powders which had not been pretreated. This corroborates the findings that hydrothermal pretreatment transforms the as-prepared powder.

Low-temperature anatase sintering at a constant rate of heating was analyzed and found to occur with an activation energy of ≈167 kJ/mol if boundary diffusion is assumed to be the dominant mass transport mechanism and an activation energy of -106 kJ/mol if volume diffusion is assumed to be the dominant mechanism. Generally, activation energies for boundary diffusion are less than those of volume diffusion. Because the opposite is displayed here, it may be that the analysis of Young and Cutler does not apply to the intra-agglomerate anatase sintering.

Differential scanning calorimeter experiments showed that the enthalpy of the transformation of as-prepared powder depended on reaction atmosphere. The enthalpy of transformation was greater for runs in air than for runs in argon, indicating that a reaction with oxygen probably occurs. It also varied among different batches of powder indicating again, that more control is needed during the powder synthesis to assure homogeneous powders.

6 FIGURES

Reference	Temperature °C	Time	Additive	Amount	Atmosphere	% Rutile	% Anatase
46	700-800						
3	610		None		Air		
4	525	24 h	None		Air	0	100
4	950	240 h	None		Air	100	0
5	1000	1 h	Fe_2O_3	0.087 wt%	Air	30	70
5	1000	1 h	Fe_2O_3	0.087 wt%	$\frac{CO_2}{H_2}$ =27.4	93	7
5	1000	1 h	None		$\frac{CO_2}{H_2}$ =27.4	35	65
5	1000	1 h	None		Air	20	80

Figure 1 Compilation of results on the study of the anatase → rutile transformation under various experimental conditions as found in the literature.

Reference	Temperature °C	Time	Additive	Amount	Atmosphere	% Rutile	% Anatase
7	700	3 h	None		Air	0	100
7	800	3 h	None		Air	0	100
7	900	3 h	None		Air	82	18
7	700	3 h	Na_2O	1 mole %	Air	0	100
7	800	3 h	Na_2O	1 mole %	Air	0	100
7	900	3 h	Na_2O	1 mole %	Air	14	86
7	700	3 h	CuO	1 mole %	Air	3	97
7	800	3 h	CuO	1 mole %	Air	100	0
7	900	3 h	CuO	1 mole %	Air	100	0
7	700	3 h	CoO	1 mole %	Air	0	100
7	800	3 h	CoO	1 mole %	Air	21	79
7	900	3 h	CoO	1 mole %	Air	100	0

Figure 1 continued.

Reference	Temperature °C	Time	Additive	Amount	Atmosphere	% Rutile	% Anatase
7	700	3 h	NiO	1 mole %	Air	0	100
7	800	3 h	NiO	1 mole %	Air	3	97
7	900	3 h	NiO	1 mole %	Air	100	0
7	700	3 h	MnO_2	1 mole %	Air	0	100
7	800	3 h	MnO_2	1 mole %	Air	0	100
7	900	3 h	MnO_2	1 mole %	Air	100	0
7	700	3 h	Fe_2O_3	1 mole %	Air	0	100
7	800	3 h	Fe_2O_3	1 mole %	Air	2	98
7	900	3 h	Fe_2O_3	1 mole %	Air	100	0
7	700	3 h	Cr_2O_3	1 mole %	Air	0	100
7	800	3 h	Cr_2O_3	1 mole %	Air	12	88
7	900	3 h	Cr_2O_3	1 mole %	Air	96	4

Figure 1 continued.

Reference	Temperature °C	Time	Additive	Amount	Atmosphere	% Rutile	% Anatase
7	700	3 h	MoO_3	1 mole %	Air	0	100
7	800	3 h	MoO_3	1 mole %	Air	16	84
7	900	3 h	MoO_3	1 mole %	Air	18	82
7	700	3 h	WO_3	1 mole %	Air	0	100
7	800	3 h	WO_3	1 mole %	Air	0	100
7	900	3 h	WO_3	1 mole %	Air	15	85
11	1000	0.25 h	LiF	1 mole %	Air	100	0
11	1000	0.25 h	Li_2CO_3	1 mole %	Air	100	0
11	1000	0.25 h	CuO	1 mole %	Air	100	0
11	1000	0.25 h	MnO_2	1 mole %	Air	95.4	4.6
11	1000	0.25 h	CdO	1 mole %	Air	91.5	8.5
11	1000	0.25 h	Fe_2O_3	1 mole %	Air	90.8	9.2

Figure 1 continued.

Reference	Temperature °C	Time	Additive	Amount	Atmosphere	% Rutile	% Anatase
11	1000	0.25 h	CoO	1 mole %	Air	90.2	9.8
11	1000	0.25 h	ZnO	1 mole %	Air	88.2	11.8
11	1000	0.25 h	NaF	1 mole %	Air	85.6	14.4
11	1000	0.25 h	PbO_2	1 mole %	Air	51.4	48.6
11	1000	0.25 h	Bi_2O_3	1 mole %	Air	49.5	50.5
11	1000	0.25 h	MoO_3	1 mole %	Air	30.6	69.4
11	1000	0.25 h	Na_2CO_3	1 mole %	Air	25.4	74.6
11	1000	0.25 h	Cr_2O_3	1 mole %	Air	9.1	90.9
11	1000	0.25 h	NiO	1 mole %	Air	8.3	91.7
11	1000	0.25 h	Al_2O_3	1 mole %	Air	0	100
11	1000	0.25 h	None	1 mole %	Air	0	100
13	1000	0.5 h	None		Still Air	6	94

Figure 1 continued.

Reference	Temperature °C	Time	Additive	Amount	Atmosphere	% Rutile	% Anatase
13	1000	0.5 h	None		O_2 2.5 ml/s	6.5	93.5
13	1000	0.5 h	None		Air 2.5 ml/s	8	92
13	1000	0.5 h	None		Ar 2.5 ml/s	13	87
13	1000	0.5 h	None		N_2 2.5 ml/s	15	85
13	1000	0.5 h	None		Steam 2.5 ml/s	21	79
13	1000	0.5 h	None		Vacuum $\approx 10^{-1}$ Pa	27	73
13	1000	0.5 h	None		5%H_2-95%N_2	97	3
23	1050	1 h	None		Air	7.5	92.5
23	1061	1 h	None		Air	13	87
23	1070	1 h	None		Air	23	77
23	1082	1 h	None		Air	56	44
16	700	24 h	None		Air	0	100

Figure 1 continued.

Reference	Temperature °C	Time	Additive	Amount	Atmosphere	% Rutile	% Anatase
16	1050	16 h	None		Air	100	0
17	625	4 h	None		Air	13	87
17	643	4 h	None		Air	24	76
17	684	1 h	None		Air	31	69
17	698	1 h	None		Air	54	46
18	708	1 h	None		Air	95	5
18	708	1 h	Zn^{2+}	5 atom %	Air	76	84
18	708	1 h	Cl^-	5 atom %	Air	49	51
18	708	8 h	Al^{3+}	5 atom %	Air	4	96
18	708	8 h	SO_4^{2-}	5 atom %	Air	0	100
18	708	8 h	PO_4^{3-}	5 atom %	Air	0	100
18	737	1 h	None		Air	100	0

Figure 1 continued.

Reference	Temperature °C	Time	Additive	Amount	Atmosphere	% Rutile	% Anatase
18	737	1 h	Zn^{2+}	5 atom %	Air	100	0
18	737	1 h	Cl^-	5 atom %	Air	79	21
18	737	8 h	Al^{3+}	5 atom %	Air	7	93
18	737	8 h	SO_4^{2-}	5 atom %	Air	9	91
18	737	8 h	PO_4^{3-}	5 atom %	Air	0	100
18	870	1 h	None		Air	100	0
18	870	1 h	Zn^{2+}	5 atom %	Air	100	0
18	870	1 h	Cl^-	5 atom %	Air	100	0
18	870	1 h	Al^{3+}	5 atom %	Air	72	28
18	870	1 h	SO_4^{2-}	5 atom %	Air	29	71
18	870	4 h	PO_4^{3-}	5 atom %	Air	6	94
21	950	0.5 h	None		5%H_2-N_2	≈7	93

Figure 1 continued.

Reference	Temperature °C	Time	Additive	Amount	Atmosphere	% Rutile	% Anatase
21	950	0.5 h	None		10%H_2-N_2	≈12	88
21	950	0.5 h	None		20%H_2-N_2	40	60
7	900	3 h	None		Flowing O_2	52	48
7	900	3 h	None		Flowing Air	70	30
7	900	3 h	None		Flowing Ar	85	15
7	900	3 h	None		Vacuum	94	6
7	900	3 h	None		Flowing H_2	95	5
7	900	3 h	None		Static Air	48	52

Figure 1 continued.

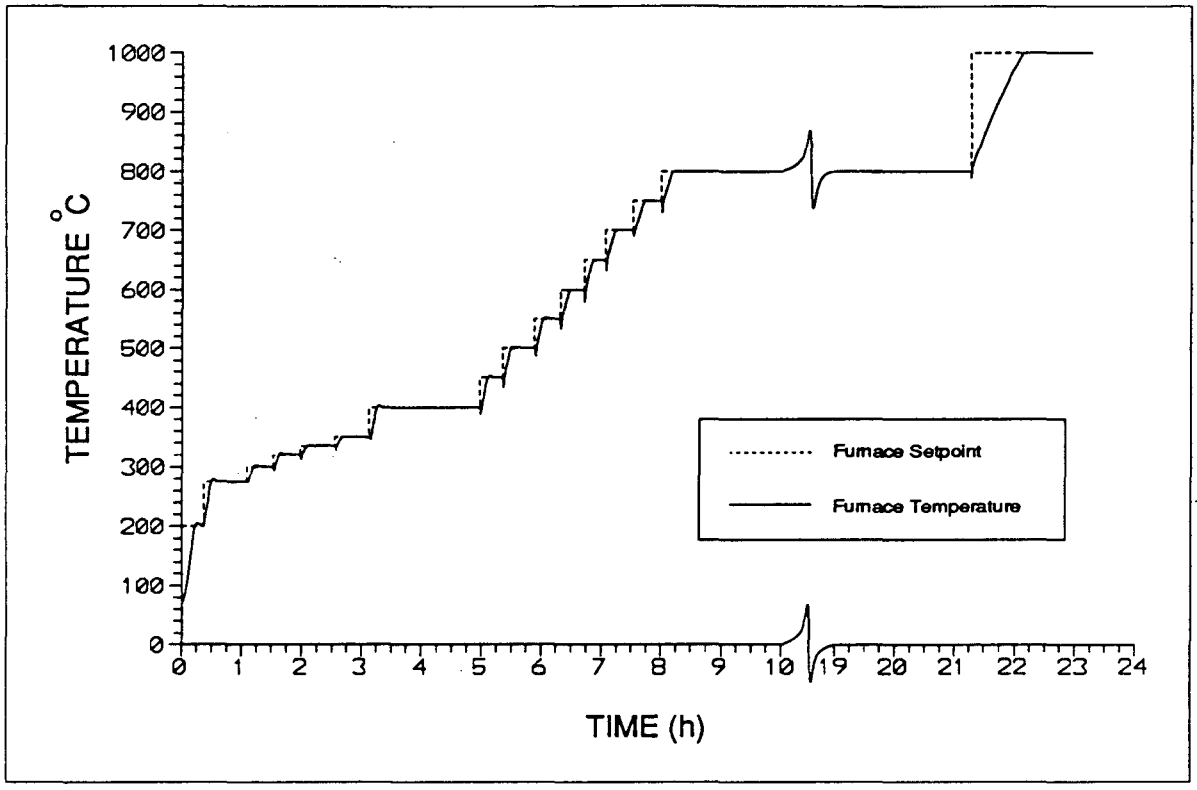

Figure 2. This figure shows the variation in furnace (Thermolyne Model No. 304000) temperature and furnace setpoint during low heating rate experiments. Samples were removed immediately after the setpoint was increased as indicated by slight drops in furnace temperature.

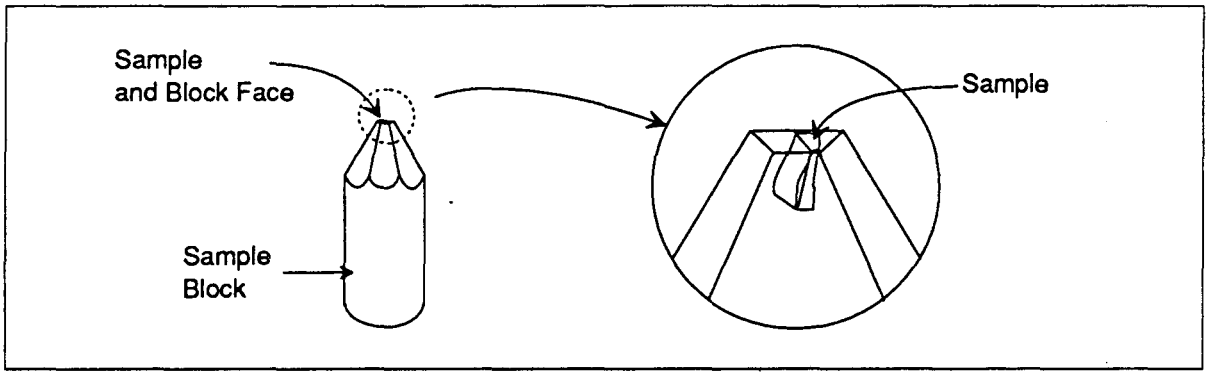

Figure 3. Sample embedded in resin for microtoming. The magnified view of the tip shows that more resin needs to be removed from around the sample before thin section can be cut.

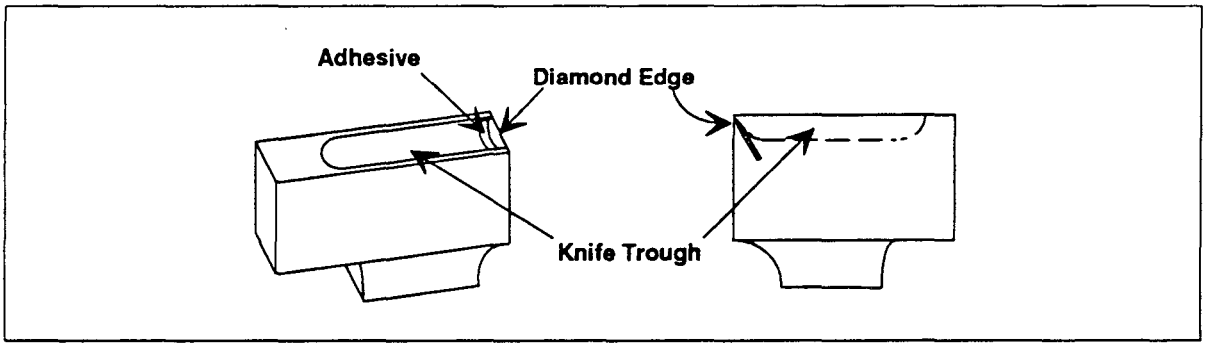

Figure 4. Diamond knife for ultramicrotomy.

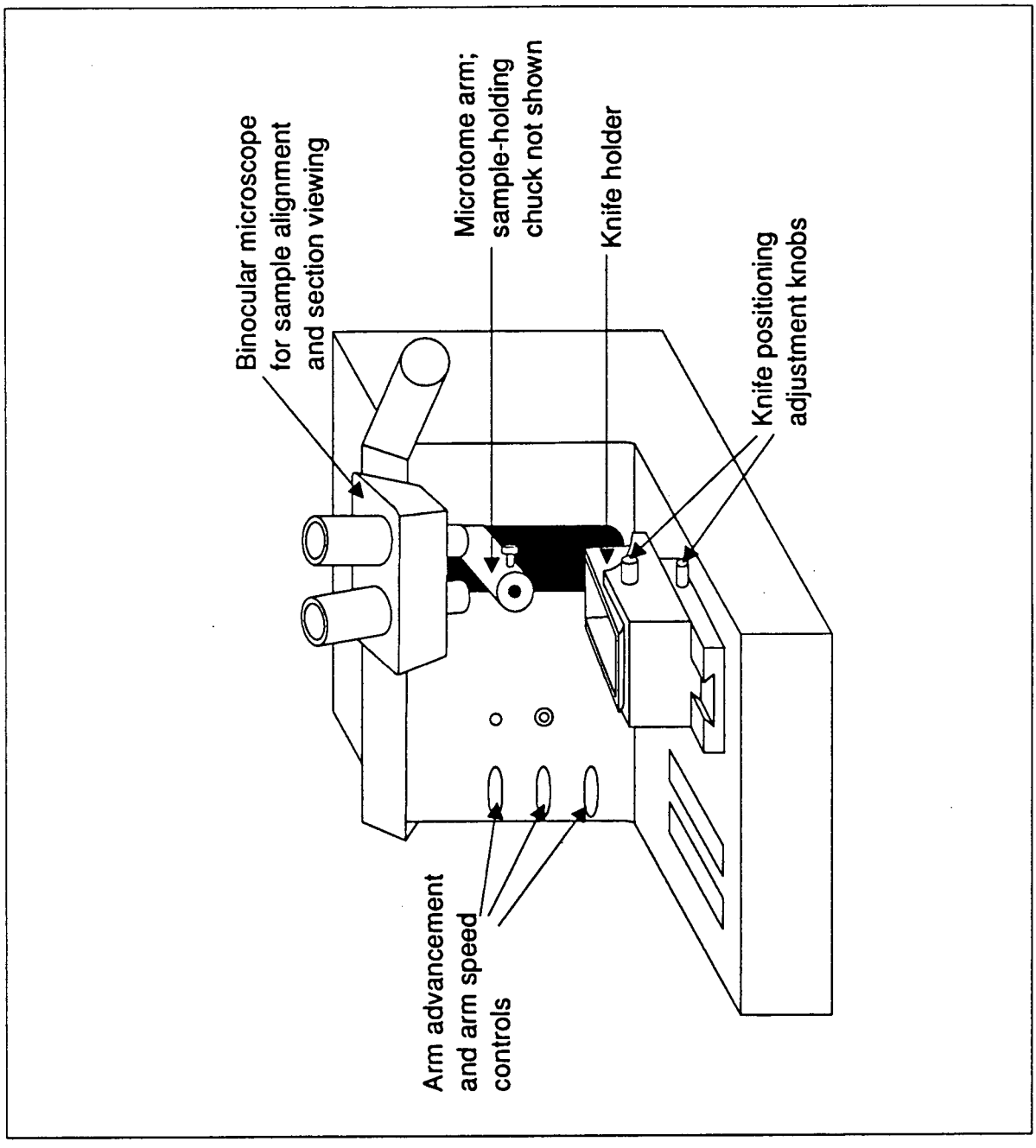

Figure 5. Modern Microtome.

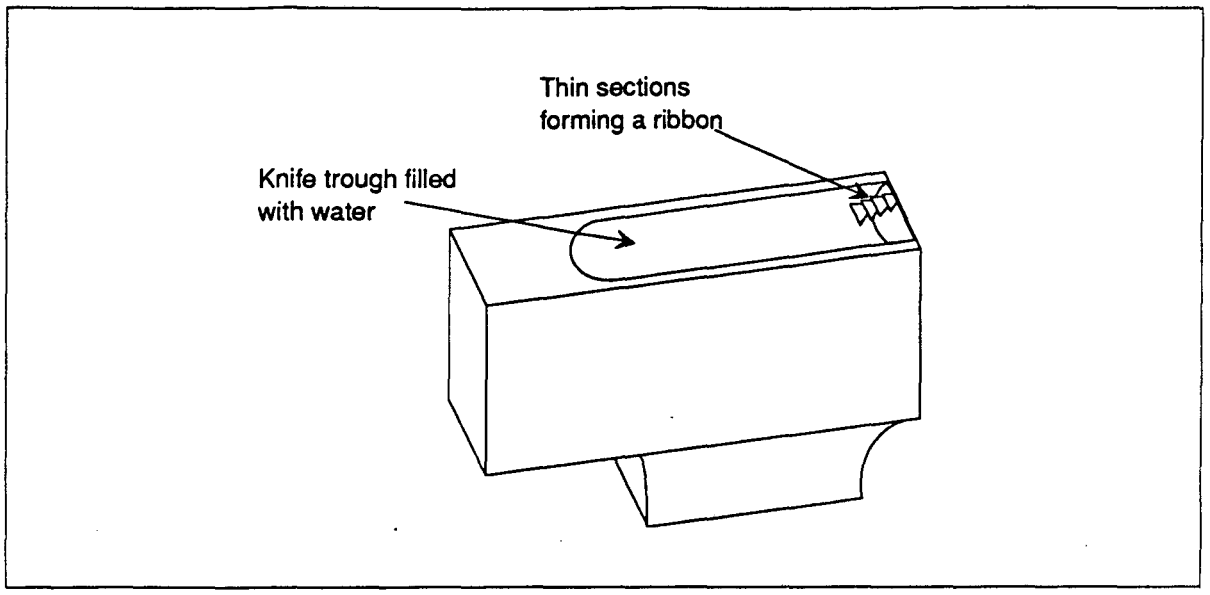

Figure 6. Cut sections form a ribbon in the knife trough. The ribbon is floating on a fluid (most often water) in the knife trough. The section size is greatly exaggerated for clarity. See Figure 14 for a micrograph of an actual blockface for microtomy.

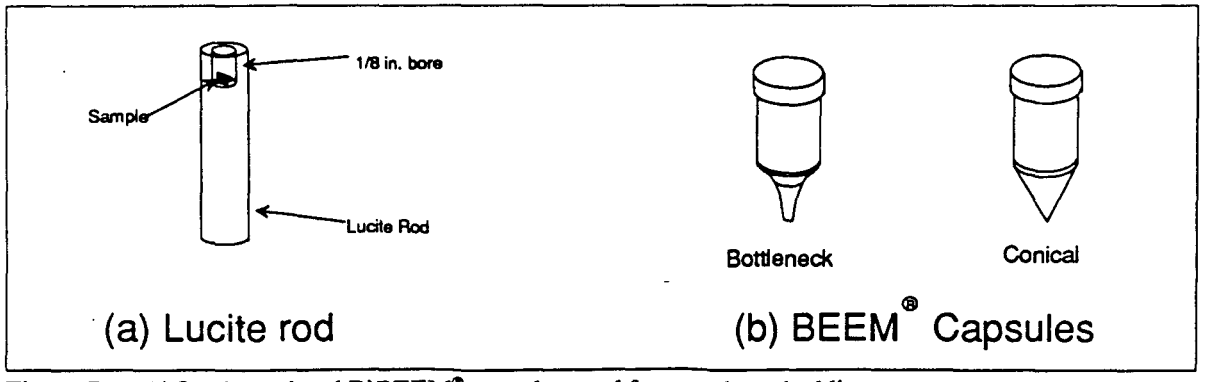

Figure 7 A) Lucite rod and B)BEEM® capsules used for sample embedding.

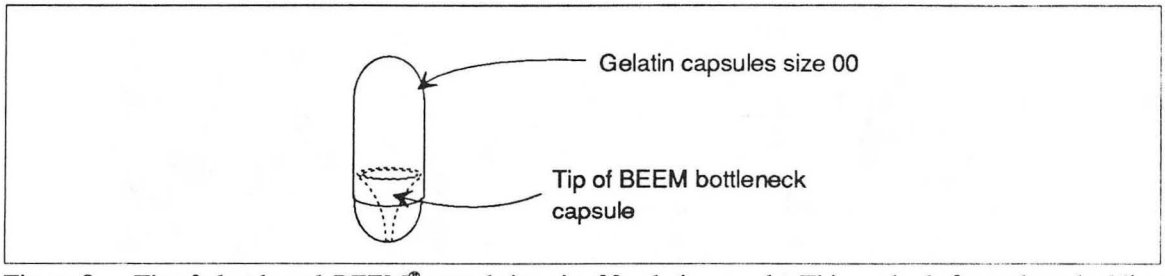

Figure 8. Tip of a bottleneck BEEM® capsule in a size 00 gelatin capsule. This method of sample embedding for ultramicrotomy was the preferred method.

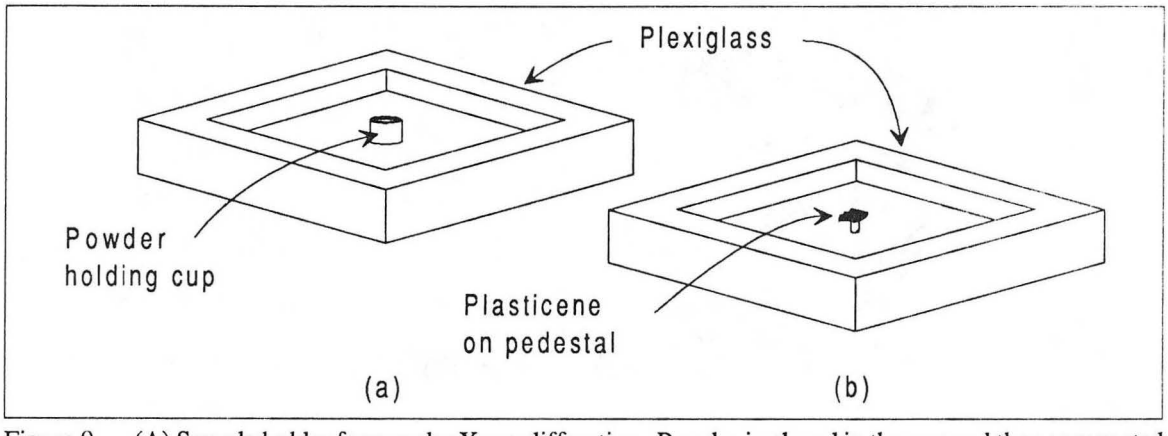

Figure 9. (A) Sample holder for powder X-ray diffraction. Powder is placed in the cup and then compacted and smoothed with a glass microscope slide. (B) Sample holder for small pieces of material which could be ground. The sample's surface is made flush with the holder's top surface by pressing with a glass slide. The plasticene allows for easy alignment and adherence of irregularly shaped specimens.

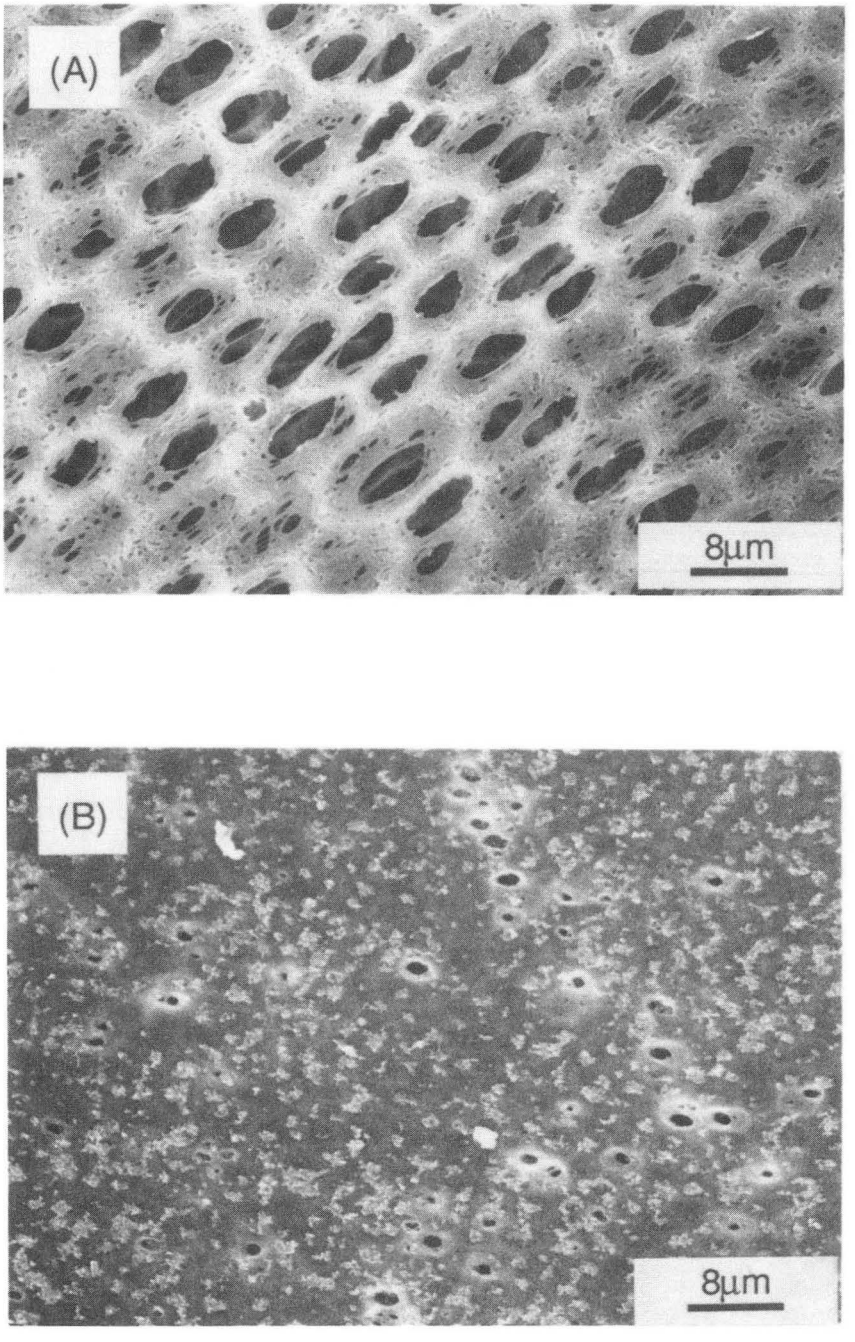

XBB 914-2710

Figure 10 (A) Unused 0.45 μm filter membrane. (B) 0.45 μ filter membrane after filtering a solution of ethanol and HPC dispersant.

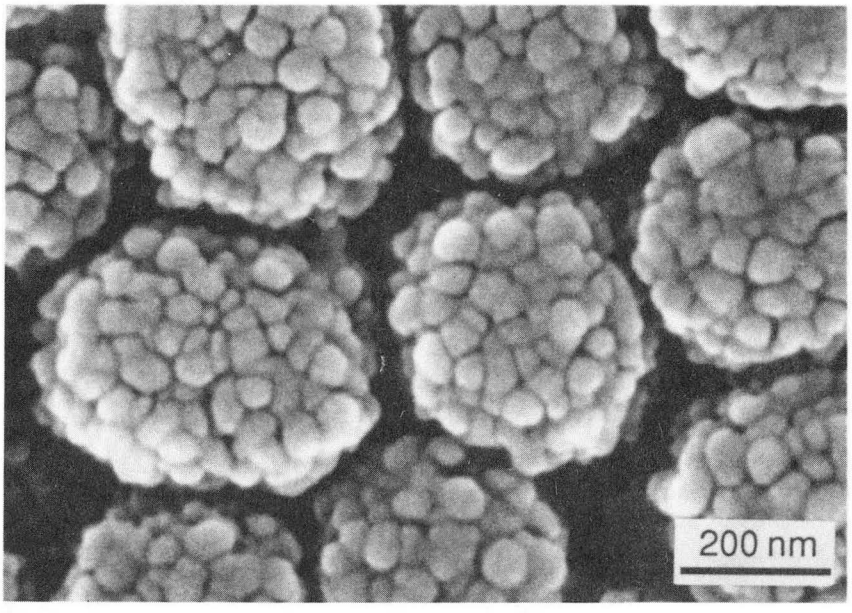

XBB 914-2711

Figure 11 Representative micrograph of ethoxide-derived titania prepared in the presence of HPC dispersant.

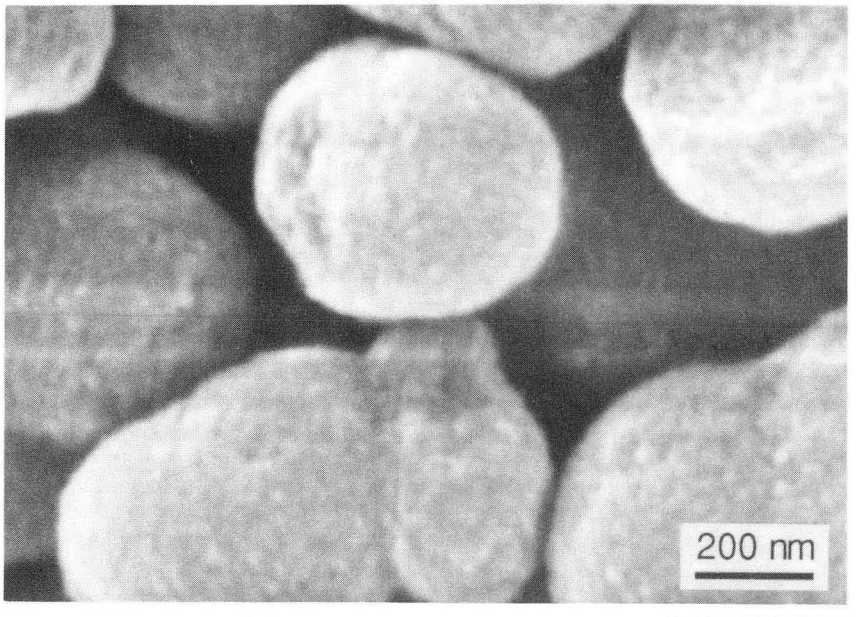

XBB 914-2712

Figure 12 Representative micrograph of ethoxide-derived titania prepared without HPC dispersant.

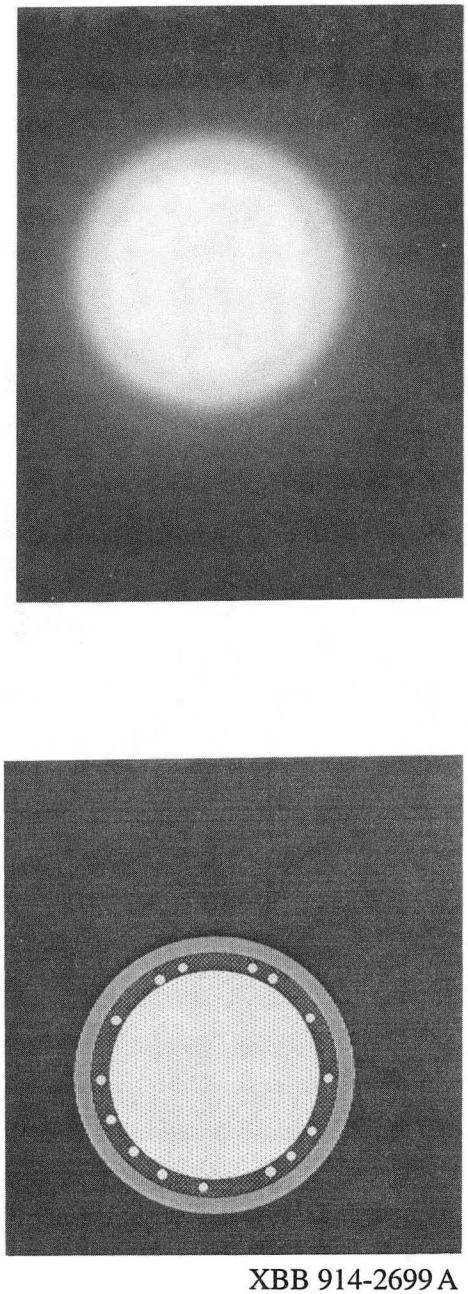

XBB 914-2699 A

Figure 13 Electron diffraction pattern of ultramicrotomed, as-prepared, ethoxide-derived titania. The schematic illustrates clearly the features in the print. Note the broad diffraction spots indicative of small crystallites. Not all of the features (rings) are visible in the print. Measurements for atomic lattice spacings were taken directly off of the negative.

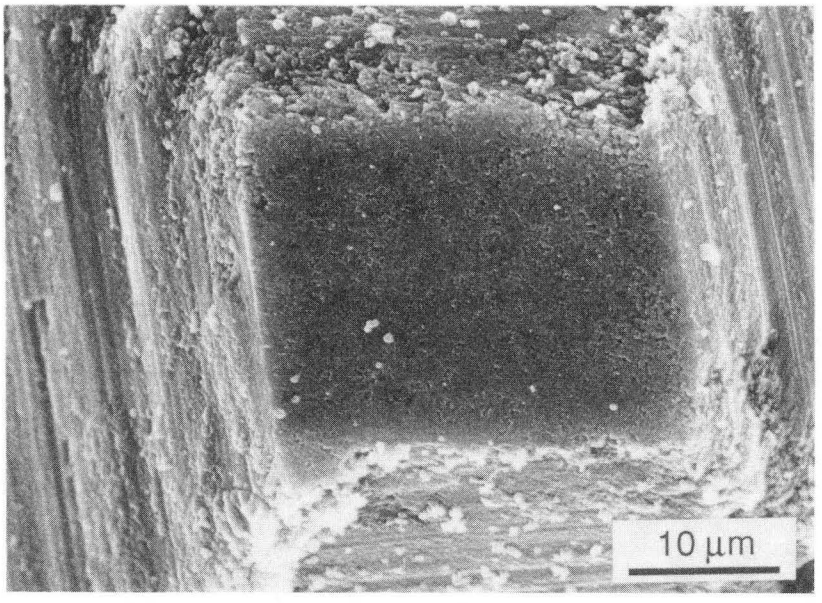

XBB 914-2713

Figure 14 SEM micrograph of a sample block face which has been shaped for microtoming.

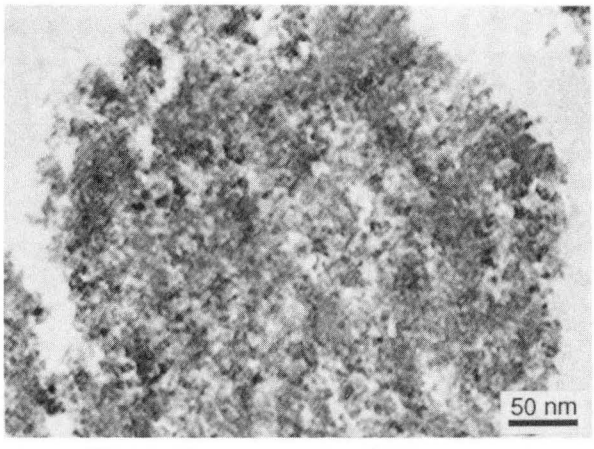

XBB 914-2700 A

Figure 15 TEM micrograph of ultramicrotomed as-prepared B3 powder. See Figure 13 for the electron diffraction pattern of the powder.

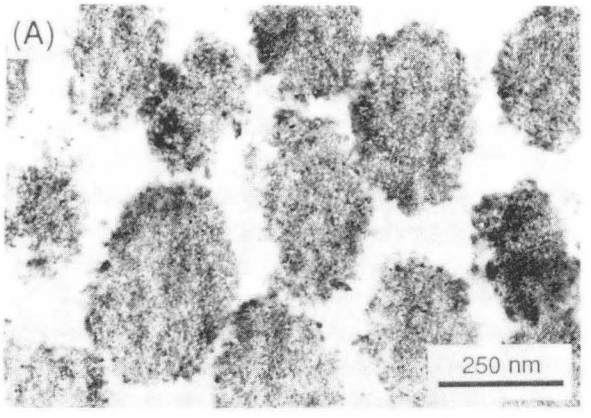

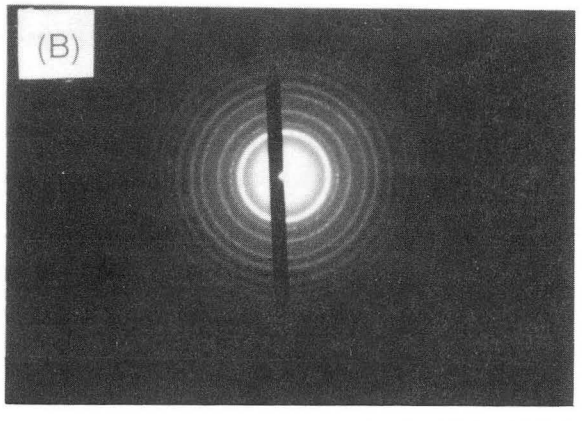

XBB 914-2701 A

Figure 16 (A) TEM micrograph of ultramicrotomed B3 powder which had been heated at 400°C for 15 min. (B) Electron diffraction pattern of powder in (A).

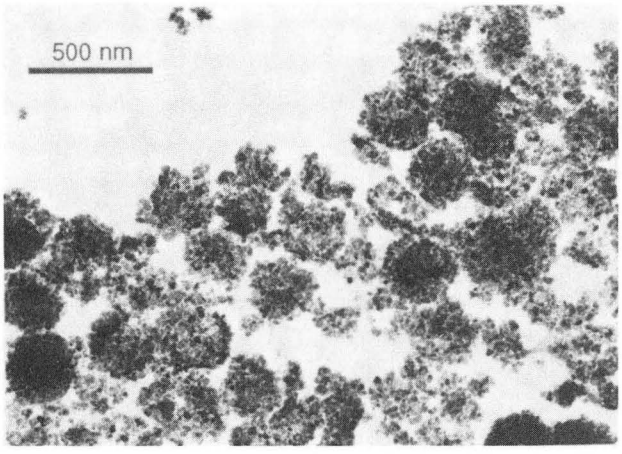

XBB 914-2702 A

Figure 17 TEM micrograph of ultramicrotomed B3 powder which had been annealed at 500°C for 24 h.

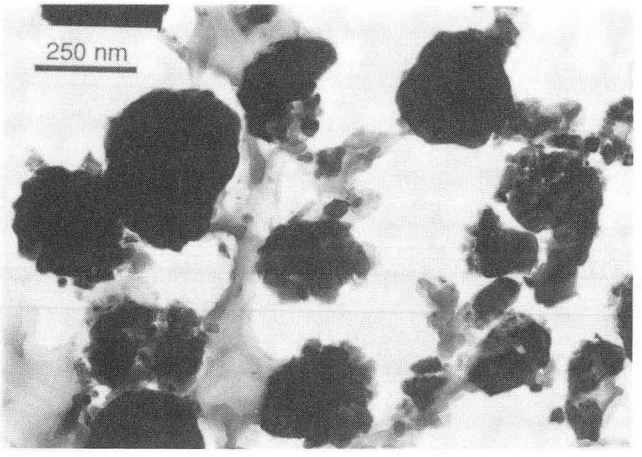

XBB 914-2703 A

Figure 18 TEM micrograph of ultramicrotomed B3 powder which had been heated at 500°C for 24 h and then subsequently annealed at 650°C for 1.5 h

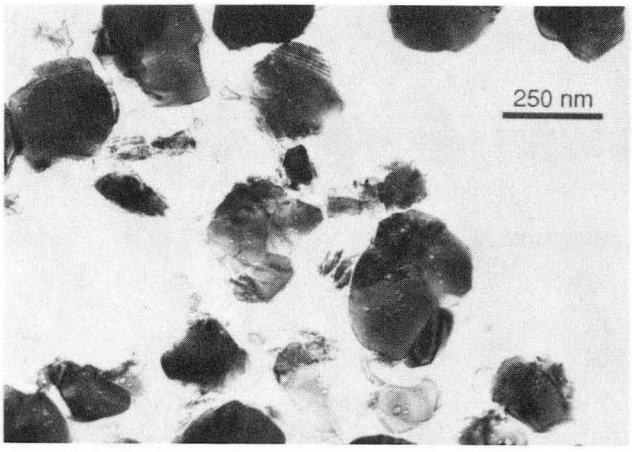

XBB 914-2704 A

Figure 19 TEM micrograph of ultramicrotomed B3 powder which had been heated at 800°C for 1 h.

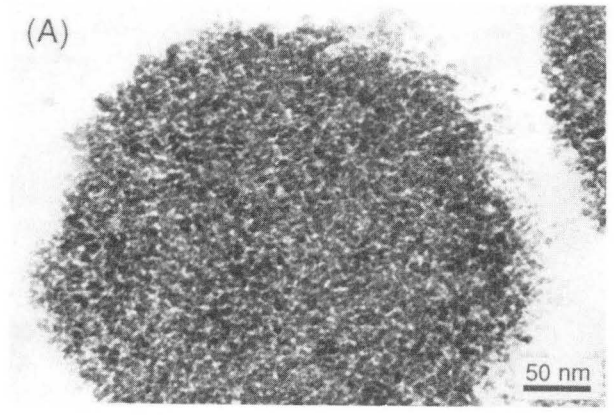

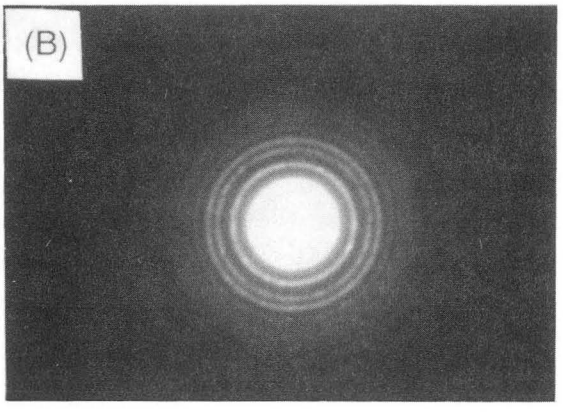

XBB 914-2705 A

Figure 20 (A) TEM micrograph of ultramicrotomed B3 powder which had been hydrothermally treated (placed for 24 h in boiling water). (B) Electron diffraction pattern of hydrothermally treated powder.

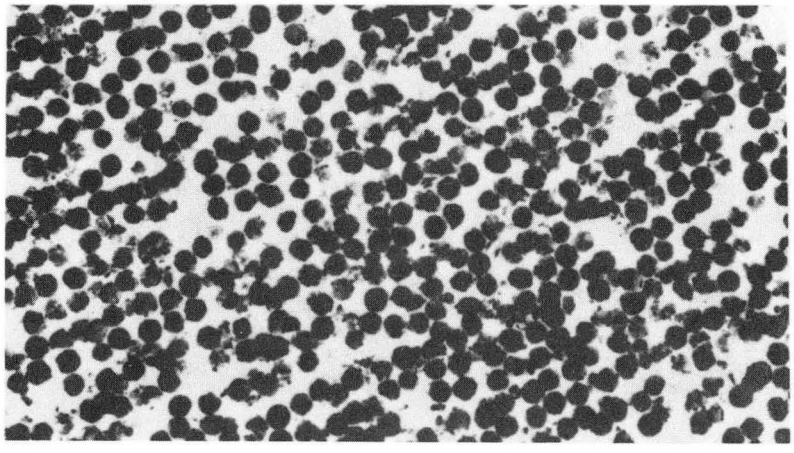

XBB 880-11104 A

Figure 21 TEM micrograph of B3 powder sectioned parallel to the powder's settling direction. Viewing the micrograph on edge along one of the diagonals shows the ordering more clearly.

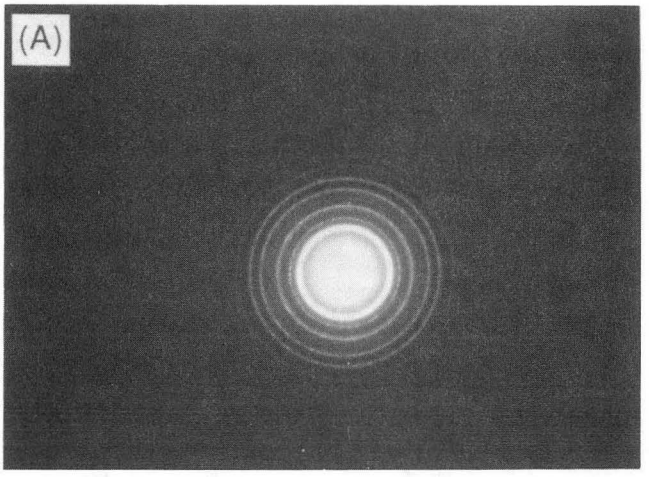

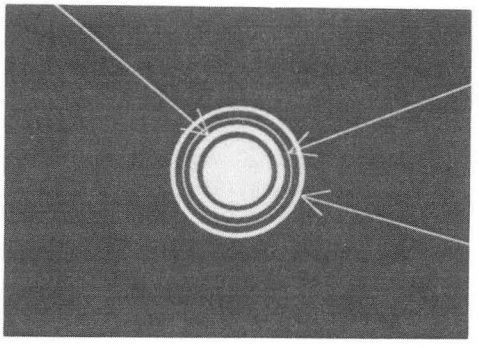

Figure 22(A) Electron diffraction pattern for B3 powder (N_2/15/45/5/VC) annealed at 400°C for 15 min.

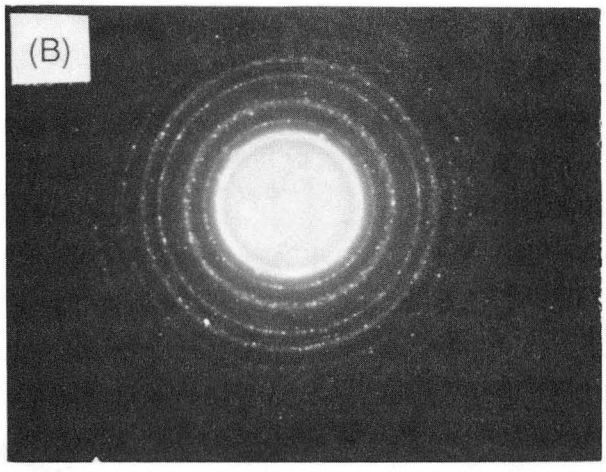

Anatase 101
Brookite 120, 111

Spots indexed as
Rutile 110

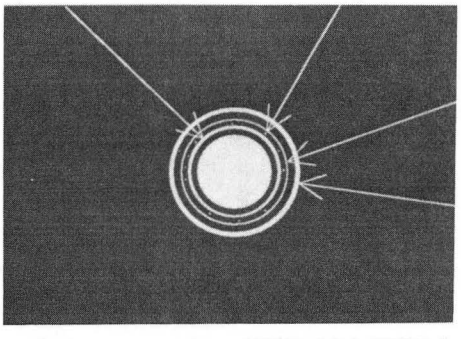

Brookite 121

Anatase 103, 004
Brookite 012, 201

XBB 914-2707 A

Figure 22(B) Electron diffraction pattern for B3 powder (N_2/15/45/5/VC) annealed at 500°C for 24 min.

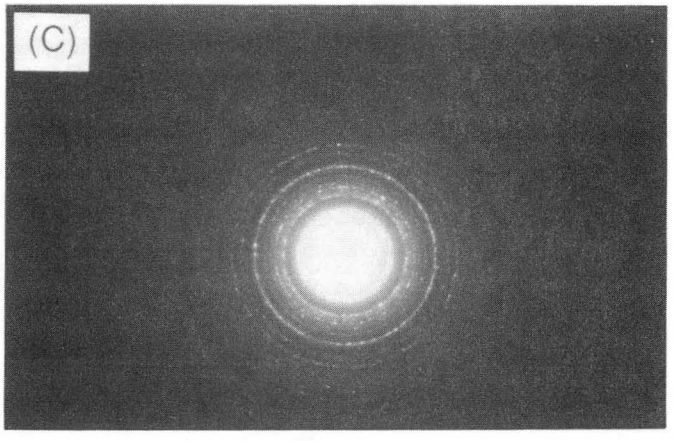

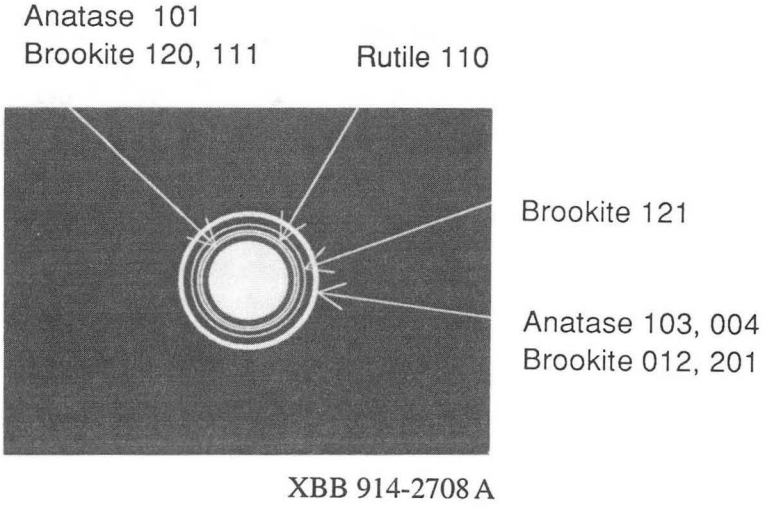

Figure 22(C) Electron diffraction pattern for B3 powder (N_2/15/45/5/VC) annealed at 600°C for 120 min.

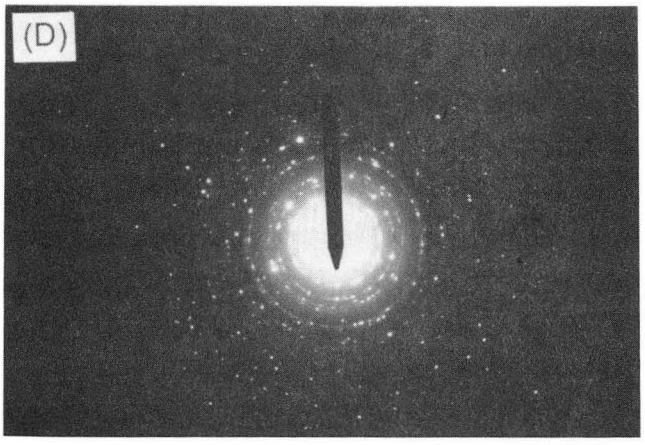

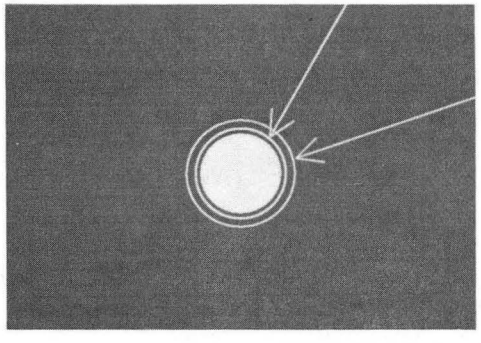

Figure 22(D) Electron diffraction pattern for B3 powder (N_2/15/45/5/VC) annealed at 700°C for 45 min.

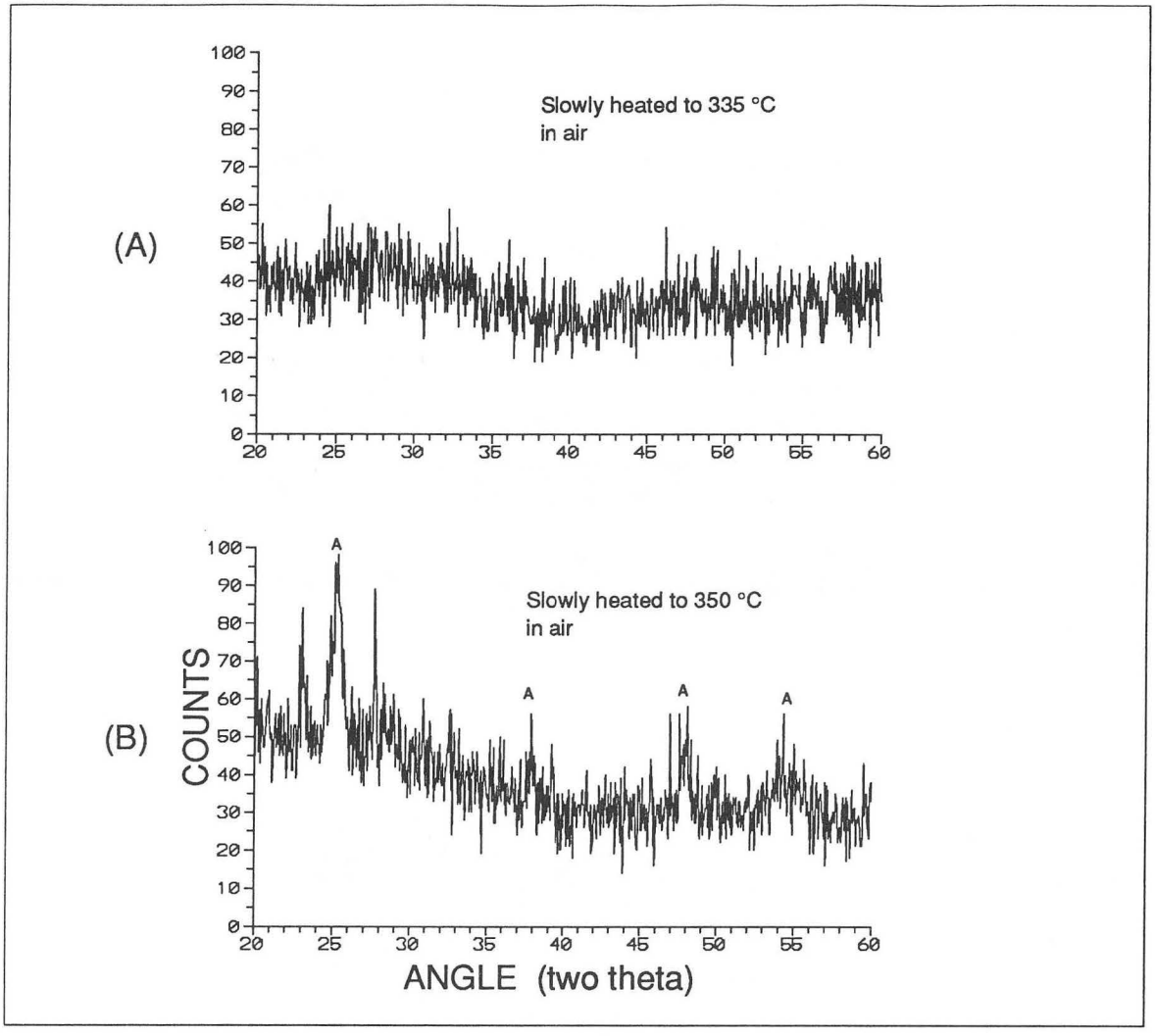

Figure 23. X-ray diffraction patterns for Batch 23, 15/45/5/CS, powder compact. Removal temperature temperatures are as follows (A) 335°C (B) 350°C (C) 400°C (D) 750°C (E) 1000°C. See Section 3.4.2 for a description of the heating schedule.

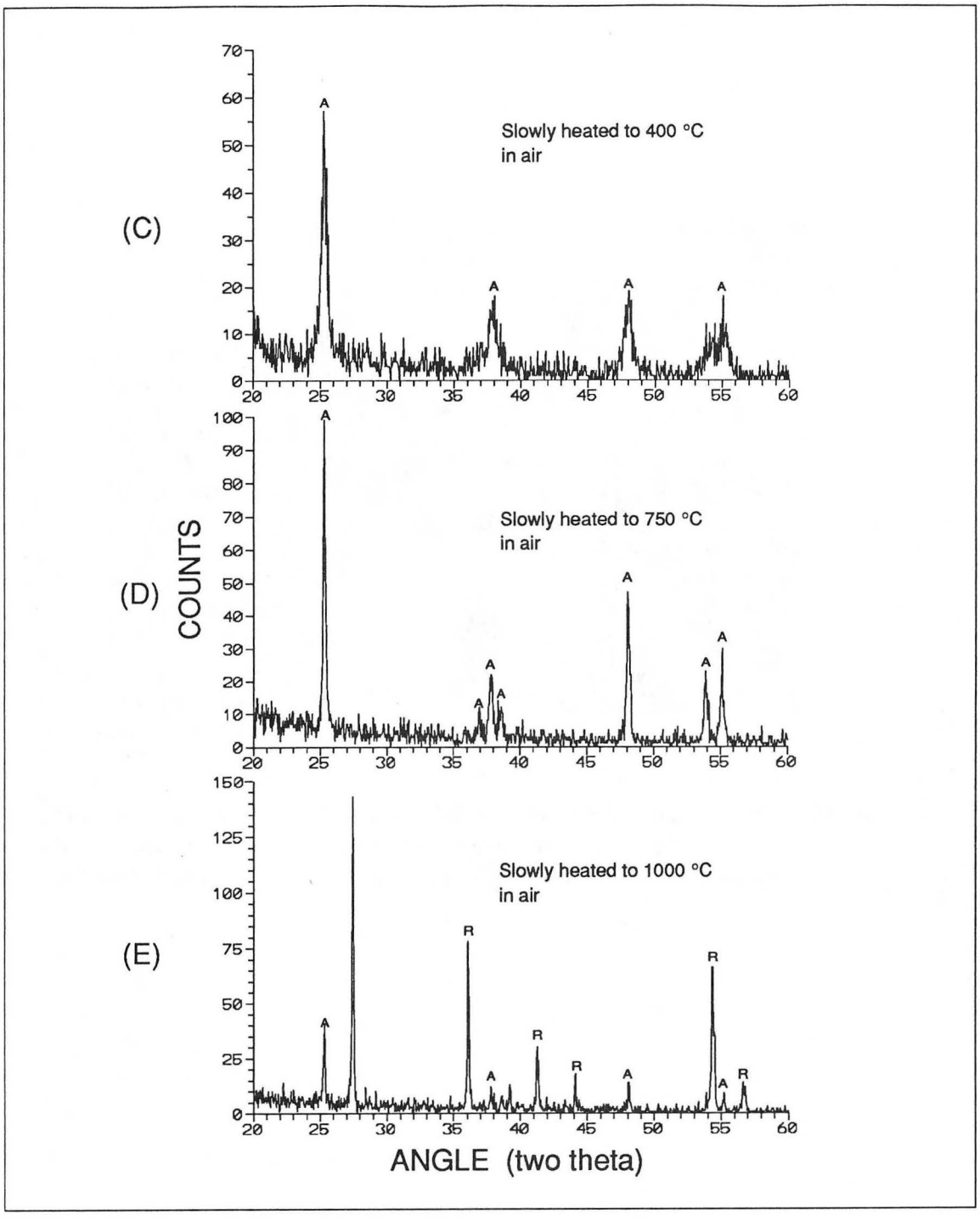

Figure 23 cont.

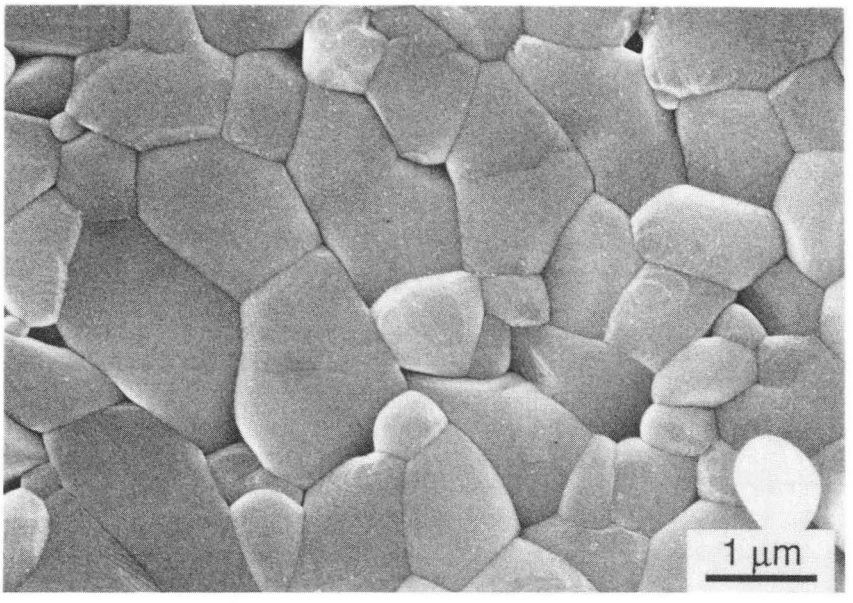

XBB 914-2714

Figure 24 Top surface micrograph of B24 powder slowly heated to 400°C, preannealed at 600°C and then annealed at 1100°C. Compare it to the fracture surface micrograph of the same sample shown in Figure 29c.

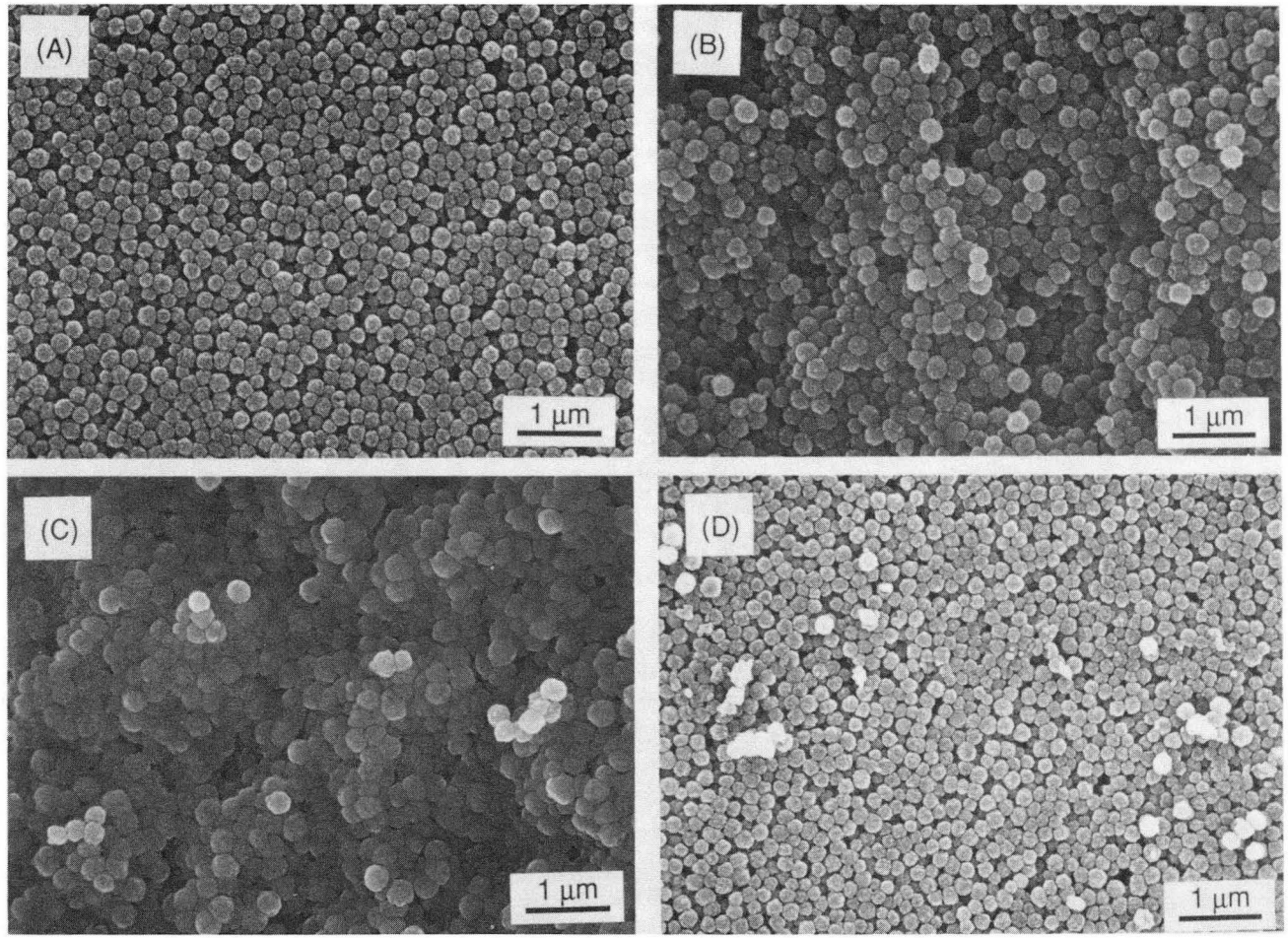

XBB 915-3430

Figure 25 B24 powder compacts heated to 400°C and then annealed for 2 h at the following temperatures: (A) 400°C, (B) 500°C, (C) 600°C, (D) 700°C.

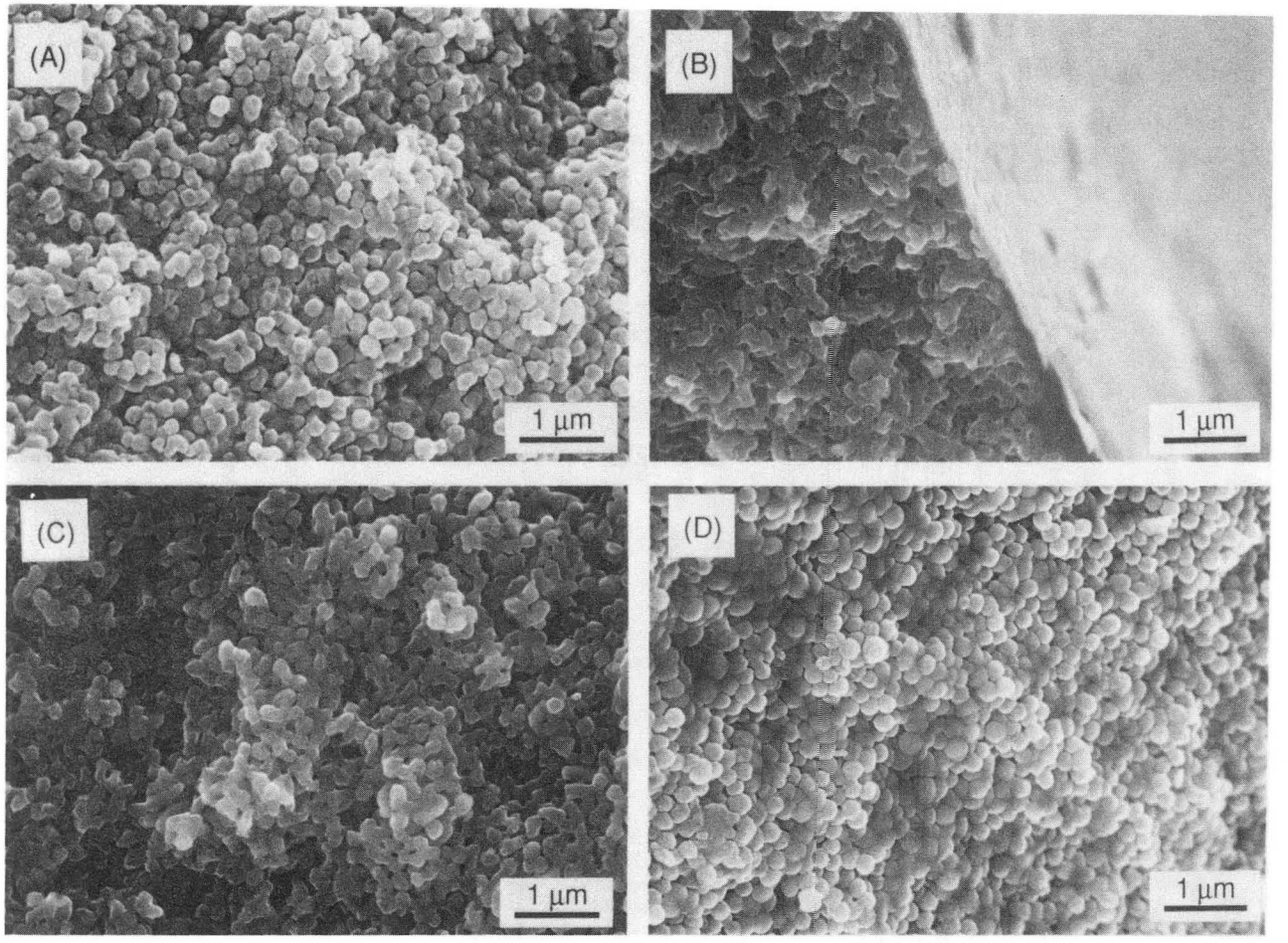

XBB 915-3431

Figure 26 All samples annealed for 1 h at 800°C after pretreatment for 2 h at (A) 400°C, (B) 500°C, (C) 600, (D) 700°C.

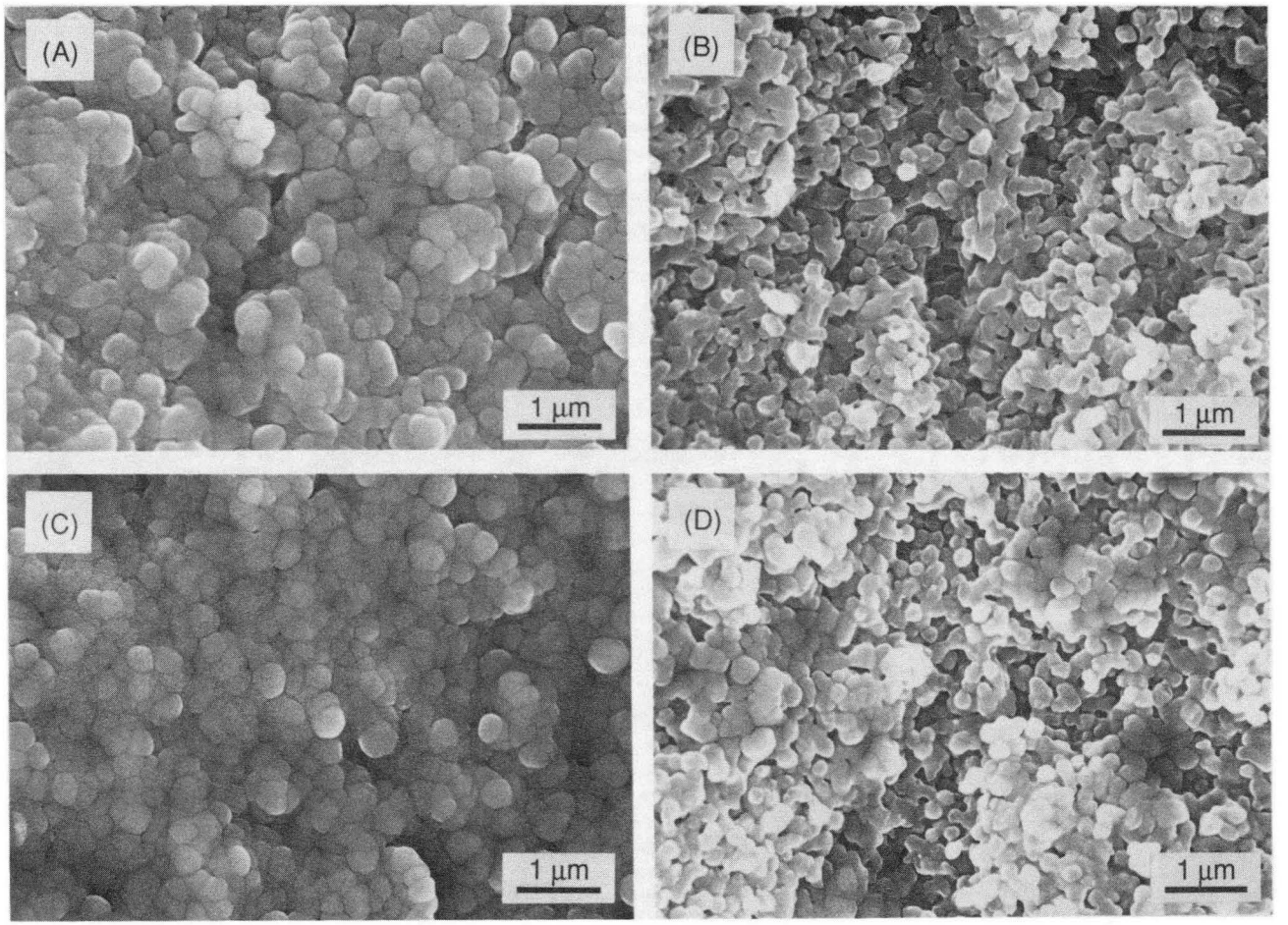

XBB 915-3432

Figure 27 All samples annealed for 1 h at 900°C after pretreatment for 2 h at (A) 400°C, (B) 500°C, (C) 600, (D) 700°C.

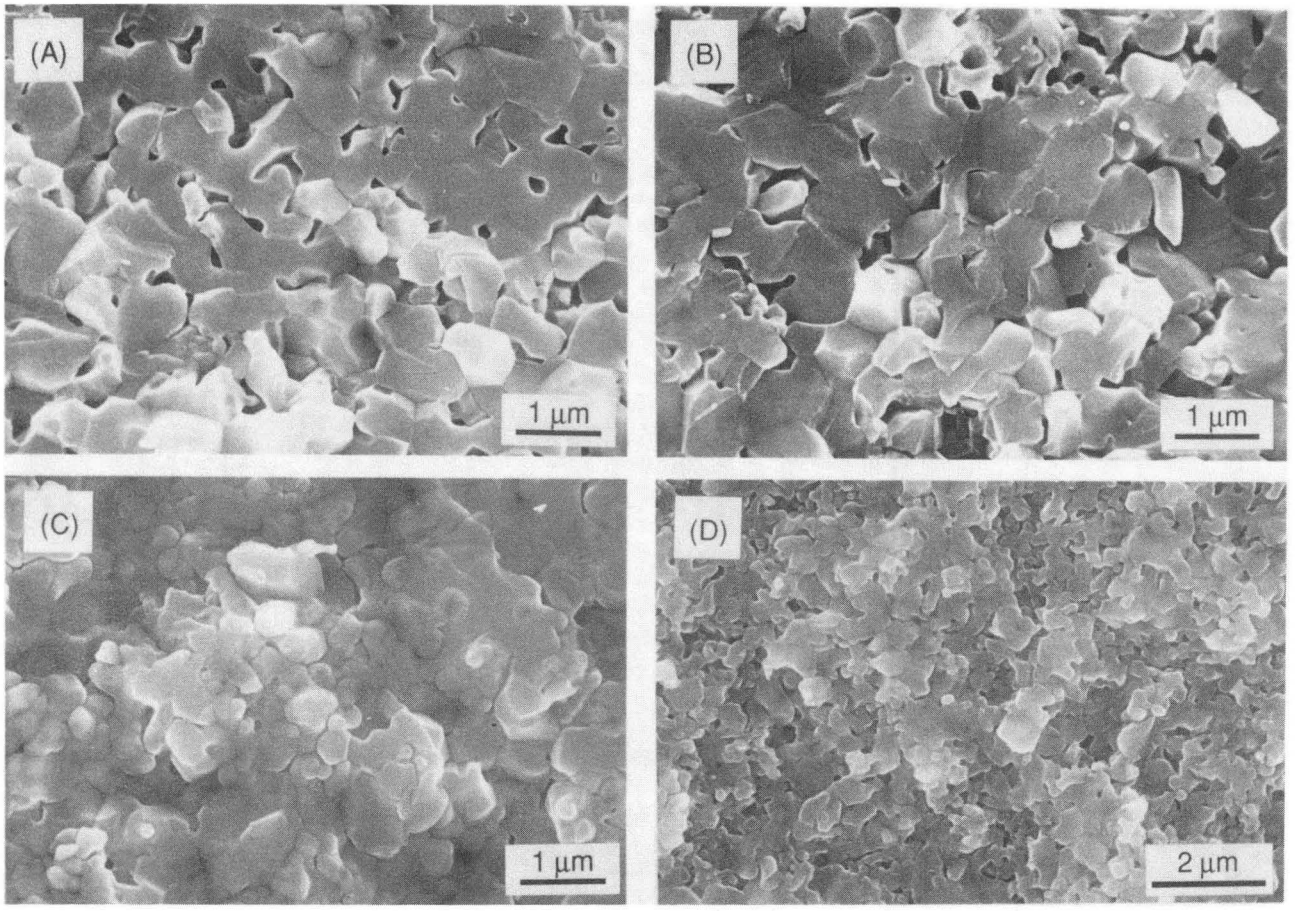

XBB 915-3433

Figure 28 All samples annealed for 1 h at 1000°C after pretreatment for 2 h at (A) 400°C, (B) 500°C, (C) 600, (D) 700°C.

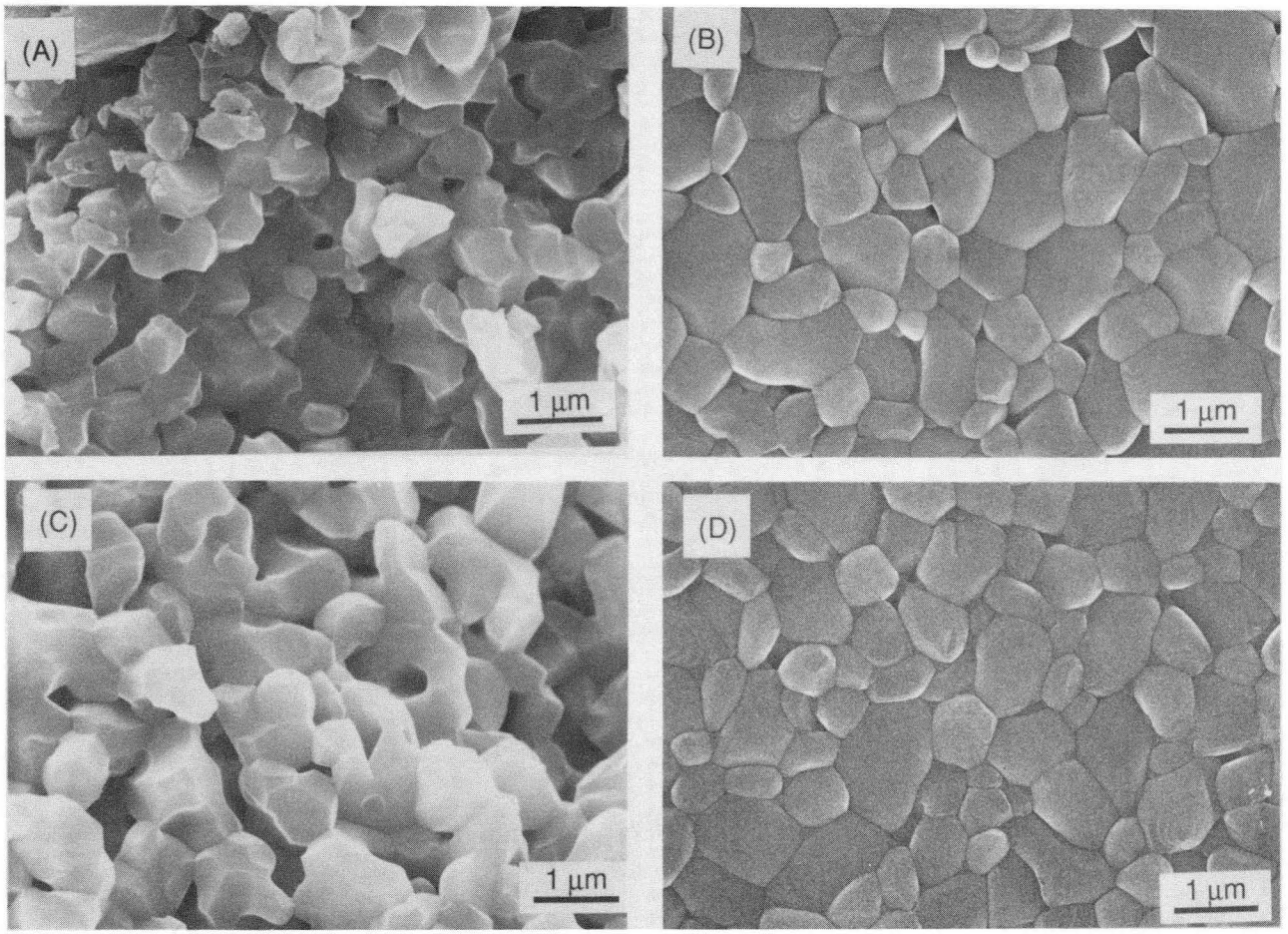

XBB 915-3434

Figure 29 All samples annealed for 1 h at 1100°C after pretreatment for 2 h at (A) 400°C, (B) 500°C, (C) 600, (D) 700°C.

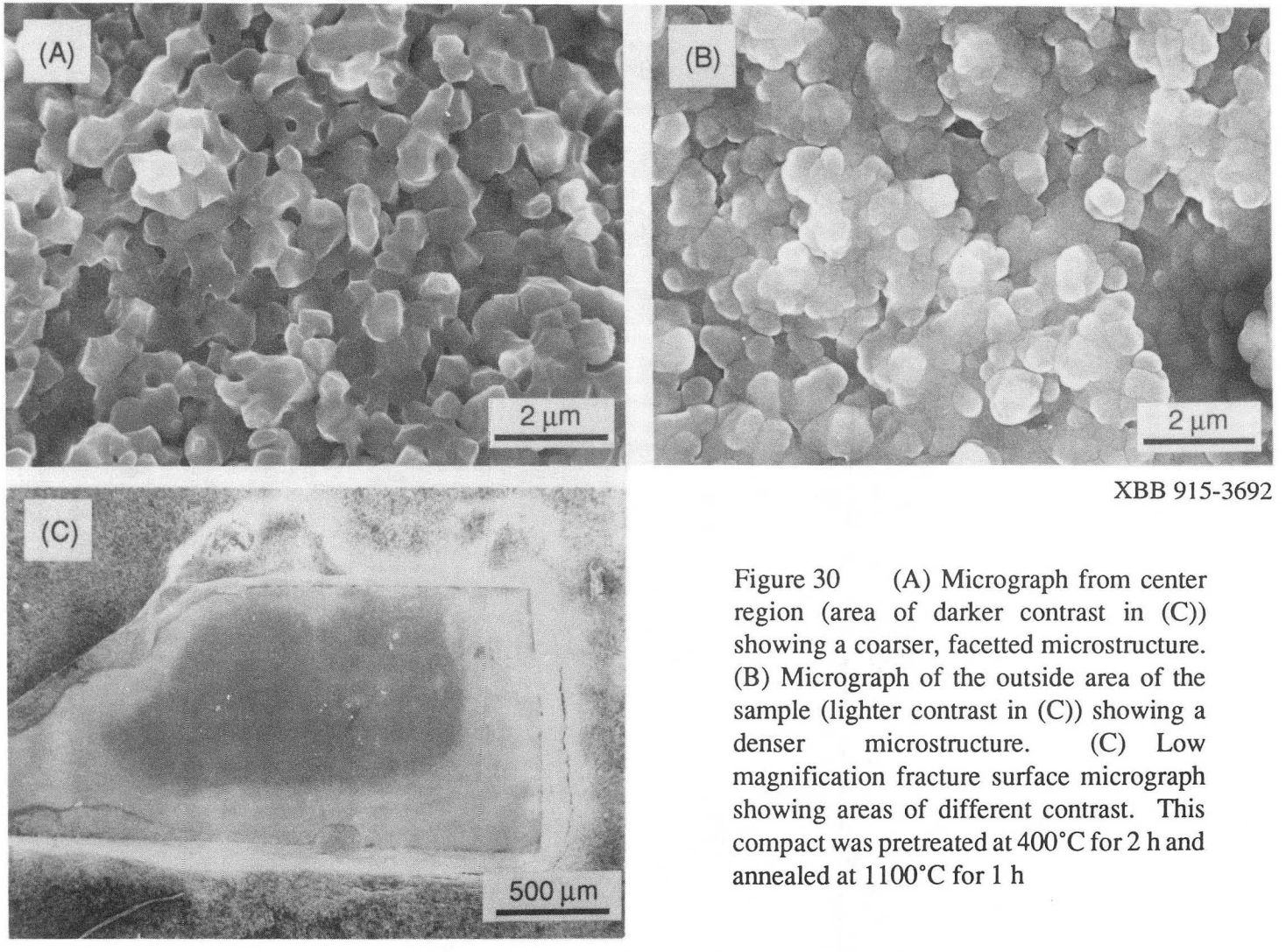

XBB 915-3692

Figure 30 (A) Micrograph from center region (area of darker contrast in (C)) showing a coarser, facetted microstructure. (B) Micrograph of the outside area of the sample (lighter contrast in (C)) showing a denser microstructure. (C) Low magnification fracture surface micrograph showing areas of different contrast. This compact was pretreated at 400°C for 2 h and annealed at 1100°C for 1 h

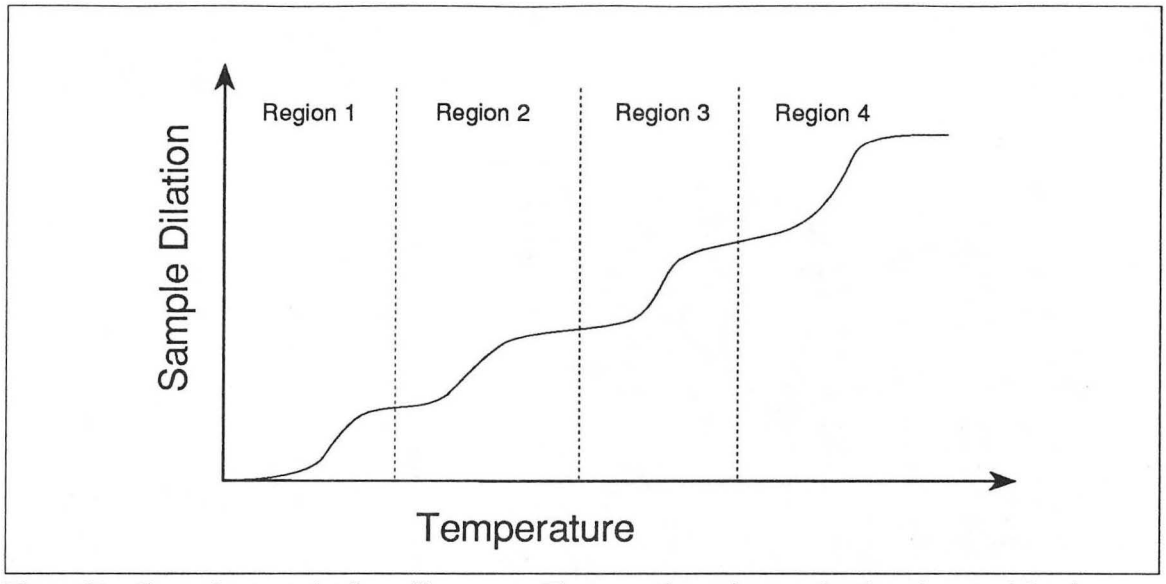

Figure 31. General output plot from dilatometer. The curve shown is smoother than the actual data however the different regions of shrinkage are distinct on the original data.

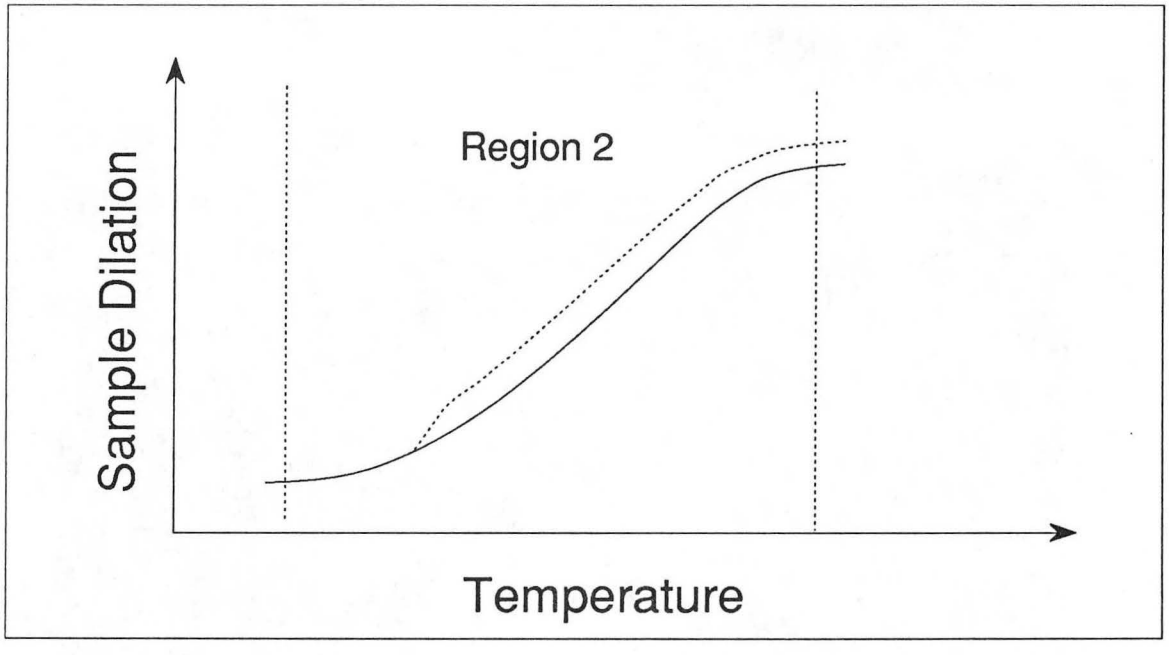

Figure 32. Second region of shrinkage in dilatometer plot. Dashed region indicates feature that would be present if second exothermic peak seen in DSC experiments contributed to shrinkage.

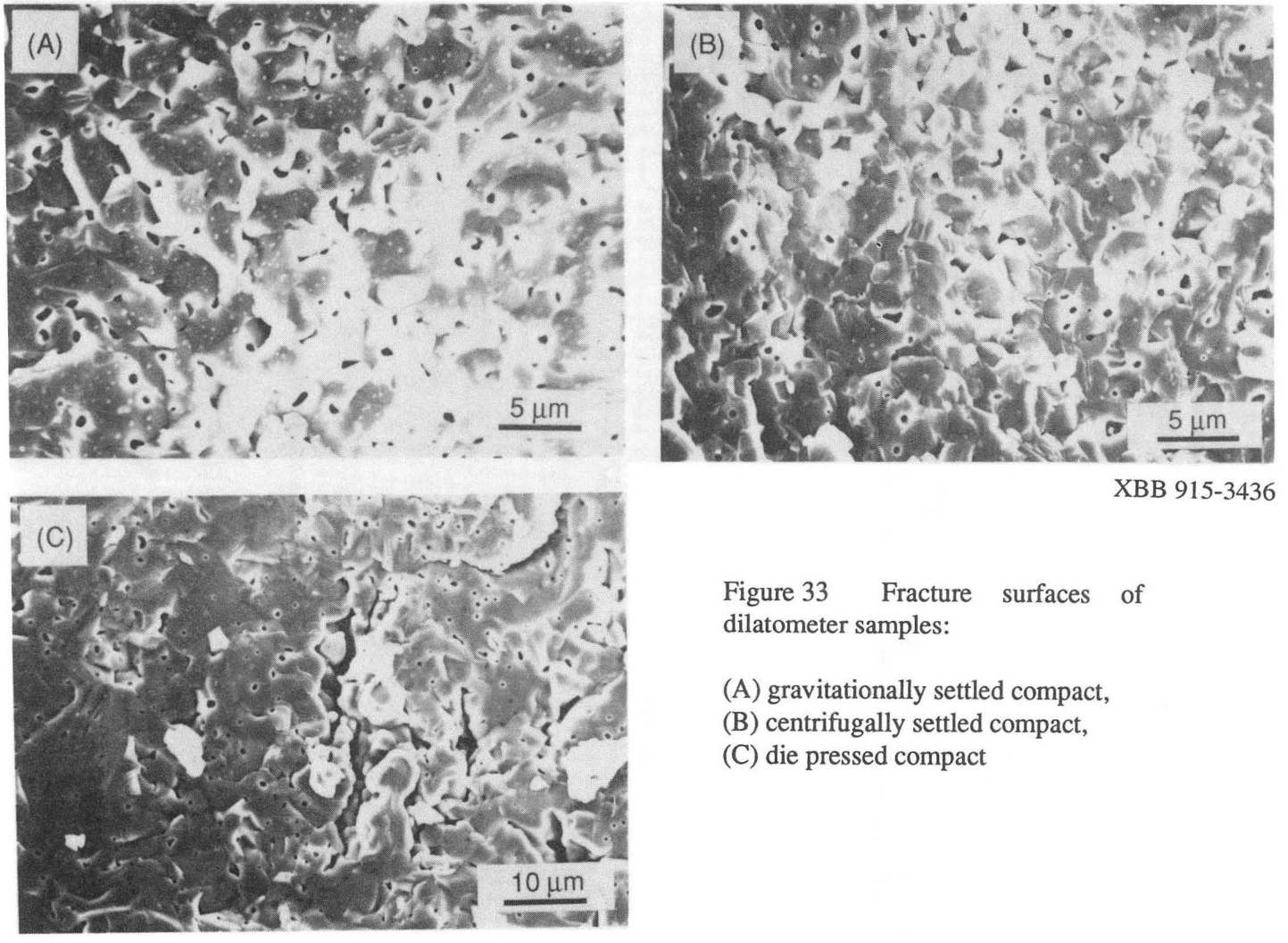

XBB 915-3436

Figure 33 Fracture surfaces of dilatometer samples:

(A) gravitationally settled compact,
(B) centrifugally settled compact,
(C) die pressed compact

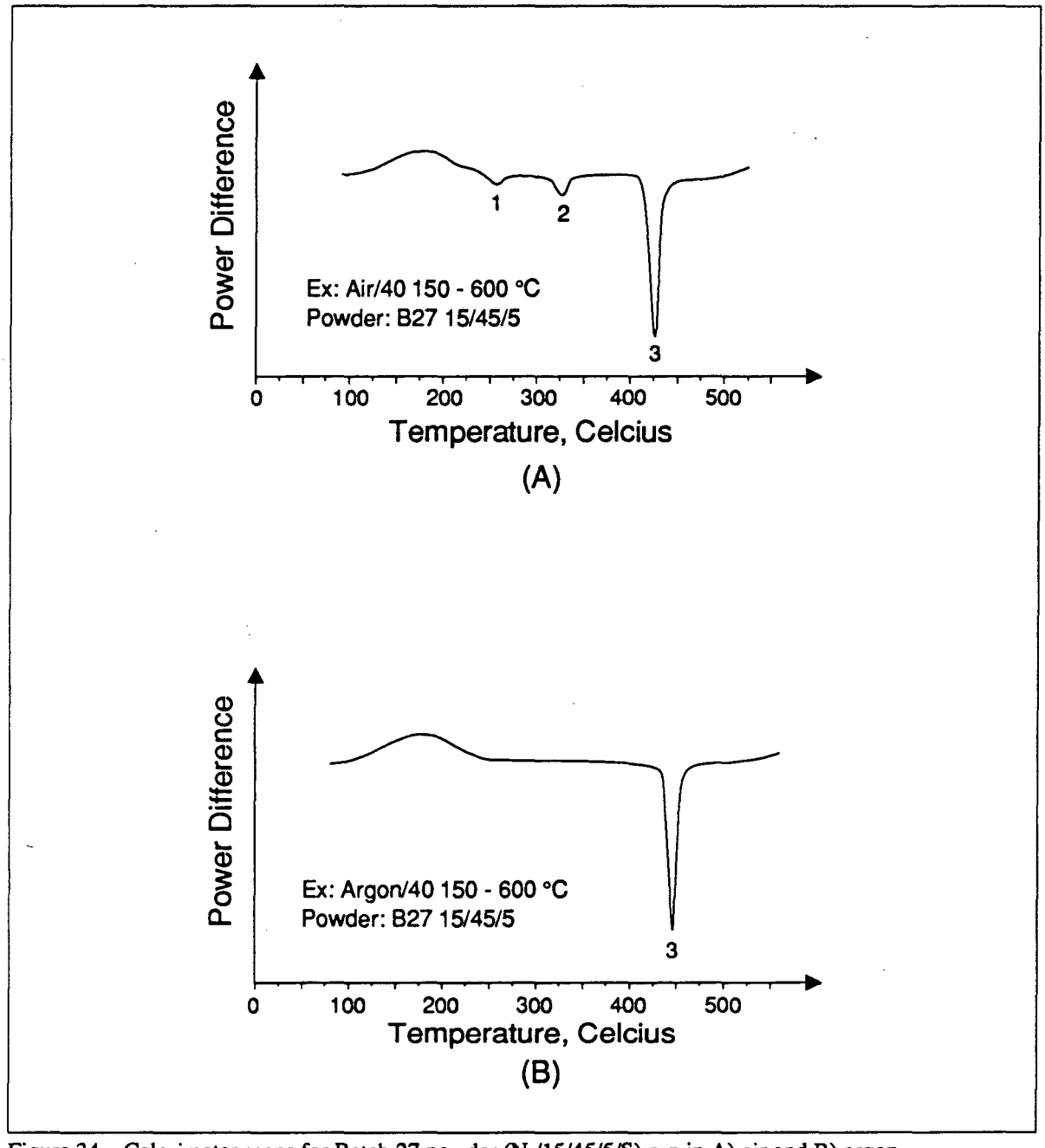

Figure 34. Calorimeter scans for Batch 27 powder (N_2/15/45/5/S) run in A) air.and B) argon.

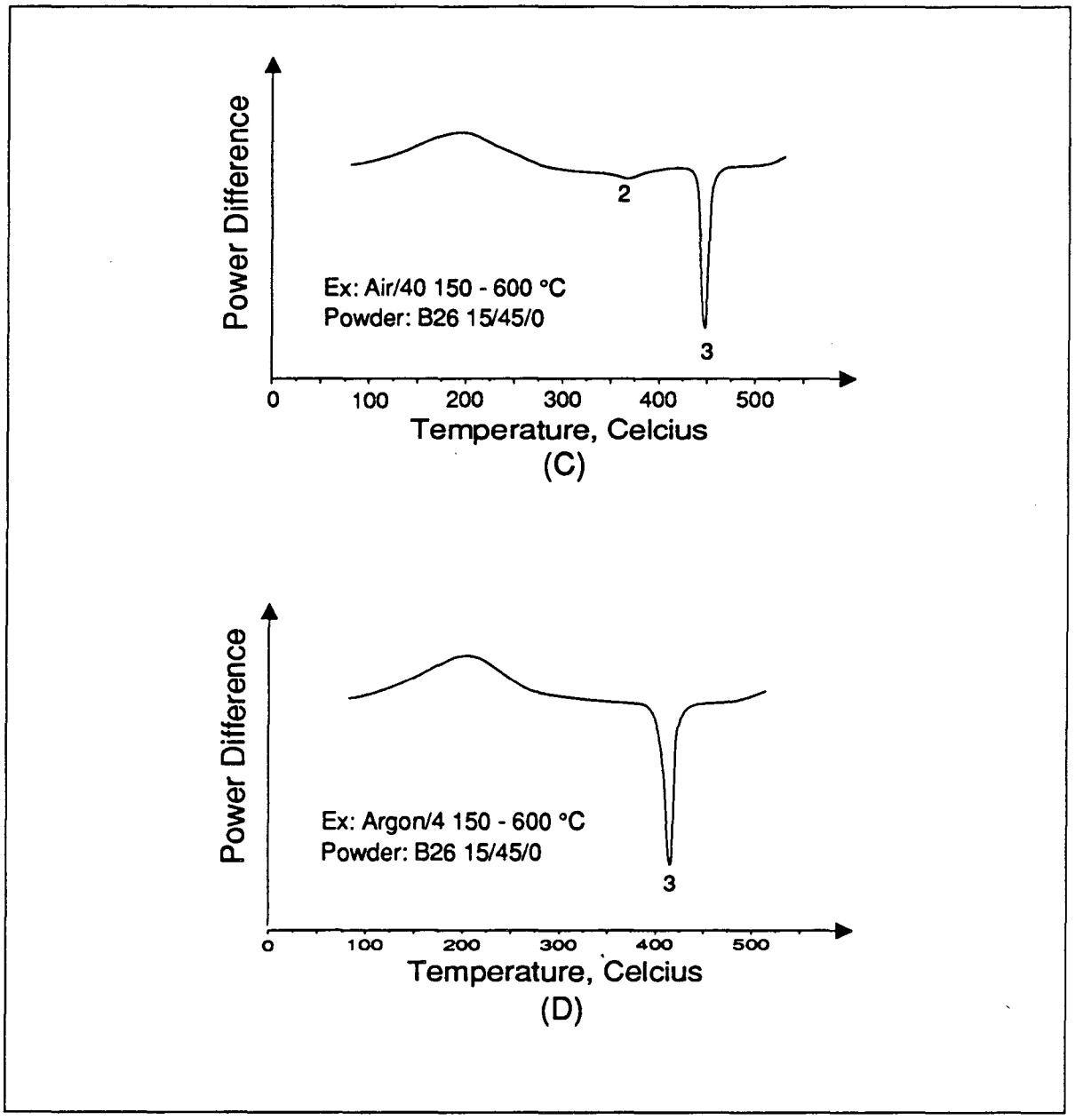

Figure 34 cont.Calorimeter scans for Batch 26 powder (N_2/15/45/0) run in C) air and D) argon.

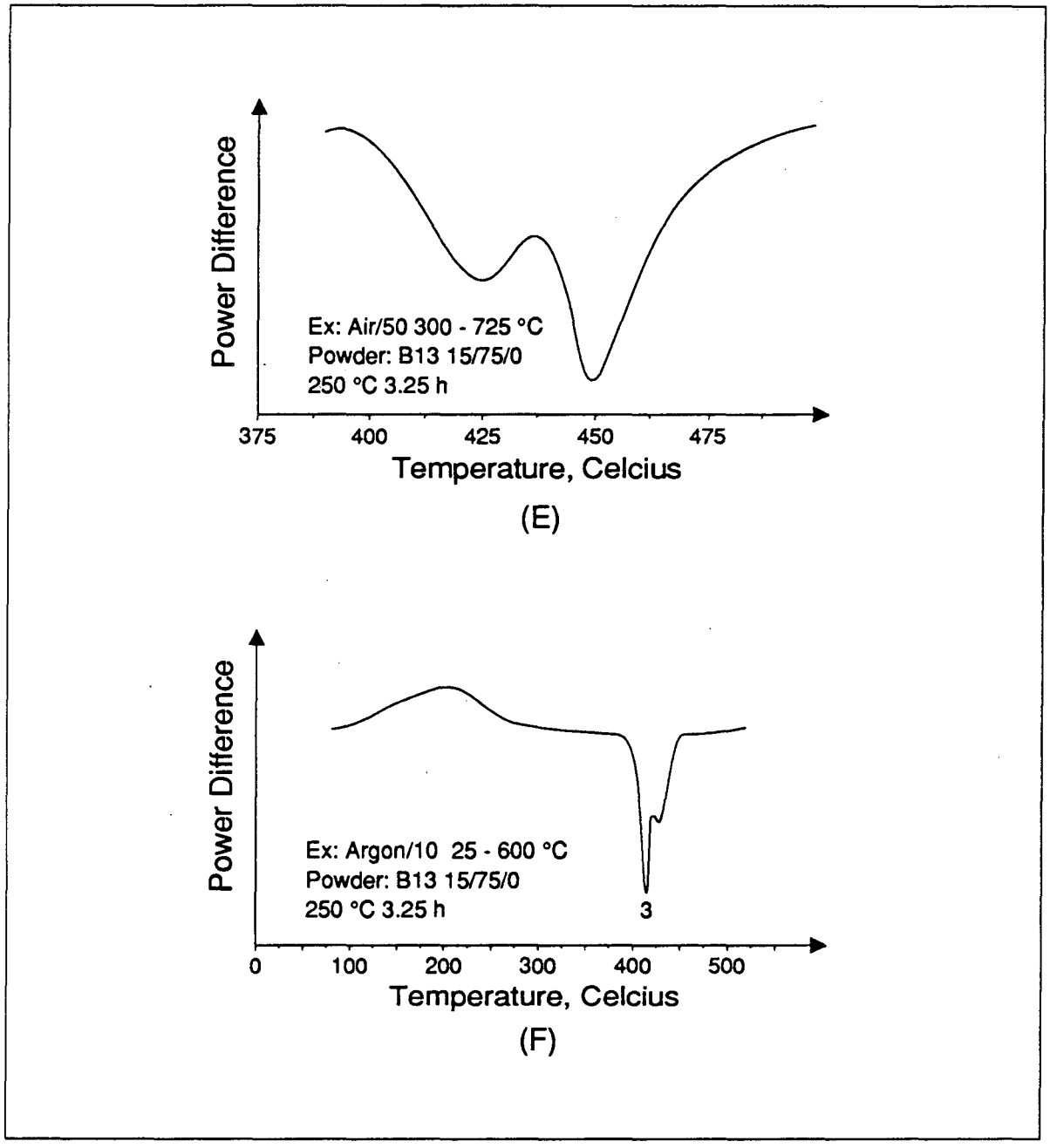

Figure 34 cont.Calorimeter scans for Batch 13 powder run in E) air and F) argon. The powder was pretreated at 250°C for 3.25 h.

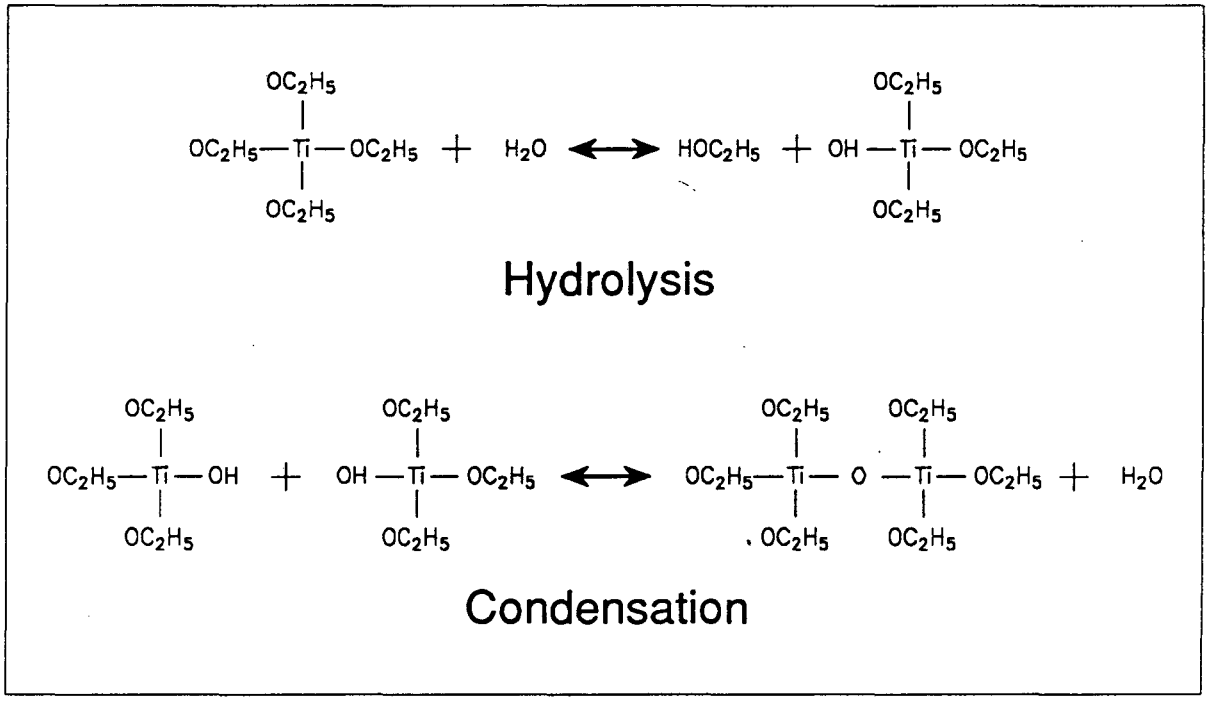

Figure 35. Hydrolysis and subsequent condensation of titanium tetraethoxide to form titania, TiO_2.

7 REFERENCES

7.1 TiO_2 - Phase Transformations

1. N. A. Bendeliani, S. V. Popova and L. F. Vereshchagin, "New Modification of Titanium Dioxide Obtained At High Pressures," Geochemistry International, 3 [3] 387-390 (1966).

2. A. Cimino, D. Gazzoli, and M. Valigi, "The Effect of the Reduction of NH_4ReO_4 Dispersed on Titanium Dioxide on the Anatase-Rutile Transformation," Journal of the Less-Common Metals, 75 85-88 (1980).

3. A. W. Czanderna, C. N. Ramachandra Rao, and J. M. Honig, "The Anatase-Rutile Transition Part 1. Kinetics of the Transformation of Pure Anatase," Trans. of the Faraday Society, 54 [7] 1069-1073 (1958).

4. Frank Dachille, P. Y. Simons and Rustum Roy, "Pressure-Temperature Studies of Anatase, Brookite, Rutile and TiO_2-II," The American Mineralogist, 53 [11-12] 1929-1939 (1968).

5. Emerson F. Heald, and Clair W. Wess, "Kinetics and Mechanism of the Anatase/Rutile Transformation, as Catalyzed By Ferric Oxide and Reducing Conditions," American Mineralogist, 57 [1-2] 10-23 (1972).

6. L. S. Hsu and C. Y. She, "Real-time Monitoring of Crystallization and Structural Transformation of Titania Films with Raman Spectroscopy," Optics Letters, 10 [12] 638-640 (1985).

7. Yoshio Ilda and Shunro Ozaki, "Grain Growth and Phase Transformation of Titanium Oxide During Calcination," J. Appl. Phys., 44 [3] 120-127 (1961).

8. John C. Jamieson and Bart Olinger, "Pressure-Temperature Studies of Anatase, Brookite, Rutile, and TiO_2(II): A Discussion," American Mineralogist, 54 [9-10] 1477-1481 (1969).

9. H. Knoll and U. Kuhnold, "Uber die Stabilitat des Anatas," Naturwissenschaften, 44 394 (1957).

10. Ronald K. Linde and Paul S. DeCarli, "Polymorphic Behavior of Titania under Dynamic Loading," The Journal of Chemical Physics, 50 [1] 319-325 (1969).

11. K. J. D. MacKenzie, "The Calcination of Titania IV. The Effect of Additives on the Anatase-Rutile Transformation," Trans. J. Brit. Cer. Soc., 73 29-34 (1975).

12. K. J. D. MacKenzie, "The Calcination of Titania V. Kinetics and Mechanism of the Anatase-Rutile Transformation in the Presence of Additives," Trans. J. Brit. Cer. Soc., 74 77-84 (1975).

13. K. J. D. MacKenzie, "The Calcination of Titania VI. The Effect of Reaction Atmosphere and Electric Fields on the Anatase-Rutile Transformation," Trans. J. Brit. Cer. Soc., 74 121-125 (1975).

14. T. Mashimo and A. Sawaoka, "Anisotropic Behavior of the Shock-induced Phase Transition of Rutile Phase Titanium-dioxide," Physics Letters A, 78A [4] 419-422 (1980).

15. T. Mitsuhashi and O. J. Kleppa, "Transformation Enthalpies of the TiO_2 Polymorphs," J. Am. Ceram. Soc., 62 [7-8] 356-357 (1979).

16. A. Navrotsky and O. J. Kleppa, "Enthalpy of the Anatase-Rutile Transformation," J. Am. Ceram. Soc., 50 [11] 626 (1967).

17. C. N. R. Rao, "Kinetics and Thermodynamics of the Crystal Structure Transformation of Spectroscopically Pure Anatase to Rutile," Can. J. Chem., 39 [3] 498-500 (1961).

18. C. N. R. Rao, A. Turner, and J. M. Honig, "Some Observations Concerning the Effect of Impurities on the Anatase-Rutile Transition," The Journal of the Physics and Chemistry of Solids, 11 [1/2] 173-175 (1959).

19. C. N. R. Rao, S. R. Yoganarasimhan, and P. A. Faeth, "Studies on the Brookite-Rutile Transformation," Trans. of the Faraday Society, 57 [3] 504-510 (1961).

20. Von F. Schossberger, "Uber die Umwandlung des Titanioxyds," Zeitschfift Fur Krystallographie, 104 pp358-374 (1942).

21. Robert D. Shannon, "Phase Transformation Studies in TiO_2 Supporting Different Defect Mechanisms in Vacuum-Reduced and Hydrogen-Reduced Rutile," J. Appl. Phys., 35 [11] 3414-3416 (1964).

22. Robert D. Shannon and Joseph A. Pask, "Topotaxy in the Anatase-Rutile Transformation," The American Mineralogist, 49 [11-12] 1707-1717 (1964).

23. Robert D. Shannon and Joseph A. Pask, "Kinetics of the Anatase-Rutile Transformation," J. Am. Ceram. Soc., 48 [8] 391-398 (1965).

24. F. W. Vahldiek, "Phase Transition of Titanium Dioxide Under Various Pressures," J. Less-Common Metals, 11 [2] 99-110 (1969)

7.2 TiO_2 - Sintering

25. M. F. Yan and W. W. Rhodes, "Low Temperature Sintering of TiO_2," Mat. Sci. Engin., 61 59-66 (1983).

26. Harlan U. Anderson, "Initial sintering of Rutile," J. Am. Ceram. Soc., 50 [5] 235-238 (1967).

27. Eric A. Barringer and H. Kent Bowen, "Formation, Packing, and Sintering of Monodisperse TiO_2 Powders," J. Am. Ceram. Soc., 67 [12] C-199-C-201 (1982).

28. Lawrence H. Edelson and Andreas M. Glaeser, "Role of Particle Substructure in the Sintering of Monosized Titania," J. Am. Ceram. Soc., 71 [4] 225-235 (1988).

29. A. G. Grotyohann and K. Herrington, "Sintering of Titanium Dioxide," J. Am. Ceram. Soc., 47 [1] 53-54 (1964).

30. K. J. D. MacKenzie, "The Calcination of Titania VII. Sintering of Rutile," Trans. J. Brit. Cer. Soc., 74 127-124 (1975).

31. H. M. O'Bryan, Jr. and G. Parravano, "On the Sintering of Single Crystal Rutile," Mat. Sci. Engin., 1 [3] 177-182 (1966).

32. Michael J. Readey and Dennis W. Readey, "Sintering TiO_2 in HCl Atmospheres," J. Am. Ceram. Soc., 70 [12] C358-C361 (1987).

33. D. H. Whitmore and Toshihiko Kawai, "Kinetics of Initial Sintering of Vacuum-Reduced Titanium Dioxide," J. Am. Ceram. Soc., 45 [8] 375-379 (1962).

34. Wayne S. Young and Ivan B. Cutler, "Initial Sintering with Constant Rates of Heating," J. Am. Ceram. Soc., 53 [12] 659-663 (1970).

7.3 TiO_2 - Synthesis

35. Yoko Suyama and Akio Kato, "Effect of Additives on the Formation of TiO_2 Particles by Vapor-Phase Reaction," J. Am. Ceram. Soc., 68 [6] C154-C156 (1985).

36. Yoko Suyama and Akio Kato, "TiO_2 Produced by Vapor-Phase Oxygenolysis of $TiCl_4$," J. Am. Ceram. Soc., 59 [3-4] 146-149 (1976).

37. R. W. Siegel, S. Ramasamy, H. Hahn, Li Zongquan, Lu Ting, and R. Gronsky, "Synthesis, Characterization and Properties of Nanophase TiO_2," J. Mater. Res., 3 [6] 1367-1372 (1988).

38. Paul Nahass and H. K. Bowen, "Precipitation of Titania in a Continuous-flow Reactor with an Organic Base Stabilizer," Mat. Sci. Engin., 100 235-240 (1988).

39. Sridhar Komarneni, Rustum Roy, and Else Breval, "A New Method of Making Titania Gels and Their Microstructure," J. Am. Ceram. Soc., 68 [2] C41-C42 (1985).

40. Lisa Lazorka, Herbert Short, Eric Johnson, "TiO_2's Future is Keyed to New Technologies," Chemical Engineering, Jan. pp37-41 (1989).

41. A. W. Czanderna, A. F. Clifford and J. M. Honig, "Preparation of Highly Purified TiO_2 (Anatase)," J. Amer. Chem. Soc., 79 [10] 5408-5410 (1957).

7.4 Titanium - Oxygen Structure

42. National Bureau of Standards, "Titanium Oxide (anatase), TiO_2 (tetraganol)(revised)," U.S. National Bureau of Standards Monograph 25, [7] p 82 (1969).

43. National Bureau of Standards, "Titanium Oxide (rutile), TiO_2 (tetraganol)(revised)," U.S. National Bureau of Standards Monograph 25, [7] p 83 (1969).

44. T. Ohsaka, S. Yamaoka and O. Shimomura, "Effect of Hydrostatic Pressure on the Raman Stectrum of Anatase (TiO_2)," Solid State Commun., 30 [6] 345-347 (1979).

45. Arne Magneli and Bengt-Olov Marinder, "On the Structural Geometry and the Metal-Metal Distances of Some Groups of Transition Metal Oxides with an Oxygen Arrangement Approaching Close Packing," Arkiv För Kemi, 407-412 (1964).

46. R. C. DeVries and Rustum Roy, "A Phase Diagram for the System Ti-TiO_2 Constructed from Data in the Literature," Am. Ceram. Soc. Bull., 33 [12] 370-372 (1954).

47. Sten Andersson, Bengt Collen, Georg Krusse, Ulf Kuylenstierna, Arne Magneli, Herbert Pestmalis and Stig Asbrink, "Identification of Titanium Oxides by X-Ray Powder Patterns," Acta Chem. Scand., 11 [10] 1653-1657 (1957).

48. Sten Andersson and Lena Jahnberg, "Crystal Structure Studies on the Homologous Series Ti_nO_{2n-1}, V_nO_{2n-1} and $Ti_n\ 2Cr_2O_{2n-1}$," Arkiv För Kemi, 413-426 (1964).

49. Sten Andersson, Bengt Collen, Ulf Kuylenstierna and Arne Magneli, "Phase Analysis Studies on the Titanium-Oxygen System," Acta Chem. Scand., 11 [10] 1641-1652 (1957).

50. Gudrun Asbrink, Stig Asbrink, Arne Magneli, Hideyuki Okinaka, Koji Kosuge and Sukeji Kachi, "A Ti_3O_5 Modification of V_3O_5-type Structure," Acta Chem. Scand., 25 [10] 3889-3890 (1971).

51. U. Balachandran and N. G. Eror, "Raman Spectra of Titanium Dioxide," Journal of Solid State Chemistry, 42 276-282 (1982).

52. Yukio Yamada and Kazuhiko Yoshida, "Electron Microscope Study of the δ-Phase in Titanium Oxide Evaporated Films," Japanese Journal of Applies Physics, 22 [1] 36-41 (1983).

53. Yukio Yamada, "Electron Microscopic Study of Transition Structures Formed from Titanium Oxide Evaporated Films," Japanese Journal of Applied Physics, 22 [1] 29-35 (1983).

54. Dieter Schwarzenbach, "The Structure of a Chelated Dinuclear Peroxytitanium(IV)," Inorganic Chemistry, 9 [11] 2391-2397 (1970).

7.5 TiO_2 - General

55. William F. Sullivan and Sandford S. Cole, "Thermal Chemistry of colliodal Titanium Dioxide," J. Am. Ceram. Soc., 42 [3] 127-133 (1959).

56. R. N. Blumenthal and D. H,. Whitmore, "Thermodynamic Study of Phase Equilibria in the Titanium-Oxygen System within the $TiO_{1.95}$-TiO_2 Region," Journal of the Electrochemical Society, 110 [1] 92-93 (1963).

57. Jau-Ho Jean and Terry A. Ring, "Processing Monosized TiO_2 Powders Generated with HPC Dispersant," Am. Ceram. Soc. Bull., 65 [12] 1574-1577 (1986).

58. T. V. Charlu, O. J. Kleppa, and T. B. Reed, "High-temperature Combustion Calorimetry III. Enthalpies of formation of Titanium Oxides," J. Chem. Thermodynamics, 6 [11] 1065-1074 (1974).

59. D. M. J. Compton and T. E. Firle, "Reduction of TiO_2 Powders and Rutile Single Crystals," J. Am. Ceram. Soc., 52 [9] 515-516 (1969).

60. Lawrence Edelson and Andreas M. Glaeser, "Effects of Thermal Pretreatment on Coarsening of Nominally Monodispersed Titania," J. Am. Ceram. Soc., 71 [4] C-198-C-201 (1988).

61. F. A. Grant, "Properties of Rutile (Titanium Dioxide)," Reviews of Modern Physics, 31 [3] 646-674 (1959).

62. K. J. D. MacKenzie, "The Calcination of Titania I. Kinetics of Crystallite Growth in TiO_2 (Anatase) Powders," Trans. J. Brit. Cer. Soc., 73 23-27 (1974).

63. K. J. D. MacKenzie, "The Calcination of Titania II. Influence of Atmosphere on Crystal Growth in Anatase Powders," Trans. J. Brit. Cer. Soc., 73 179-183 (1974).

64. K. J. D. MacKenzie, "The Calcination of Titania III. Effect of Electric Fields on Crystal Growth in Anatase," Trans. J. Brit. Cer. Soc., 73 185-189 (1974).

65. Rene Marchand, Luc Brohan and Michel Tournoux, "TiO_2(B) A New Form of Titanium Dioxide and the Potassuim Octatitanate $K_2Ti_8O_{17}$," Mat. Res. Bull., 15 [3] 1129-1133 (1980).

66. C. Howard Shomate, "Heat Capacities at Low Temperatures of Titanium Dioxide (Rutile and Anatase)," J. Amer. Chem. Soc., 69 [2] 218-219 (1947).

67. M. E. Straumanis, T. Ejima and W. J. James, "The TiO_2 Phase Explored by the Lattice Constant and Density Method," Acta Cryst., 14 [5] 493-497 (1961).

68. D. A. Venkatu and L. E. Poteat, "Diffusion of Titanium in Single Crystal Rutile," Mat. Sci. Engin., 5 258-262 (1970).

69. Lawrence H. Edelson, Masters Thesis, Department of Materials Science, University of California, Berkeley CA (1986).

70. Eric A. Barringer, PhD. Thesis, Department of Materials Science and Engineering, MIT,Cambridge MA (1983).

71. Lawrence H. Edelson, private communications.

72. Simon Moss, private communications.

7.6 Ultramicrotomy

73. Jean-Dominique Acetarin, Eric Carlemalm, Eduard Kellenberger, and Werner Villiger, "Correlation of Some Mechanical Properties of Embedding Resins with Their Behaviour in Microtomy," J. of Electron Microscopy Technique, Vol. 6 [1] 63-79 (1987).

74. Specimen Preparation for Transmission Electron Microscopy of Materials, Materials Reserach Society Symposium Proceedings Vol. 115 Ed. John C. Bravman et al. (1988)

75. Roseann Csencsits and Ronald Gronsky, "Preparation of Zeolites for TEM Using Microtomy," in Specimen Preparation for Transmission Electron Microscopy of Materials, Mat. Res. Soc. Symp. Proc., Vol. 115 (1988).

76. David G. Pickles and Edward Lilley, "Ultramicrotoming of Ceramic Powders for Electron Microscopy," J. Am. Ceram. Soc., 68 [9] C-222 - C223 (1985).

77. Norma Reid, "Ultramicrotomy," in Practical Methods in Electron Microscopy Vol. 3 Part II North-Holland Publishing Company: Amsterdam (1976).

78. D. F. Blake, T. E. Bunch, D. E. Philpott, and R. Zeiger, "A Simple Device for the Preparation of Embedded Materials Science Specimens for Ultramicrotomy," Journal of Electron Microscopy Technique, 6 305-306 (1987).

7.7 Sol-Gel Processing of Ceramics

79. Rustem Roy, "Ceramics by the Solution-Sol-Gel Route," Science, Vol. 238 1664-1669 (1987).

80. Donald R. Ulrich, "Chemical Processing Ceramics," Chenical and ENgineering News, Vol. 68 Jan. 28-40 (1990)

81. Paola Gherardi and Egon Matijevic, "Interactons of Precipitated Hematite with Preformed Colloidal Titania Dispersions," Journal of Colloid and Iterface Science, Vol. 109, No. 1, 57-68 January (1986).

82. J.M. Bind, T Dupin, H. Schafer and M. Titeux, "Industrial Synthesis of Coprecipitated $BaTiO_3$ Powders," Journal of Metals, Vol. 39 60-61 (1987).

83. Shin-Ichi Hirano, Takashi Hayashi, and Tomoyuki Kageyama, "Synthesis of $LiAlO_2$ Powder by Hydrolysis of Metal Alkoxides," J. Am. Ceram. Soc., 70 [3] 171-74 (1987).

84. David W. Johnson, Jr., "Sol-Gel Processng of Ceramics and Glass," Am. Ceram. Soc. Bull., 64 [12] 1597-1602 (1985).

85. Nikola Kallay and Darko Babic, "Adsorption at Solid/Solution Interfaces II. Surface Charge and Potential of Spherical Colloidal Titania," Colloids and Surfaces, Vol. 19 375-386 (1986).

86. Egon Matijevic, "Monodispersed Colloids: Art and Science," Langmuir, Vol. 2 [1] 12-20 (1986).

87. K.S. Mazdiyasni, R.T. Dolloff, and J.S. Smith II, "Preparation of High-Purity Submicron Barium Titanate Powders," Journal of The American Ceramic Society, Vol. 52 [10] 523-526 (1969).

88. L.S. Millberg, "The Synthesis of Ceramic Powders," Journal of Metals, Vol 39 9-13 (1987).

89. Jim Johnston, "Metal Alkoxides for Sol-Gel Applications," Applications Research Group Dynamit Nobel Chemicals.

90. Egon Matijevic and Paul Scheiner, "Ferric Hydrous Oxide Sols," Journal of Colloid and Interface Science, **63** [3] 509-524 (1978).

91. Masataka Ozaki, Stanka Kratohvil, and Egon Matijevic, "Formation of Monodispersed Spindle-Type Hematite Particles," Journal of Colloid and Interface Science, **102** [1] 146-151 (1984).

92. Shuichi Hamada and Egon Matijevic, "Ferric Hydrous Oxide Sols. IV. Preparation of Uniform Cubic Hematite Particles by Hydrolysis of Ferric Chloride in Alcohol-Water Solutions," Journal of Colloid and Interface Science, **84** [1] 274-277 (1981).

93. Shuichi Hamada nad Egon Matijevic, "Formation of Monodispersed Colloidal Cubic Haematite Particles in Ethanol + Water Solutions," J. Chem. Soc., Faraday Trans. I, **78** 2147-2156 (1982).

7.8 Phase Transformation - General

94. J. M. Honig, "Application of Order-Disorder Concepts to Kinetics of Diffusionless Transitions in Solids," J. Of Chemical Physics, 28 [4] (1958).

95. Melvin Avrami, "Kinetics of Phase Change. I General Theory," Journal of Chemical Physics, 7 [12] 1103-1112 (1939).

96. Melvin Avrami, "Kinetics of Phase Change. II Transformation-Time Relations for Random Distribution of Nuclei," J. Chem. Phys., 8 [3] 212-224 (1940).

7.9 Sintering - General

97. B. E. Yoldas, "Effect of Variations in Polymerized Oxides on Sintering and Crystalline Transformations," J. Am. Ceram. Soc., 65 [8] 387-393 (1982)

98. M. F. Ashby and R. M. A. Centamore, "The Dragging of Small Oxide Particles By Migrating Grain Boundaries on Copper," Acta Met., 16 [9] 1081-1092 (1968).

99. W. Beere, "A Unifying Theory of the Stability of Penetrating Liquid Phases and Sintering Pores," Acta Met., 23 [1] 131-138 (1975).

100. W. Beere, "The Second Stage Sintering Kinetics of Powder Compacts," Acta Met., 23 [1] 139-145 (1975).

101. R. J. Brook, "Pore-Grain Boundary Interactions and Grain Growth," J. Am. Ceram. Soc., 52 [1] 56-57 (1969).

102. J. E. Burke and J. H. Rosolowski, "Sintering," in Treatise on Solid State Chemistry, [Reactivity of Solids, Vol. IV], Ed., N. Hannay, Plennum Press, 1976, pp. 621-659.

103. John W. Cahn, "The Impurity-Drag Effect in Grain Boundary Motion," Acta Met., 10 [9] 789-798 (1962).

104. F. M. A. Carpay, "Discontinous Grain Growth and Pore Drag," J. Am. Ceram. Soc., 60 [1-2] 82-83 (1977).

105. R. L. Coble, "Sintering Crystalline Solids. II. Experimental Test of Diffusion Models in Powder Compacts," J. Appl. Phys., 32 [5] 793-799 (1961).

106. R. L. Coble, "Sintering Crystalline Solids. I. Intermediate and Final State Diffusion Models," J. Appl. Phys., 32 [5] 787-792 (1961).

107. J. Frenkel, "Viscous Flow of Crystalline Bodies Under the Action of Surface Tension," Journal of Physics (USSR), 9 [5] 385-391 (1945).

108. C. Greskovich and J. H. Rosolowski, "Sintering of Covalent Solids," J. Am. Ceram. Soc., 59 [7-8] 336-343 (1976).

109. C. Greskovich and K. W. Lay, "Grain Growth in Very Porous Al_2O_3 Compacts," J. Am. Ceram. Soc., 55 [3] 142-146 (1972).

110. Conyers Herring, "Effect of Change of Scale on Sintering Phenomena," J. Appl. Phys., 21 [4] 301-303 (1950).

111. M. Hillert, "On the Theory of Normal and Abnormal Grain Growth," Acta Met., 13 [3] 227-238 (1965).

112. D. Lynn Johnson and Ivan B. Cutler, "Diffusion Sintering: I, Initial Stage Sintering Models and Their Application to Shrinkage of Powder Compacts," J. Am. Ceram. Soc., 46 [11] 541-544 (1963)

113. D. Lynn Johnson and Ivan B. Cutler, "Diffusion Sintering: II, Initial Sintering Kinetics of Alumina," J. Am. Ceram. Soc., 46 [11] 545-550 (1963)

114. D. Lynn Johnson, "New Method of Obtaining Volume, Grain-Boundary, and Surface Diffusion Coefficients from Sintering Data," J. Appl. Phys., 40 [1] 192-200 (1969).

115. W. D. Kingery and M. Berg, "Study of the Initial Stages of Sintering Solids by Viscous Flow, Evaporation-Condensation, and Self Diffusion," J. Appl. Phys., 26 [10] 1205-1212 (1955)

116. W. D. Kingery and B. Francois, "Grain Growth in Porous Compacts," J. Am. Ceram. Soc., 48 [10] 546-547 (1965).

117. G. C. Kuczynski, "Self-diffusion in Sintering of Metallic Particles," Trans. A.I.M.M.E., 185 [2] 169-178 (1949).

118. F. V. Lenel, "Sintering of A Single Phase Metal Powder - Mechanism of Sintering," in Powder Metallurgy - Principles and Applications, Metal Powder Industries Federation, Princeton, New Jersey, 1980, pp. 241-267.

119. K. Lucke and H. P. Stuwe, "On the Theory of Impurity Controlled Grain Boundary Motion," Acta Met., 19 [10] 1087-1099 (1971).

120. M. N. Rahaman and L. C. De Jonghe and R. J. Brook, "Effect of Shear Stress on Sintering," J. Am. Ceram. Soc., 69 [1] 53-58 (1986).

121. M. N. Rahaman, L. C. De Jonghe and C. H. Hsueh, "Creep During Sintering of Porous Compacts," J. Am. Ceram. Soc., 69 [1] 58-60 (1986).

7.10 General

122. Man F. Yan, "Microstructural Control in the Processing of Electronic Ceramics," Mat Sci. Engin., 48 53-72 (1981).

123. L. C. De Jonghe and M. N. Rahaman, "Loading Dilatometer," Rev. Sci. Instrum., 55 [12] 2007-2010 (1984).

124. V. N. Filipovich and A. M. Kalinina, "Critical Amorphization Radius of Crystals," Structural Transformations in Glass At High Temperatures, 5 34-38 (1965).

125. R. L. Fullman, "Measurement of Particle Sizes in Opaque Bodies," Trans AIME, 5 [3] 447-452 (1953).

126. G. W. Greenwood, "The Growth of Dispersed Precipitates in Solutions," Acta Met., 4 [5] 243-248 (1956).

127. Conyers Herring, "Diffusional Viscosity of a Polycrystalline Solid," J. Appl. Phys., 21 [5] 437-445 (1950).

128. I. M. Lifshitz and V. V. Slyozov, "The Kinetics of Precipitation From Supersaturated Solid Solutions," J. Phys. Chem. Solids, 19 [1-2] 35-50 (1961).

129. Bengt-Olov Marinder and Arne Magneli, "Metal-Metal Bonding in Some Transition Metal Dioxides," Acta Chem. Scand., 11 [10] 1635-1640 (1957).

130. E. F. Osborn, "Subsolidus Reactions in Oxide Systems in the Presence of Water at High Pressures," J. Am. Ceram. Soc., 36 [5] 147-151 (1953).

131. Jenqdaw Wang and Rishi Raj, "Estimate of the Activation Energies for Boundary Diffusion from Rate-Controlled Sintering of Pure Alumina, and Alumina Doped with Zirconia or Titania," J. Am. Ceram. Soc., 73 [5] 1172-1175 (1990).

132. CRC Handbook of Physics and Chemistry, Sixty Third Edition, Published by the Chemical Rubber Company.

8 APPENDIX 1: Ultramicrotomy

8.1 Razor Blade

The mechanical stresses produced at the block tip while employing this method were relatively large and difficult to control. Because an extremely small block face was required this method of preparation proved inadequate. The samples tended to crack and break off long before a small enough block face was produced. However, biologists may use this method because their specimens (most of which are relatively soft plant and animal tissue) do not require as small a block face as material science samples do and because the resin used by most biologists is not as hard as the LR White® resin.

8.2 Sanding Jig

The blockface dimensions which could be achieved reproducibly by this method were on the order or 100 μm. However, the device described by Blake was very cumbersome to use and did not work well. The hole in the jig, in which the lucite was held, was made to very accurate dimensions however the acrylic rods available were not. Therefore when the rod was in the jig, the axis of the rod and the hole did not coincide. This caused the axes to shift relative to one another when the rod was rotated. Thus, tedious and often incorrect alignment resulted. Frequently the sample was accidentally sanded completely away. This method had less than a 30% success rate and was eventually abandoned.

8.3 Hand Sanding

Using this method one could produce a block face of similar dimensions as if the jig were used. After some practice, this method proved somewhat more effective than using the jig but still frequently resulted in oversanding and subsequent loss of the specimen.

8.4 Minisander

Using a miniature sanding wheel and aided by a 40 power binocular microscope, block faces with dimensions on the order of 25 μm were routinely fashioned. The minisander method resulted in a success ratio greater than 85%. Compared to the other methods, this

one offered a greater success rate and improved blockface size. In addition, time is also saved. It takes nominally 20 minutes to shape a block-face to proper dimensions using the minisander compared to at least 40 minutes using one of the other methods.

9 APPENDIX 2: Sample Data

9.1 Sample Identification Tables

Batch ID#	Description
B2	N_2/15/45/0.635/C
B3	N_2/15/45/0.635/C
B4	N_2/15/45/0.635/C
B5	N_2/15/45/0.635/C
B6	N_2/15/45/0.635/C
B7	Air/15/75/5
B8	Air/15/75/5
B9	Air/15/75/5
B10	Air/15/75/5
B11	Air/15/75/5
B12	Air/15/75/5
B13	N_2/15/75/0/C
B14	N_2/15/75/0.34/C
B15	N_2/15/45/5/SC
B16	N_2/15/45/5/SC
B17	N_2/15/45/5/SC
B18	N_2/15/45/5/SC
B19	N_2/15/45/5/SC
B20	N_2/15/45/5/SC
B21	N_2/15/45/5/SC
B22	N_2/15/45/5/SC
B23	N_2/15/45/5/SC
B24	N_2/15/45/5/SC
B25	N_2/15/45/5/SC
B26	N_2/15/45/0
B27	N_2/15/45/5
B28	N_2/15/45/5

Table 14. Powder synthesis variables. Nomenclature: Atmosphere / [$Ti(C_2H_5)_4$] (Molarity) * 100 / [H_2O] (Molarity) * 100 / [HPC] (gm/cc) * 1000 / S = stock solution used; C=centrifugally classified.

9.2 Dilatometry Sample Identification

SAMPLE	PREPARATION	PRETREATMENT	HEATING SCHEDULE
D4	Batch 17, Compact 2, Centrifugally settled	Boiled in H_2O for 24h	• RT to 335°C over 2.5 h • hold 25 min at 335°C • 4°C/min to 1200°C
D5	Batch 17, Compact 2, Centrifugally settled	Boiled in H_2O for 24h	• Direct insertion into 300°C hot zone of dilatometer furnace • 300 to 1300°C at 4°C/min
D7	Batch 17, Compact 2, Centrifugally settled	Boiled in H_2O for 24h	• RT to 300°C over 1.5 h • 1°C/min to 350°C • hold 30 min at 350°C • 4°C/min to 1350°C
D8	Batch 16, Compact 1, Gravationally settled	None	• RT to 300°C over 1.5 h • 2°C/min to 400°C • 4°C/min to 1350°C
D9	Batch 16, Compact 1, Gravationally settled	None	• RT to 300°C over 1.5 h • 2°C/min to 400°C • 4°C/min to 1350°C
D10	Batch 17, Compact 1, Centrifugally settled	None	• RT to 300°C over 1.5 h • 2°C/min to 400°C • 4°C/min to 1350°C
D13	Batch 24, Die pressed compact	Heated slowly to 200°C	• RT to 300°C over 1.5 h • 2°C/min to 400°C • 4°C/min to 1350°C
D15	Batch 21, Die pressed compact	Heated 3.5 h at 400°C	• 4°C/min to 1350°C
D17	Batch 24, Centrifugally settled	Heated slowly to 200°C	• RT to 300°C over 1.5 h • 2°C/min to 400°C • 4°C/min to 1350°C
D18	Batch 20, Die pressed compact	None	• RT to 300°C over 1.5 h • 4°C/min to 1350°C

Table 15. Dilatometer sample identification and description.

9.3 Differential Scanning Calorimetry Runs

Batch	ID#	Heating Rate°C/min	Atm.	Temp. Range°C	Pretreatment
13	25	4	Air	250-725	250C, 3.25 h
13	29	4	Air	25-700, 60 min	250C, 3.25 h
13	8,9	10	Ar	30-600	250C, 3.25 h
13	30	10	Air	250-450	250C, 3.25 h
13	16,17	50	Ar	30-725	250C, 3.25 h
13	23	50	Air	300-725	250C, 3.25 h
13	43	50	Air	25-725, 3 min	250C, 3.25 h
13	14	100	Ar	30-725, 20 min	250C, 3.25 h
13	15	100	Ar	30-725	250C, 3.25 h
13	20	100	Air	300-725	250C, 3.25 h
13	42	100	Air	25-725, 3 min	250C, 3.25 h
13	12,13	200	Ar	30-725	250C, 3.25 h
13	18	200	Air	300-725, 10 min	250C, 3.25 h
13	19	200	Air	300-725	250C, 3.25 h
13	41	200	Air	25-725, 3 min	250C, 3.25 h
13	40	300	Air	25-725, 3 min	250C, 3.25 h
13	39	400	Air	25-725, 3 min	250C, 3.25 h
13	26	500	Air	25-700, 15 min	250C, 3.25 h
13	34,37	500	Air	300-725	250C, 3.25 h
13	35,36	500	Air	300-600	250C, 3.25 h
13	38	500	Air	25-725, 3 min	250C, 3.25 h

Table 16. DSC experimental parameters. Continued next page.

Batch	ID#	Heating Rate°C/min	Atm.	Temp. Range°C	Pretreatment
14	1	10	Ar	30-600	
14	2	40	Ar	30-600	
14	3	100	Ar	30-600	
16	1	40	Ar	30-600	
18	1	4	Ar	30-600, 240 min	
18	2	20	Ar	30-600, 30 min	as prepared ground
18	3	100	Ar	30-600, 30 min	as prepared ground
18	4	20	Ar	30-600, 30 min	as prepared ground 200C, 1h air
18	5	20	Ar	30-600, 840 min	as prepared ground 200C, 1h air
18	6	20	Ar	30-600, 30 min	as prepared ground 450C, 1h air
18	7	20	Ar	30-600, 840 min	as prepared ground 450C, 1h air

Table 16. Continued.

LAWRENCE BERKELEY LABORATORY
UNIVERSITY OF CALIFORNIA
INFORMATION RESOURCES DEPARTMENT
BERKELEY, CALIFORNIA 94720